Study of Nonstrange Mesons Produced in K^-p Interactions at 3.9 and 4.6 GeV/c*

M. Aguilar-Benitez, S. U. Chung, R. L. Eisner, and N. P. Samios
Brookhaven National Laboratory, Upton, New York 11973
(Received 29 February 1972)

An investigation is presented on the production and decay properties of pseudoscalar, vector, and tensor mesons produced in association with Λ, Σ^0, and $Y^*(1385)$ from K^-p interactions at 3.9 and 4.6 GeV/c. The data have been compared with SU(3) and quark-model predictions. New measurements of the mass, width, and branching ratios of the $\phi(1019)$, $f'(1519)$, and $Y^*(1385)$ resonances are given. Our analysis of the η' meson favors the $J^{PC} = 0^{-+}$ classification. The properties of this well-known meson are compared with those of our previously proposed $M(953)$ meson. An important aspect of this study is that we have placed particular emphasis on taking the background into account when we extracted resonance quantities such as the density-matrix elements.

I. INTRODUCTION

An extensive study of K^-p interactions at 3.9 and 4.6 GeV/c consisting of 700 000 pictures in the BNL 80-in. hydrogen bubble chamber has been completed. The more dramatic results have already been published in a series in *Physical Review Letters* and *Physics Letters*. This publication represents the second of a number of articles describing the experimental details as well as presenting the final corrected data. The first paper[1] was concerned with strange mesons, namely the production and decay properties of the $K(890)$ and $K(1420)$ mesons. Here we turn our attention to the study of nonstrange-meson systems recoiling against Λ^0 and Σ^0 hyperons as well as numerous exclusive two-body resonant reactions. Particular emphasis has been placed upon a systematic evaluation of the properties of many of these meson states, i.e., mass, width, production, and decay distributions, etc. All such information is tabulated and compared with a limited number of dynamical models which vary in degree in their agreement with the data. Noteworthy among these has been the validity of an SU(3) approach in describing many of the dominant features of numerous reactions.

After the presentation of the event-selection procedure and a general description of the final states in Sec. II, the analysis of mesons produced with Λ (Sec. III), Σ^0 (Sec. IV), and $Y^*(1385)$ (Sec. IV) is given. In Sec. VI a general summary of this experimental study is presented, and in Secs. VII–IX detailed comparisons between the data and the theoretical predictions of SU(3) and quark models are given.

TABLE I. Microbarn equivalent of the different topologies used in the present study.

Topology	Events/μb 3.9 GeV/c	4.6 GeV/c
Zero-prong + vee	2.6	4.0
Two-prong + vee	5.1	7.4
Four-prong	6.4	3.6
Four-prong + vee	2.0	6.5
Multistrange[a]	7.1	10.4

[a] 2-vee, 3-vee, 2-prong + 2-vee.

II. DESCRIPTION OF FINAL STATES

A. Event Selection

The data for this analysis come from exposures of the BNL 80-in. hydrogen bubble chamber to incident K^- beams of 3.9- and 4.6-GeV/c momenta. The events used for this study mainly involve the presence of Λ^0 (or Σ^0) hyperons in the final state. A list of such topologies is shown in Table I. This corresponds to a total of $\approx$25 events/μb; the actual breakdown is listed in the table and includes corrections for scanning efficiency, film coverage, fiducial volume, and throughput efficiency.

The final states of interest for this study are indicated in Table II. In general, the selection procedure was based on χ^2 kinematic probability criteria as well as ionization estimates (as measured by the BNL Flying-Spot Digitizer). When the ionization was consistent with several kinematic interpretations, the one in the highest-constraint class was chosen provided the probability selections listed in Table II were satisfied.

Most of the following investigation will focus on the two-prong-plus-vee topology. There, the most common ambiguities were between reactions 2 and 7 as well as between 3 and 7. In order to illustrate the clean separation between the hypotheses 2 and 7 afforded by the above criteria, we

TABLE II. Experimental details of the final states used in the present study.

Topology	Final state	Prob. cut	No. of events 3.9 GeV/c	No. of events 4.6 GeV/c	Reaction No.
Zero-prong+vee	$K^-p \to \Lambda MM$	···	1168	2169	1
Two-prong+vee	$K^-p \to \Lambda\pi^+\pi^-$	1%	1178	1237	2
	$K^-p \to \Lambda\pi^+\pi^-\pi^0$	5%	2981	3552	3
	$K^-p \to \Lambda\pi^+\pi^-MM$	···	3560	5976	4
	$K^-p \to \Lambda K^+K^-$	1%	204	268	5
	$K^-p \to \Lambda K^+K^-\pi^0$	5%	172	358	6
	$K^-p \to \Sigma^0\pi^+\pi^-$	5%	405	429	7
	$K^-p \to \Sigma^0K^+K^-$	5%	87	95	8
Four-prong+vee	$K^-p \to \Lambda\pi^+\pi^+\pi^-\pi^-$	1%	309	1130	9
	$K^-p \to \Lambda\pi^+\pi^+\pi^-\pi^-\pi^0$	5%	432	1987	10
Multistrange	$K^-p \to \Lambda K_1^0K_1^0$		42	54	11
	$K^-p \to \Lambda K_1^0(K^0)$		154	159	12
	$K^-p \to \Lambda K^\pm\pi^\mp K_1^0$		227	322	13
	$K^-p \to \Sigma^0K_1^0K_1^0$		18	19	14

present for a portion of the final sample and after the 5% probability selection on reaction 7 a study of the distribution of the angle between the normal to the production plane and the outgoing Λ direction in the Σ^0 rest frame. We expect this angle to peak at $\cos(\hat{n}\cdot\hat{\Lambda})=0$ for $\Lambda\pi^+\pi^-$ events and to be isotropic for true $\Sigma^0\pi^+\pi^-$ events. The distribution for the unique events of reaction 7 and for events ambiguous between reactions 2 and 7 are shown in Figs. 1(a) and 1(b), respectively. They show that nearly all of the ambiguous events are not from reaction 7 and they were included in reaction 2 [four-constraint (4c)].

The remainder of the $\Sigma^0\pi^+\pi^-$ ambiguities were with reaction 3 ($\Lambda\pi^+\pi^-\pi^0$). That a clean separation of these two channels was achieved is illustrated from an investigation of the correlation between the MM^2 distribution, from $K^-p \to \Lambda\pi^+\pi^-MM$, and the MM distribution from $K^-p \to \pi^+\pi^-MM$ for events that fitted either reaction 3 and/or 7 or 4 (after removal of events that fitted reaction 2). These distributions are, respectively, shown in Figs. 2(a) and 2(b). The shaded areas represent events that fitted reaction 7. The clear γ signal [Fig. 2(a)], correlated with the Σ^0 peak [Fig. 2(b)], indicates that nearly all events which fitted the $\Sigma^0\pi^+\pi^-$ hypothesis were correctly assigned to reaction 7 (2c). Also apparent from the strong π^0 signal in Fig. 2(a) is the clear separation of reaction 3, $\Lambda\pi^+\pi^-\pi^0$, from reaction 4, $\Lambda\pi^+\pi^-MM$.

The separation of reactions 5, 6, and 8 was checked in a similar manner to that described above.

B. General Description of Final States

The dominant feature of the final states listed in Table II and used in the present study is copious

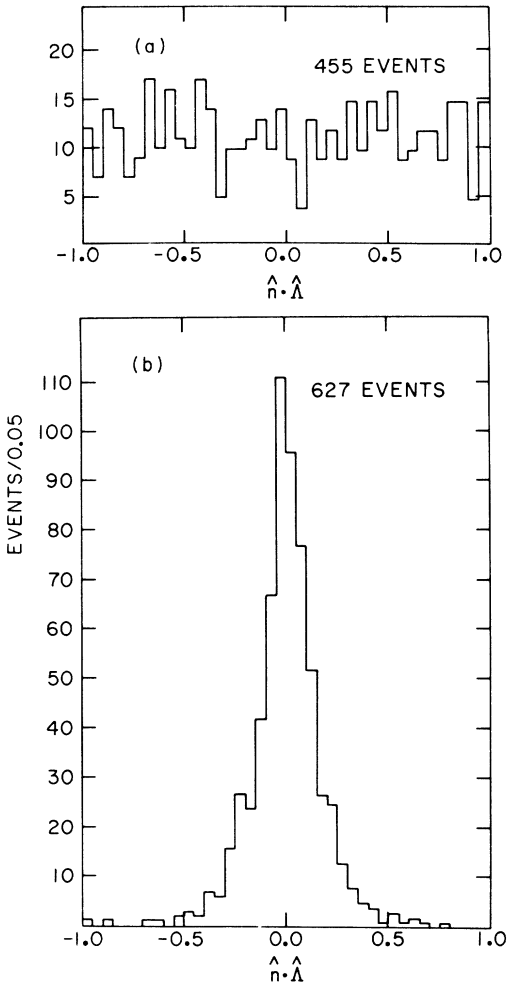

FIG. 1. (a) $\hat{n}\cdot\hat{\Lambda}$ distribution for a subsample of unique events of reaction 7. (b) Same as (a), but for events ambiguous between reactions 7 and 2.

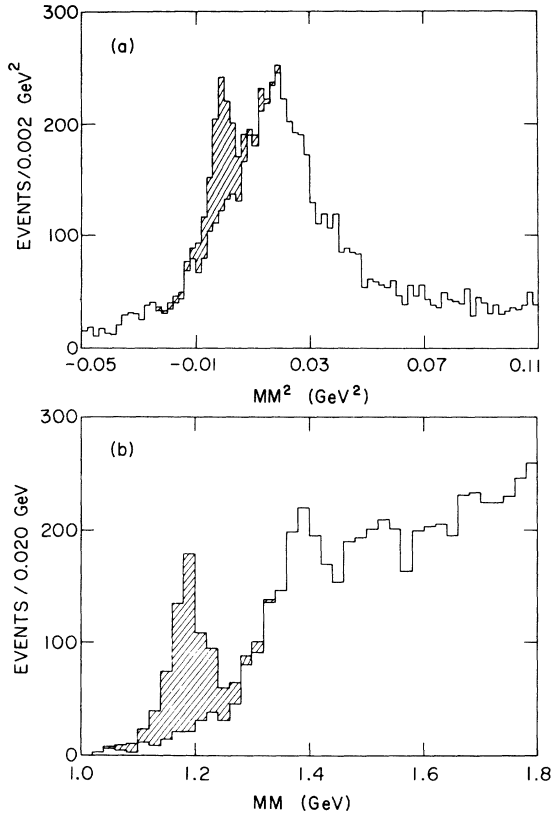

FIG. 2. (a) MM^2 distribution from $K^-p \to \Lambda\pi^+\pi^-$MM for events that fitted reactions 3 and/or 7 or 4. (b) MM distribution from reaction $K^-p \to \pi^+\pi^-$MM for the same sample of events as in (a). The shaded area represents events that fitted reaction 7.

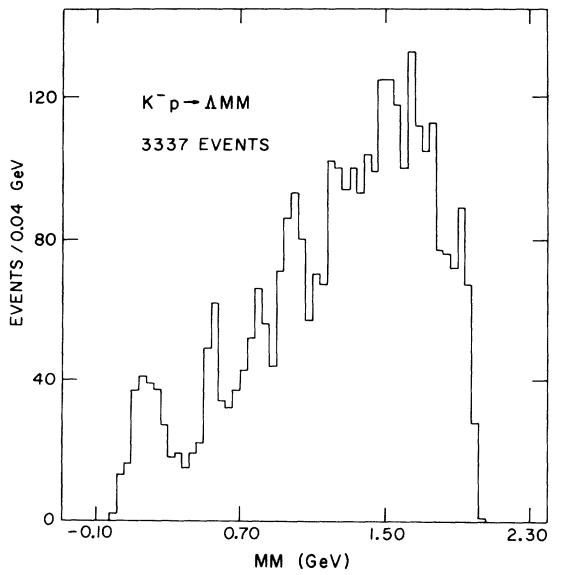

FIG. 3. MM distribution from reaction 1.

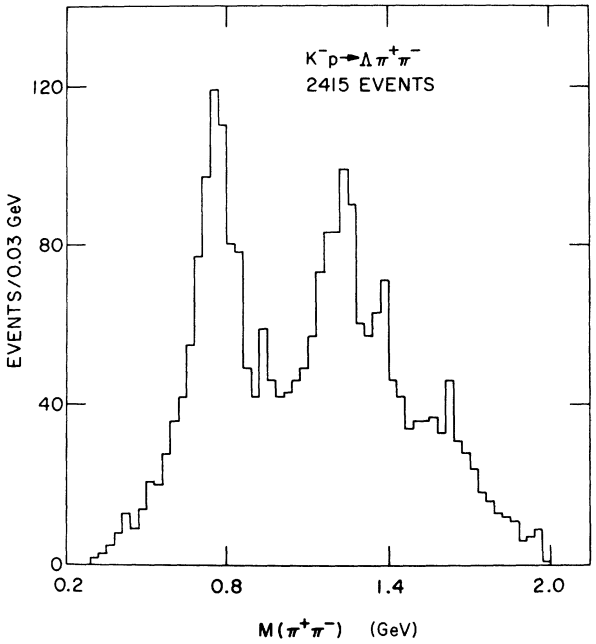

FIG. 4. $\pi^+\pi^-$ effective-mass distribution from reaction 2.

production of both meson and baryon resonances. The relevant mass distributions are displayed in Figs. 3–21. Single π^0 production as well as neutral decay modes of well-known resonances ($\eta, \omega, \eta', \phi$) are identified in the missing-mass distribution of reaction 1 (Fig. 3). The final states 2 and 7 exhibit strong contributions from meson (ρ^0, f^0) and hyperon [$Y^*(1385), Y(1660)\ldots$] resonance production (see Figs. 4–7). Strong ω production, a clear η signal, and a significant en-

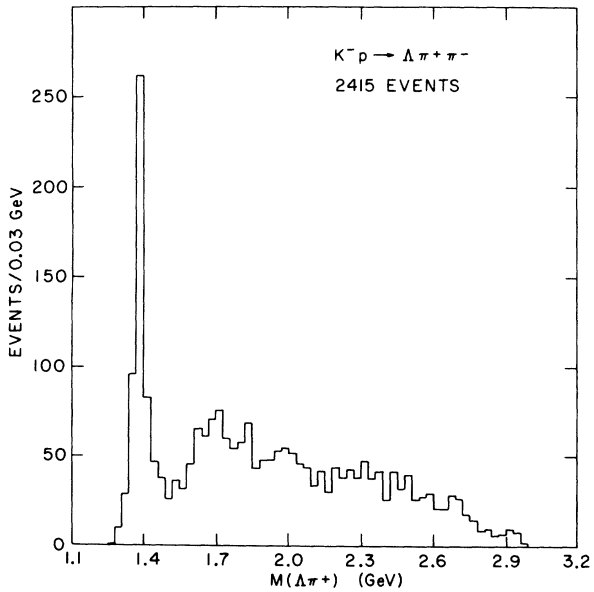

FIG. 5. $\Lambda\pi^+$ effective-mass distribution from reaction 2.

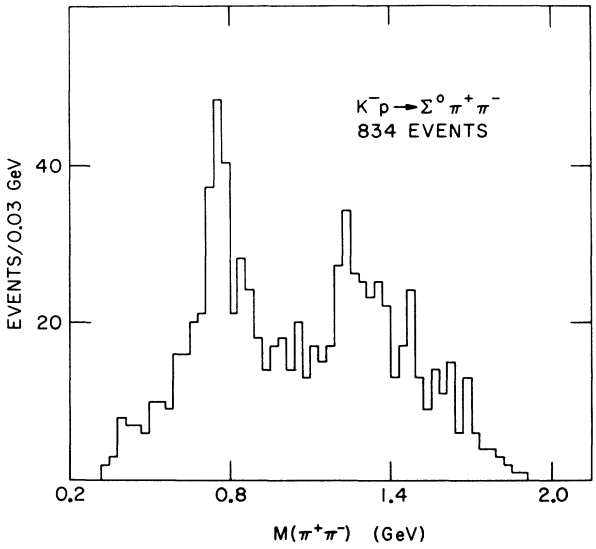

FIG. 6. $\pi^+\pi^-$ effective-mass distribution from reaction 7.

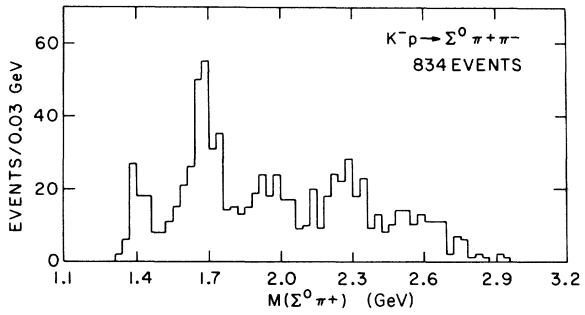

FIG. 7. $\Sigma^0\pi^+$ effective-mass distribution from reaction 7.

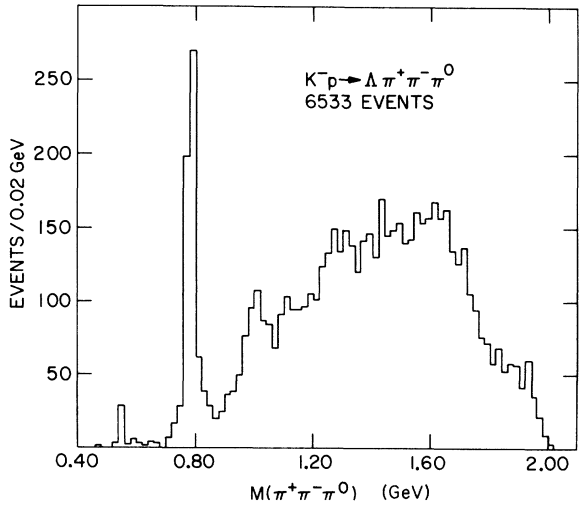

FIG. 8. $\pi^+\pi^-\pi^0$ effective-mass distribution from reaction 3.

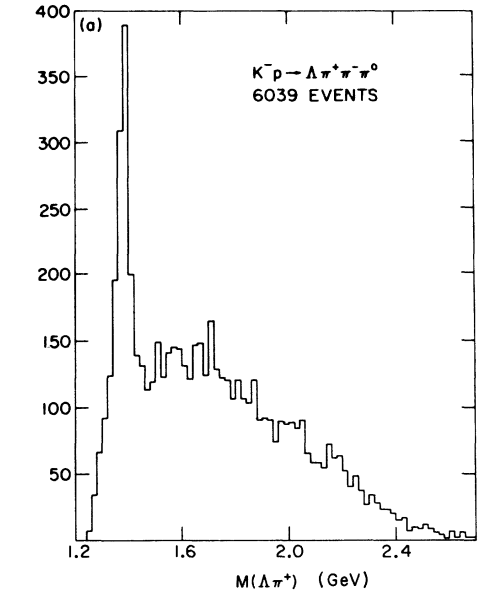

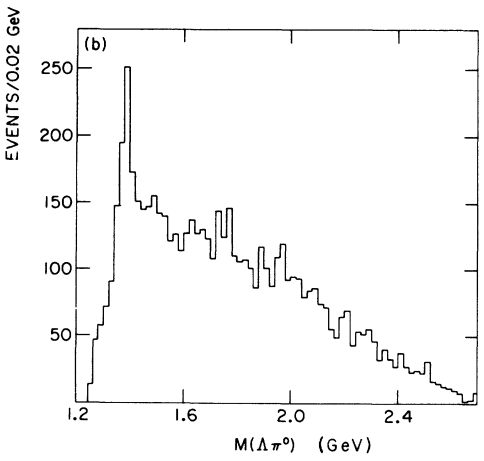

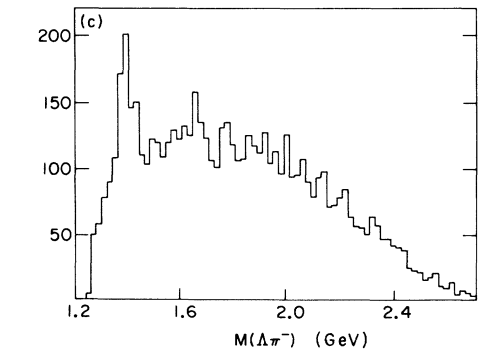

FIG. 9. (a)–(c) $\Lambda\pi^+$, $\Lambda\pi^0$, and $\Lambda\pi^-$ effective-mass distributions from reaction 3.

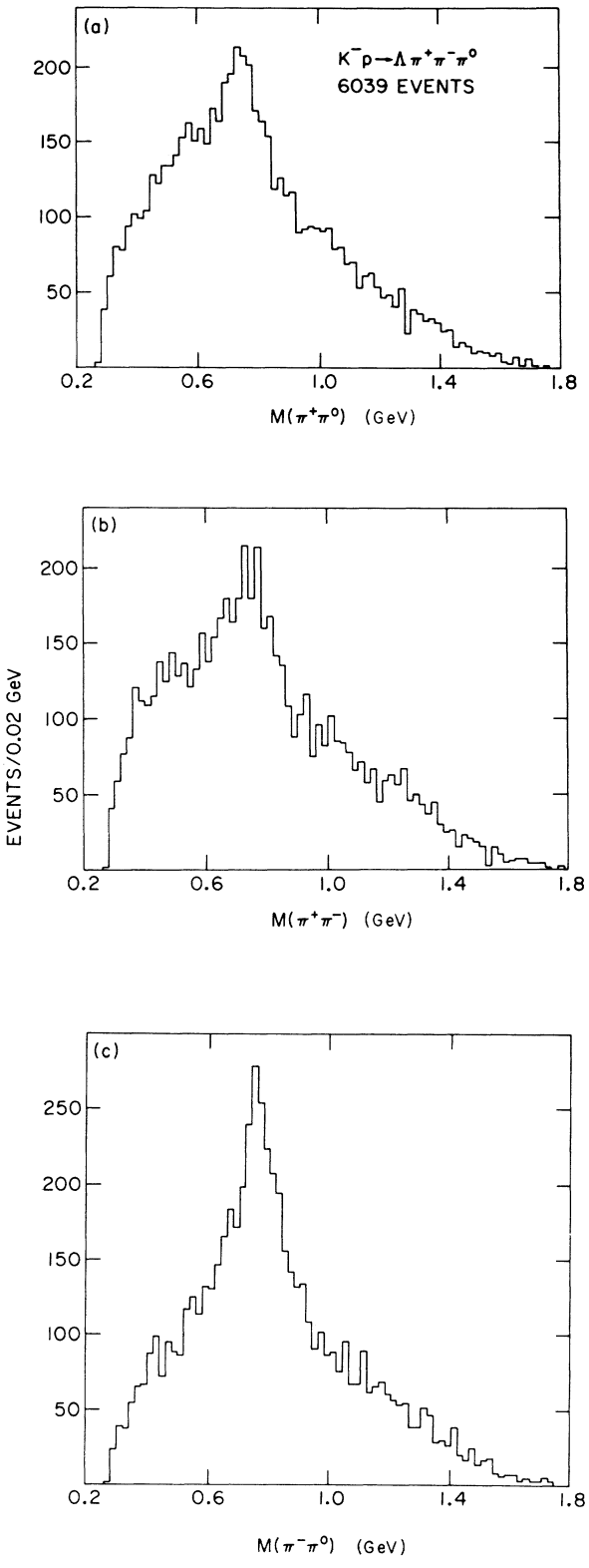

FIG. 10. (a)–(c) $\pi^+\pi^0$, $\pi^+\pi^-$, and $\pi^-\pi^0$ effective-mass distributions from reaction 3.

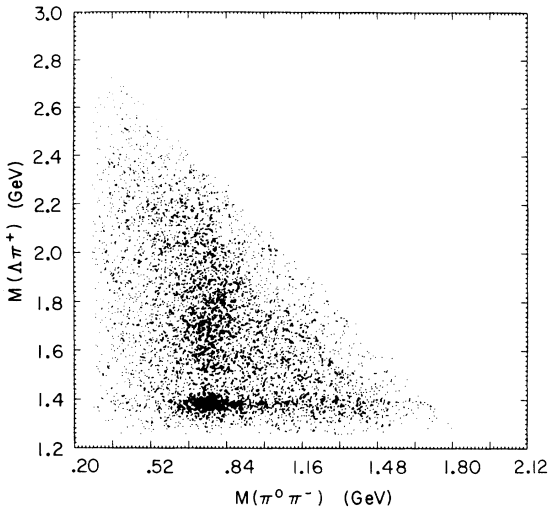

FIG. 11. $M(\pi^0\pi^-)$-vs-$M(\Lambda\pi^+)$ distribution from reaction 3.

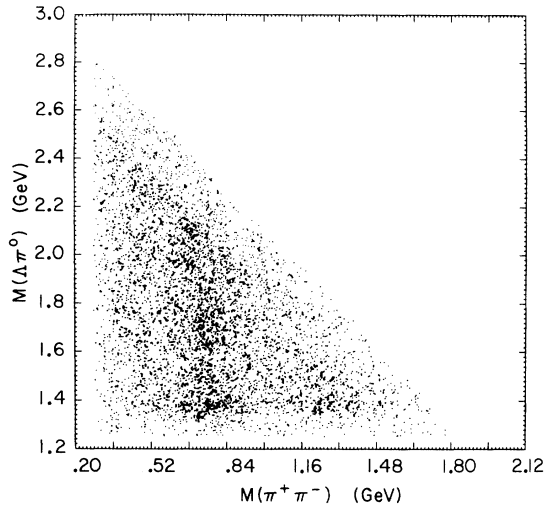

FIG. 12. $M(\pi^+\pi^-)$-vs-$M(\Lambda\pi^0)$ distribution from reaction 3.

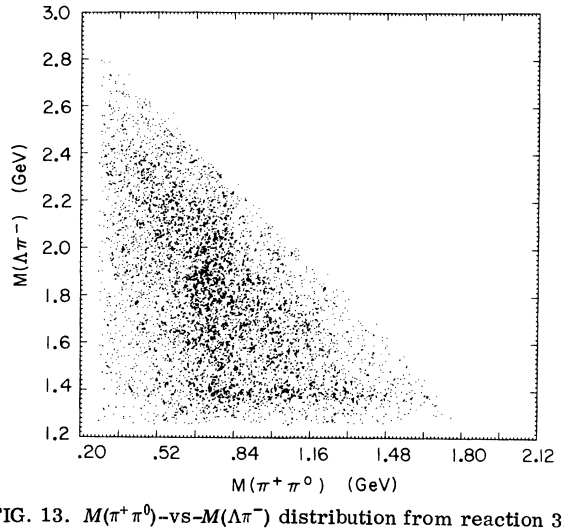

FIG. 13. $M(\pi^+\pi^0)$-vs-$M(\Lambda\pi^-)$ distribution from reaction 3.

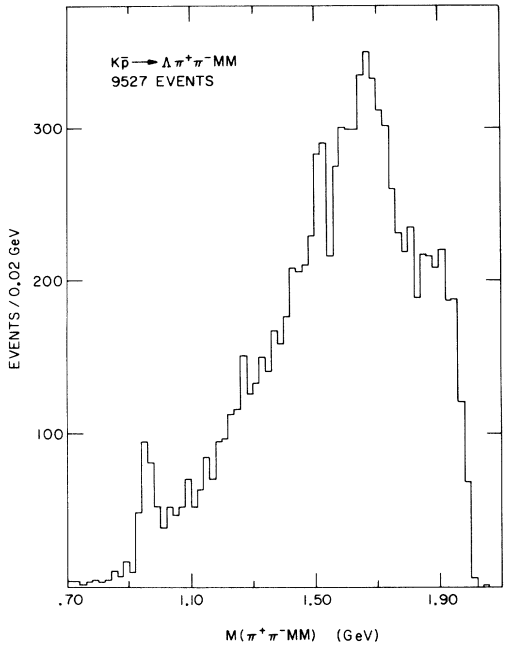

FIG. 14. $\pi^+\pi^-$MM effective-mass distribution from reaction 4.

hancement in the 1-GeV region are the main characteristics in the $\pi^+\pi^-\pi^0$ mass distribution of reaction 3 (Fig. 8). Important contributions from quasi-two-body (i.e., $Y^*\rho$) and quasi-three-body (i.e., $Y^*\pi\pi$ and $\Lambda\pi\rho$) channels to the final state (3) are apparent in the pertinent mass distribution and triangular plots shown in Figs. 9–13. The presence of the η' meson represents the only striking effect in the $\pi^+\pi^-$MM and $\pi^+\pi^+\pi^-\pi^-\pi^0$ effective-mass distributions from reactions 4 and 10 (Figs. 14 and 15). As seen in Figs. 16 and 17, strong production of ϕ and the observation of the f' meson characterize the $K\bar{K}$ mass distributions from reactions 5, 8, 11, 12, and 14. Contributions from $\phi, Y^*(1385)$ and the quasi-two-body channel $Y^*(1385)\phi$ to the final state (6) is apparent from the $M(K^+K^-)$-vs-$M(\Lambda\pi^0)$ distribution and corresponding effective-mass projections (Figs. 18 and 19). Finally, the $\pi^+\pi^+\pi^-\pi^-$ (Fig. 20) and $K_1^0K^\pm\pi^+$ (Fig. 21) mass distributions from reactions 9 and 13 do not exhibit any significant structure and will be used to establish upper limits in decay rates of well-established meson resonances.

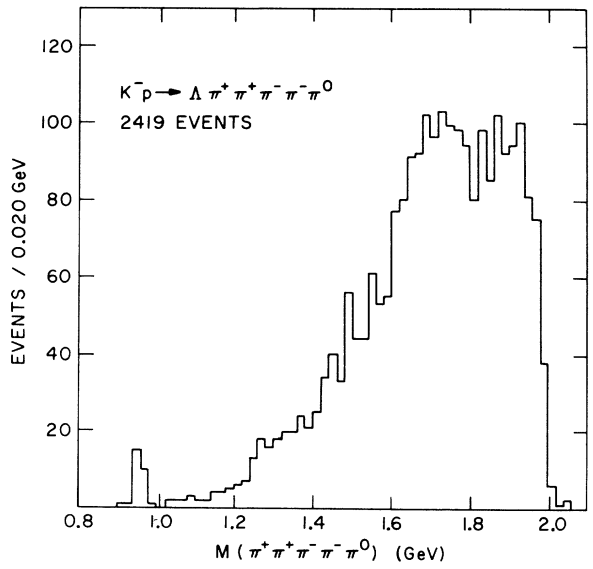

FIG. 15. $\pi^+\pi^+\pi^-\pi^-\pi^0$ effective-mass distribution from reaction 10.

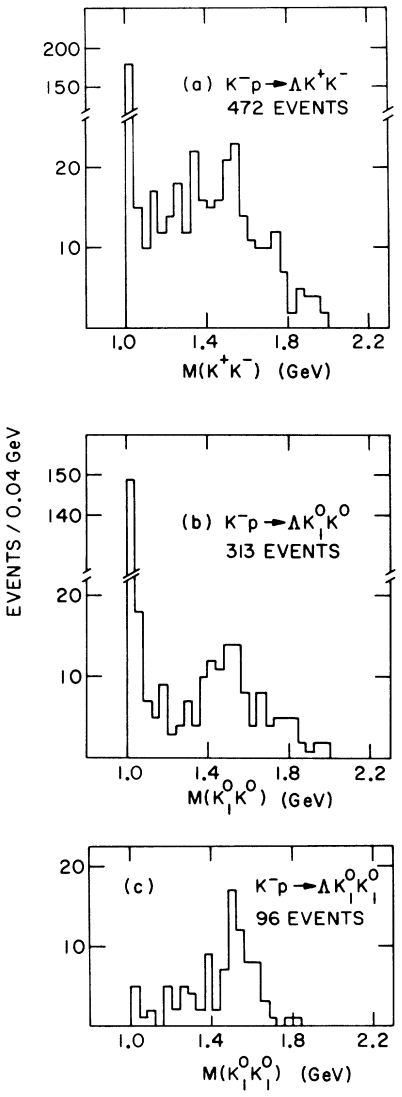

FIG. 16. $K\bar{K}$ effective-mass distribution from (a) reaction 5, (b) reaction 12, (c) reaction 11.

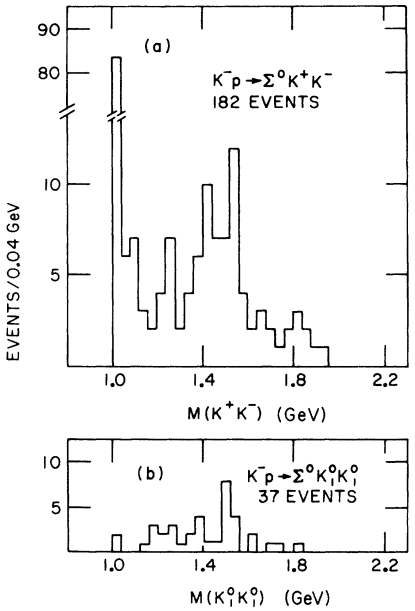

FIG. 17. $K\bar{K}$ effective-mass distribution from (a) reaction 8, (b) reaction 14.

III. STUDY OF REACTIONS $K^-p \to \Lambda$+MESONS

A. Pseudoscalar Mesons

1. *Reaction* $K^-p \to \Lambda\pi^0$

The missing-mass-squared distribution from reaction 1 is shown in Fig. 22(a) [22(b)] at 3.9 [4.6] GeV/c. The number of events at each momentum of the reaction

$$K^-p \to \Lambda\pi^0$$

was obtained from fits to these spectra using a linear form as background plus a Gaussian shape with central value fixed at the π^0 mass and with a variable width. The solid curves in Fig. 22(a) [(b)] represent the results of the fits. The number of events and the corrected cross sections so obtained are

3.9 GeV/c: 109 ± 10 events; $\sigma = 67 \pm 6$ μb,

4.6 GeV/c: 111 ± 12 events; $\sigma = 44 \pm 5$ μb.

The corresponding differential cross sections as a function of $-t'$,[2] shown in Figs. 23(a) and 23(b) and listed in Table III, were obtained by normalizing the number of events in the π^0 region

$$-0.02 \leq \mathrm{MM}^2 \leq 0.06 \text{ GeV}^2$$

to the total cross sections quoted above. There is an estimated 10% (15%) background contamination at 3.9 (4.6) GeV/c which has not been folded into the numbers in the tables. The forward region of

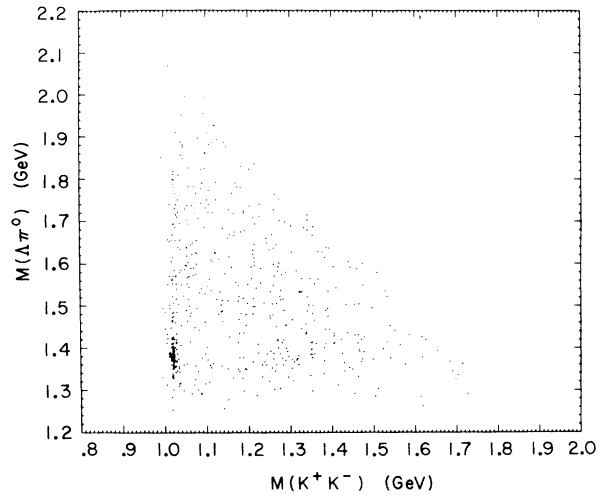

FIG. 18. $M(K^+K^-)$-vs-$M(\Lambda\pi^0)$ distribution from reaction 6.

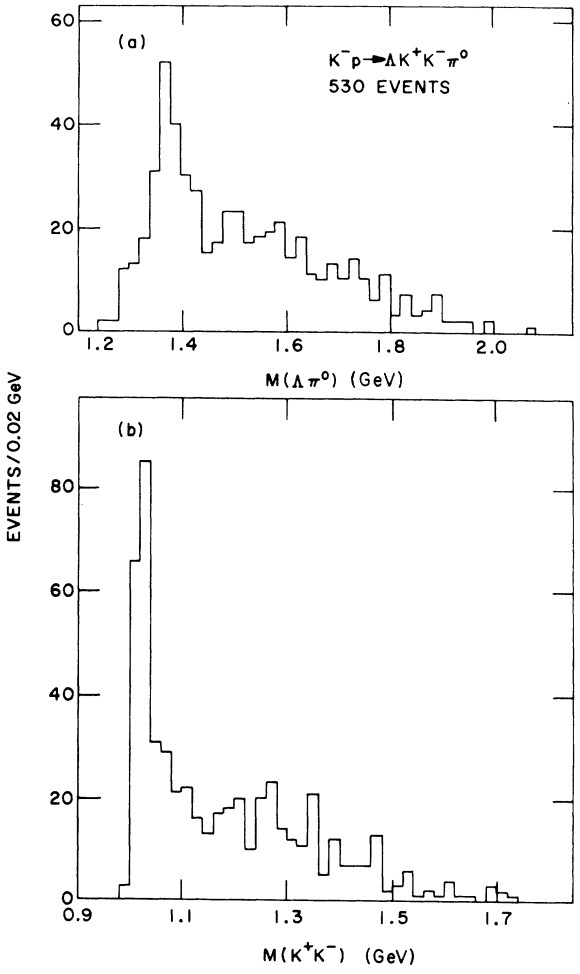

FIG. 19. (a) $\Lambda\pi^0$ effective-mass distribution from reaction 6. (b) K^+K^- effective-mass distribution from reaction 6.

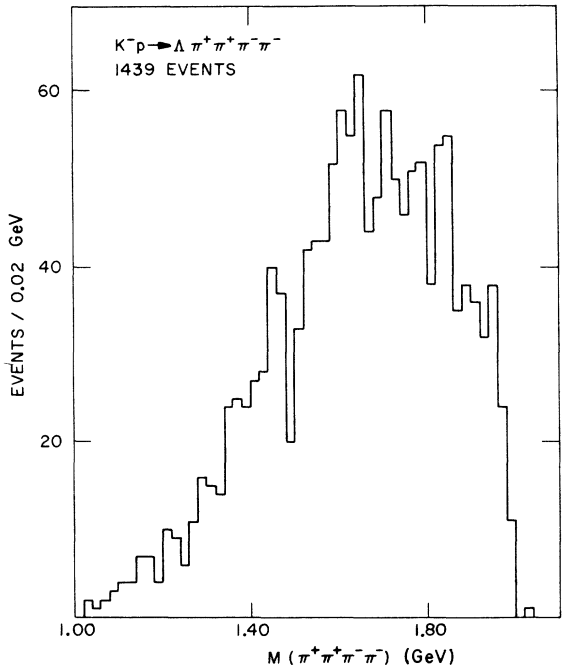

FIG. 20. $\pi^+\pi^+\pi^-\pi^-$ effective-mass distribution from reaction 9.

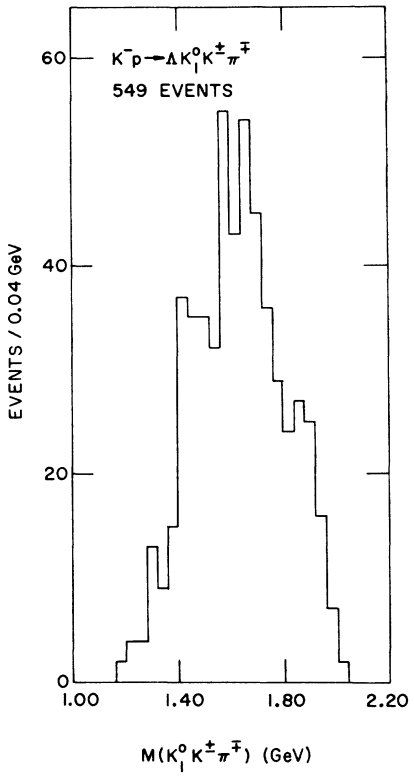

FIG. 21. $K_1^0K^{\pm}\pi^{\mp}$ effective-mass distribution from reaction 13.

$d\sigma/dt'$ ($|t'|<1.0$ GeV^2) was fitted to the form $d\sigma/dt' \sim e^{At'}$, and the following values for the slope parameter A were obtained:

3.9 GeV/c: $A=3.1\pm0.5$ GeV^{-2},

4.6 GeV/c: $A=4.6\pm0.5$ GeV^{-2}.

The Λ polarization P_Λ as a function of t' was obtained by the maximum-likelihood technique,[3] and the values are shown in Fig. 24 and listed in Table IV for the combined 3.9- and 4.6-GeV/c sample. The data are consistent with positive polarization throughout the t' interval investigated. Our results of positive P_Λ up to $|t'|=1.0$ GeV^2 are in agreement with those obtained in the reaction $K^-n\to\Lambda\pi^-$ at 3.9 GeV/c,[4] and at 4.5 GeV/c.[5]

The backward production cross section ($\cos\theta^*\leq 0.0$) at 3.9 and 4.6 GeV/c is 6.1 ± 1.9 and 2.4 ± 1.0 μb, respectively.

2. *Reaction $K^-p\to\Lambda\eta(549)$*

We now turn our discussion to the investigation of the reaction

$$K^-p\to\Lambda\eta.$$

The data on charged η production ($\eta_C\to\pi^+\pi^-\pi^0$) come from reaction 3, while those for neutral η production ($\eta_N\to$ neutrals) come from reaction 1. The number of η_C events was estimated from the $\pi^+\pi^-\pi^0$ effective-mass spectra at 3.9 and 4.6 GeV/c

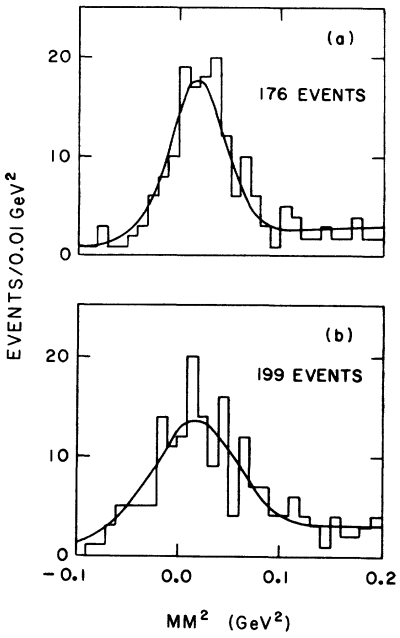

FIG. 22. MM^2 distribution from reaction 1: (a) at 3.9 GeV/c, (b) at 4.6 GeV/c.

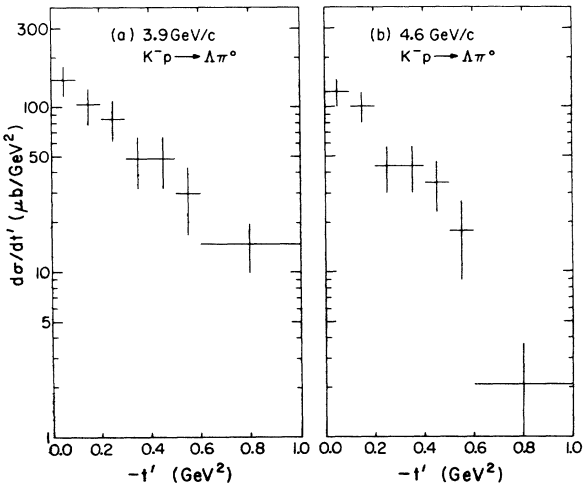

FIG. 23. Differential cross section for reaction $K^-p \to \Lambda\pi^0$: (a) at 3.9 GeV/c, (b) at 4.6 GeV/c.

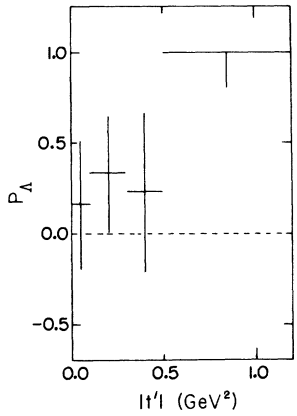

FIG. 24. Λ polarization for reaction $K^-p \to \Lambda\pi^0$.

(combined 3.9- and 4.6-GeV/c data are shown in Fig. 8). The number of events and the total corrected cross sections[6] so obtained are given in Table V.

The number of η_N events at 3.9 and 4.6 GeV/c was obtained from a fit to the missing-mass-squared spectrum of Fig. 25, using a linear form in the missing mass squared as background and a Gaussian shape with central value fixed at the η mass and with a variable width. The number of events and corrected cross sections are listed in Table V. Using the cross sections for $\Lambda\eta_C$ and $\Lambda\eta_N$ in Table V we obtain a branching ratio

$$\frac{\eta_C \to \pi^+\pi^-\pi^0}{\eta_N \to \text{neutrals}} = 0.29 \pm 0.09,$$

which is in excellent agreement with the world-averaged value[7] of 0.32 ± 0.02.

The differential cross section for the reaction $K^-p \to \Lambda\eta$ for the combined 3.9- and 4.6-GeV/c data is given in Table VI and Fig. 26 and was obtained by adding the $\pi^+\pi^-\pi^0$ spectrum and the background subtracted missing-mass-squared distribution of reaction 1 and normalizing to the total cross section given in Table V. A large forward peak ($|t'| < 0.20$ GeV^2) is observed, but the limited statistics preclude the extraction of the slope parameter.

The Λ polarization obtained from all the $K^-p \to \Lambda\eta$

TABLE III. Differential cross sections for reaction $K^-p \to \Lambda\pi^0$ at 3.9 and 4.6 GeV/c.

$\lvert t'\rvert$ Interval (GeV^2)	3.9 GeV/c No. of events[a]	3.9 GeV/c Corrected cross section[b] (μb/GeV^2)	4.6 GeV/c No. of events[a]	4.6 GeV/c Corrected cross section[b] (μb/GeV^2)
0.0–0.1	24± 5	146 ± 30	28± 5	123 ± 23
0.1–0.2	17± 4	103 ± 25	23± 5	101 ± 21
0.2–0.3	14± 4	85 ± 23	10± 3	44 ± 14
0.3–0.4	8± 3	49 ± 17	10± 3	44 ± 14
0.4–0.5	8± 3	49 ± 17	8± 3	35 ± 12
0.5–0.6	5± 2	30 ± 13	4± 2	18 ± 9
0.6–1.0	10± 3	15 ± 5	2± 1	2.2± 1.5
1.0–2.0	10± 3	6 ± 2	6± 2	2.6± 1.1
2.0–3.0	4± 2	2.4± 1.2	2± 1	0.9± 0.6
3.0–4.0	0	0	1± 1	0.4± 0.4
4.0–5.0	4± 2	2.4± 1.2	0	0
5.0–6.0	6± 2	3.7± 1.5	1± 1	0.4± 0.4
6.0–7.0	...	...	4± 2	1.8± 0.9
7.0–8.0	...	...	1± 1	0.4± 0.4

[a] In the region $-0.02 \leq \text{MM}^2 \leq 0.06$ GeV^2.

[b] Obtained by normalizing total number of events to the $K^-p \to \Lambda\pi^0$ cross section given in the text.

TABLE IV. Λ polarization from reaction $K^-p \to \Lambda\pi^0$.

$\lvert t' \rvert$ interval (GeV^2)	No. of events [a]	P_Λ
0.0–0.1	49	0.16 ± 0.36
0.1–0.3	62	0.33 ± 0.32
0.3–0.5	30	0.23 ± 0.44
0.5–1.2	26	$1.00^{+0.00}_{-0.20}$

[a] In the region $-0.02 \leq \mathrm{MM}^2 \leq 0.06$ GeV^2.

events of reaction 3 is

$$P_\Lambda = 0.8^{+0.2}_{-0.6}.$$

3. *Reaction $K^-p \to \Lambda\eta'(958)$*

Our study of the reaction $K^-p \to \Lambda\eta'$ represents the first comprehensive analysis of η' production and decay properties for incident K^- momentum above 3.0 GeV/c. We will first discuss the properties of the $\eta\pi\pi$ and $\rho^0\gamma$ decay modes of the η'. As will be seen, the $\rho\gamma/\eta\pi\pi$ branching ratio which we obtain is significantly smaller than the value quoted by Rittenberg,[8] whose data represent the largest statistical sample of η's available up to now. The question of the spin-parity determination of the η' is also investigated. Previous Dalitz-plot studies favor the J^{PC} assignment of 0^{-+}; however, as discussed by Oglievetsky, Tybor, and Zaslavsky,[9] these analyses are also consistent with the 2^{-+} assignment. We present a Dalitz-plot analysis and reach the same conclusions as the previous investigations: The $\eta_N\pi^+\pi^-$ Dalitz plot can be fitted with a simple 0^{-+} matrix element as well as with a mixture of the two simplest 2^{-+} decay amplitudes. We also observe the $\sin^2\theta$ helicity angular distribution for the ρ^0 from the $\eta' \to \rho^0\gamma$ decay mode which is consistent with the $J^P = 0^-$ classification. In addition, we present a production-dependent analysis of the decay angular correlations of the η'. We find no statistically significant deviation from zero in the moments of the normal to the decay plane from either the $\eta\pi\pi$ or $\rho\gamma$ decay modes. Moreover, in the $\rho\gamma$ case we find no significant correlations between production and decay

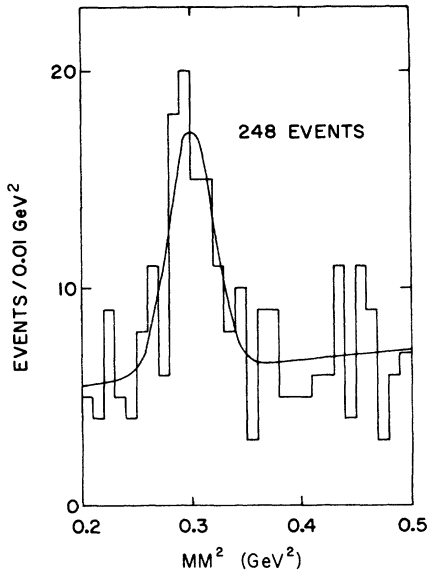

FIG. 25. MM^2 distribution, in the η region, from reaction 1.

of the ρ^0. The absence of significant angular correlations in η' production has now been observed for incident K^- momentum between 2 and 5.0 GeV/c and thus strongly favors the 0^- J^P assignment; only peculiar (and unlikely) production characteristics, which conspire at all energies so far investigated to destroy the η' polarization, must be invoked to allow the 2^- J^P assignment.

a. Mass, width, decay modes, and branching ratios. Figures 27(a) and 27(b) show the $\pi^+\pi^-$MM effective-mass spectrum from reaction 4, $\Lambda\pi^+\pi^-$MM, at 3.9 and 4.6 GeV/c, respectively. A clear enhancement is seen in the 0.9–1.0-GeV region which we associate with the η'. The shaded area represents the same mass spectrum after requiring that the missing mass squared be in the η_N region defined as

$$0.27 \leq \mathrm{MM}^2 \leq 0.33 \text{ GeV}^2,$$

and provides clear evidence for the $\eta' \to \eta_N\pi^+\pi^-$ decay mode.

We show in Fig. 28(a) [28(b)] the MM^2 projection

TABLE V. Cross sections for reaction $K^-p \to \Lambda\eta$.

Reaction \ Momentum	3.9 GeV/c No. of events	3.9 GeV/c Corrected σ (μb)	4.6 GeV/c No. of events	4.6 GeV/c Corrected σ (μb)	Combined 3.9 and 4.6 GeV/c No. of events	Combined 3.9 and 4.6 GeV/c Corrected σ (μb)
$K^-p \to \Lambda\eta_C$	18 ± 4	6 ± 1	11 ± 3	2.5 ± 0.7	29 ± 5	3.9 ± 0.7
$K^-p \to \Lambda\eta_N$					56 ± 14	13.5 ± 3.4
$K^-p \to \Lambda\eta$ [a]		26 ± 6		11 ± 3		

[a] Obtained from the $\eta_C \to \pi^+\pi^-\pi^0$ decay mode and using the η branching ratios from Ref. 7.

TABLE VI. Differential cross section for reaction $K^-p \to \Lambda\eta$ at 3.9 and 4.6 GeV/c (combined sample).

$\lvert t'\rvert$ interval (GeV^2)	No. of events	Corrected $\frac{d\sigma}{d\lvert t'\rvert}\left(\frac{\mu b}{\text{GeV}^2}\right)$
0.0–0.2	33 ± 9	37.2 ± 9.8
0.2–0.6	10 ± 3	5.6 ± 1.8
0.6–1.0	9 ± 3	5.1 ± 1.7
1.0–2.0	9 ± 3	2.0 ± 0.7
2.0–7.0	14 ± 5	0.6 ± 0.2

of the η' region defined as

$$0.9 \leq M(\pi^+\pi^-\text{MM}) \leq 1.0 \text{ GeV}$$

in which a large η_N signal is observed. Since there is no evidence for production of η_N in the side bands adjacent to the η' region, the number of η_N events in Fig. 28 allows the determination of the $\eta' \to \eta\pi^+\pi^-$ cross sections at the two momenta. The number of events and the corrected cross sections so obtained are given in Table VII.

In order to obtain the cleanest sample of resonance events for branching-ratio and spin-parity

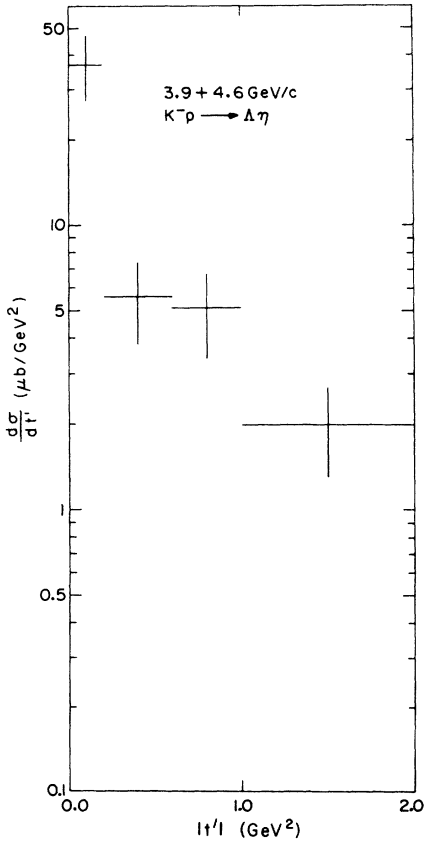

FIG. 26. Differential cross section for reaction $K^-p \to \Lambda\eta$.

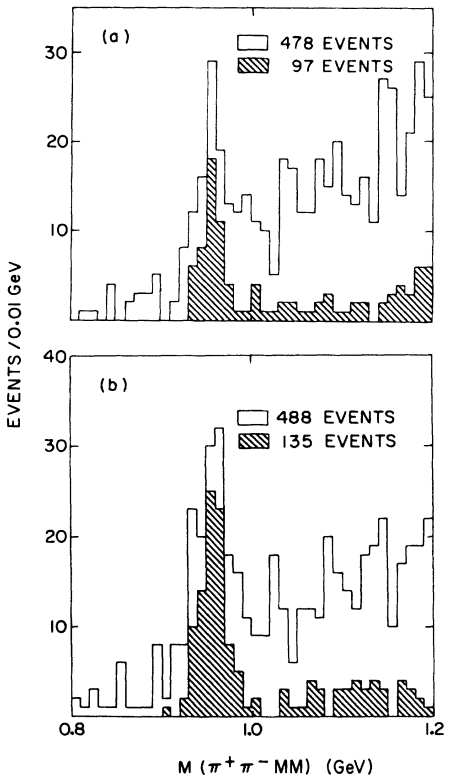

FIG. 27. $\pi^+\pi^-$MM effective-mass distribution from reaction 4. The shaded area is for events with $0.27 \leq \text{MM}^2 \leq 0.33$ GeV^2: (a) at 3.9 GeV/c, (b) at 4.6 GeV/c.

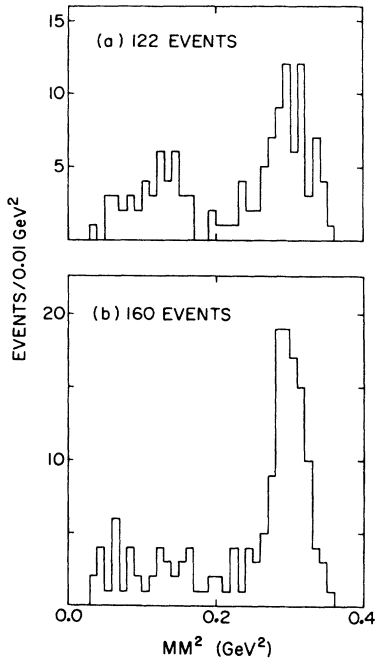

FIG. 28. MM^2 distribution for events in the region $0.9 \leq M(\pi^+\pi^-\text{MM}) \leq 1.0$ GeV: (a) at 3.9 GeV/c, (b) at 4.6 GeV/c.

TABLE VII. Cross sections for reaction $K^-p \to \Lambda\eta'$.

Reaction	Momentum	3.9 GeV/c No. $\eta_N\pi^+\pi^-$ events	3.9 GeV/c Corrected σ (μb)	4.6 GeV/c No. $\eta_N\pi^+\pi^-$ events	4.6 GeV/c Corrected σ (μb)
$K^-p \to \Lambda\eta'$, $\eta' \to (\pi\pi\eta)$		56±8	36±5	89±10	39±5
$K^-p \to \Lambda\eta'$ [a]			45±7		50±6

[a]Only $\pi\pi\gamma$ and $\eta\pi\pi$ decay modes are included.

analyses, we make use of the extreme peripherality of η' production, and we show in Fig. 29(a) the $\pi^+\pi^-$MM and $\pi^+\pi^-$"η_N" (shaded area) mass distributions after a $\cos\theta^* > 0.8$ (θ^* is the angle between target proton and outgoing Λ in the total center-of-mass system) selection for both momenta combined. The number of $\eta' \to \eta_N\pi^+\pi^-$ events estimated from the MM^2 projection of the η' region shown in Fig. 29(b) is given in Table VIII. We have fitted the shaded mass spectrum of Fig. 29(a) using a linear form in the mass as background plus a Gaussian shape with variable parameters. The values so obtained for the mass and width of the η' are

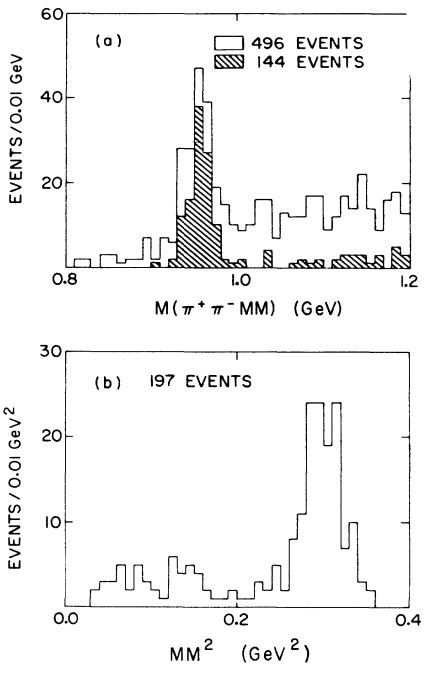

FIG. 29. (a) $\pi^+\pi^-$MM effective-mass distribution from reaction 4 after the selection $\cos\theta^*(p\cdot\Lambda) > 0.8$. The shaded area is for events with $0.27 \le \mathrm{MM}^2 \le 0.33$ GeV^2. (b) MM^2 distribution for events in the region $0.9 \le M(\pi^+\pi^-\mathrm{MM}) \le 1.0$ GeV after the selection $\cos\theta^*(p\cdot\Lambda) > 0.8$.

$$M = 955.7 \pm 2.0 \text{ MeV},$$

$$\Gamma = 23.5 \pm 3.7 \text{ MeV}.$$

The quoted value of Γ [full width at half-maximum (FWHM)] is comparable with the experimental resolution which makes the real width of the η' consistent with zero.

We now proceed to investigate the $\pi^+\pi^-\gamma$ decay mode of the η'. The reaction $K^-p \to \Lambda\pi^+\pi^-\gamma$ was not originally fitted, but events of this channel can in fact be found in a subsample of events of reaction 3, $\Lambda\pi^+\pi^-\pi^0$. Therefore, in order not to lose γ events, we have retained all the one-constraint π^0 fits with probability greater than 0.1% which are consistent with ionization. We have also investigated the unfitted mass spectrum recoiling off Λ and found no evidence for an η' signal in the events that fitted the $\Sigma^0\pi^+\pi^-$ (reaction 7) hypothesis. As can be seen in the fitted $\pi^+\pi^-\pi^0$ effective mass spectrum of Fig. 8, a broad enhancement exists in the 1.0-GeV mass region which we interpret as being composed of signals from the $\eta'(\to\pi\pi\gamma)$ and $\phi(\to\pi^+\pi^-\pi^0)$ mesons. We note that the η' peak position moves from ~0.96 to ~0.98 GeV when the γ's are incorrectly fitted as π^0's. In order to avoid the difficulty of having to resolve the η' signal from the total fitted $\pi^+\pi^-\pi^0$ mass spectrum, we examine the unfitted $\pi^+\pi^-\pi^0$ mass spectrum for the combined data at 3.9 and 4.6 GeV/c after a $\cos\theta^*$

TABLE VIII. η' decay modes.

Final state	Selection	No. of observed events
$\pi^+\pi^-\eta_N/\Lambda$	$\cos\theta^* > 0.8$	120±11
$\pi^+\pi^-\gamma/\Lambda$	$\cos\theta^* > 0.8$	65±10
$\rho^0\gamma/\Lambda$ [a]	$\cos\theta^* > 0.8$	59±10
Branching Ratios		

$$\frac{\rho^0\gamma}{\pi^+\pi^-\gamma} = 0.94 \pm 0.20, \quad \frac{\pi^+\pi^-\gamma}{\pi^+\pi^-\eta_N} = 0.54 \pm 0.10$$

[a]Obtained from a Dalitz-plot fit using events with $0.93 \le M(\pi^+\pi^-\gamma) \le 0.98$ GeV. This region contains 63±9 $\eta' \to \pi^+\pi^-\gamma$ events.

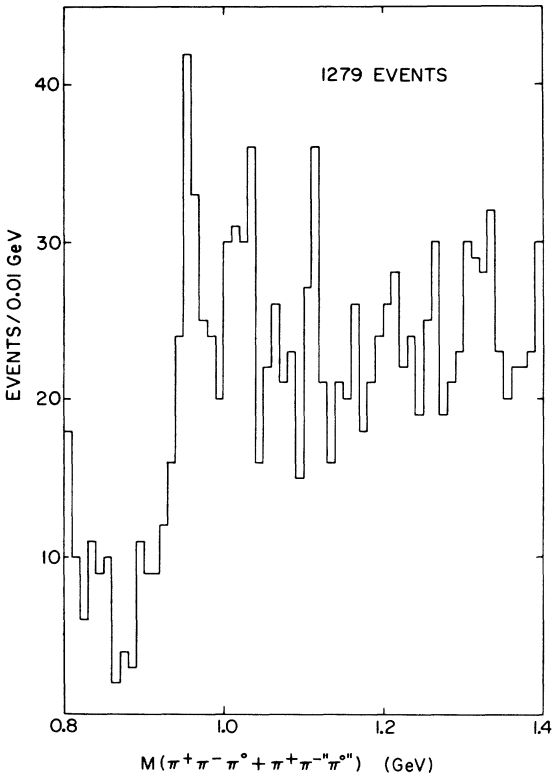

FIG. 30. Unfitted $\pi^+\pi^-\pi^0$ effective-mass spectrum for events which fit the reaction $K^-p \to \Lambda\pi^+\pi^-\pi^0$ after a $\cos\theta > 0.8$ selection.

>0.8 selection has been imposed (Fig. 30), which results in a clear separation between the ϕ and η' peaks. That the observed η' signal is, in fact, consistent with $\pi^+\pi^-\gamma$ events is shown in Fig. 31, in which the background-subtracted[10] MM^2 distribution for events in the η' region minus events in the adjacent background regions is presented; a clear γ signal peaking at $MM^2 \simeq 0.0$ GeV^2 with a width consistent with the experimental resolution is observed. The ability to separate the $\pi^+\pi^-\gamma$ signal is also apparent from comparison of the $\pi^+\pi^-$"π^0" ($MM^2 < 0.01$ GeV^2) and $\pi^+\pi^-\pi^0$ ($MM^2 > 0.01$ GeV^2) effective mass spectra shown in Figs. 32 and 33, respectively. An enhancement in the 960-MeV region is apparent only in the γ favored spectrum ($MM^2 < 0.01$ GeV^2), with no evidence for a signal in the π^0 favored spectrum ($MM^2 > 0.01$ GeV^2). This feature, of course, rules out a $\pi^+\pi^-\pi^0$ decay mode of the η'. A maximum-likelihood fit, using a Gaussian plus a polynomial background in the mass on the $\pi^+\pi^-$"π^0" spectrum, yields a mass

$$M = 956 \pm 2 \text{ MeV},$$

whose value is consistent with that obtained from the $\eta_N\pi^+\pi^-$ decay mode. The number of $\eta' \to \pi^+\pi^-\gamma$ events so obtained is given in Table VIII.

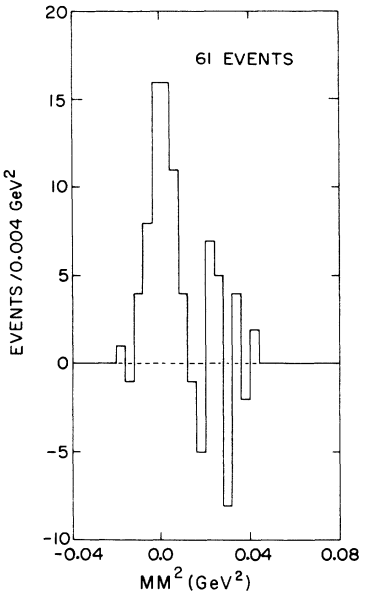

FIG. 31. Subtracted missing-mass-squared distribution for events in the η' region.

We now show that the observed $\pi^+\pi^-\gamma$ signal is consistent with being entirely $\rho^0\gamma$. The shaded area in Fig. 32 represents the $\pi^+\pi^-$"π^0" effective-mass spectrum for events with $\pi^+\pi^-$ effective mass in the ρ^0 region defined as

$$0.64 \leq M(\pi^+\pi^-) \leq 0.82 \text{ GeV}.$$

We observe that essentially all the $\eta' \to \pi^+\pi^-\gamma$ signal remains after this selection on the $\pi^+\pi^-$ effective mass. [To confirm further that the $MM^2 < 0.01$ GeV^2 selection is consistent with selecting all the

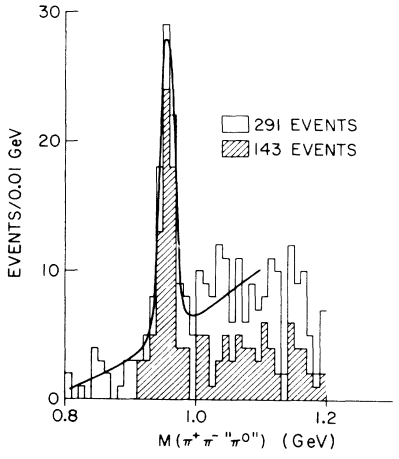

FIG. 32. Unfitted $\pi^+\pi^-$"π^0" effective-mass spectrum for events that fitted $K^-p \to \Lambda\pi^+\pi^-\pi^0$ with $\cos\theta^* > 0.8$ and $MM^2 < 0.01$ GeV^2. The shaded histogram is for events with $\pi^+\pi^-$ effective mass in the ρ^0 region.

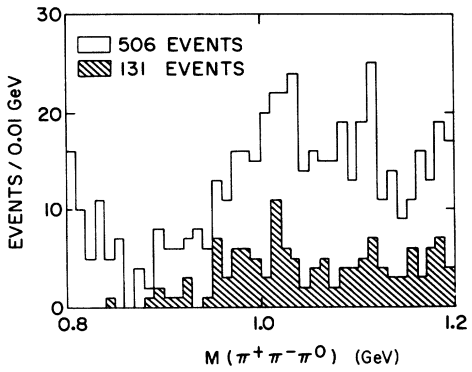

FIG. 33. Unfitted $\pi^+\pi^-\pi^0$ effective-mass spectrum for events that fitted $K^-p \to \Lambda\pi^+\pi^-\pi^0$ with $\cos\theta^* > 0.8$ and $MM^2 > 0.01$ GeV^2. The shaded histogram is for events with $\pi^+\pi^-$ effective mass in the ρ^0 region.

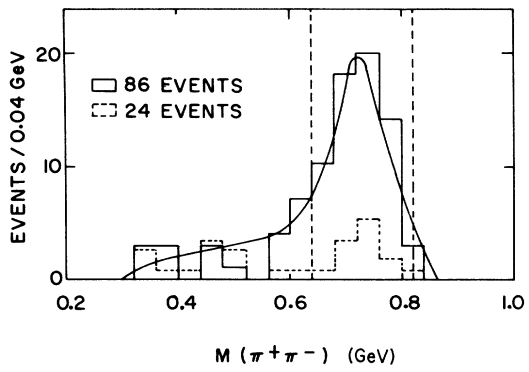

FIG. 34. $\pi^+\pi^-$ mass projection for events in the η' region. The dotted curve represents the $\pi^+\pi^-$ mass projection of the adjacent control bands normalized to the total number of events in the background under the resonance.

$\eta' \to \pi^+\pi^-\gamma$ events, we show in the shaded area of Fig. 33 the $\pi^+\pi^-\pi^0$ effective-mass distribution ($MM^2 > 0.01$ GeV^2) after the ρ^0 selection. No evidence for an η' enhancement is observed in this mass spectrum.]

A quantitative estimate of the $\rho^0\gamma/\pi^+\pi^-\gamma$ branching ratio is provided from an analysis of the data shown in Fig. 34, where the $\pi^+\pi^-$ effective-mass projection of the η' region is exhibited. The dotted distribution is a suitably adjusted[11] $\pi^+\pi^-$ mass projection from control regions adjacent to the resonance region. A maximum-likelihood fit to the Dalitz plot for events in the η' region, using phase space plus a ρ Breit-Wigner function modified by a matrix element corresponding to the decay of a $J^{PC} = 0^{-+}$ particle into $\rho^0\gamma$, gives 64 ± 9 events.[12] As shown by the solid curve in Fig. 34, a good fit is obtained with the $\pi^+\pi^-$ mass peaking at 0.730 GeV, as do the data. The fit to Fig. 32 gave 63 ± 9 η' events in the mass region 0.93–0.98 GeV. Moreover, outside this region the $\pi^+\pi^-$ projection shows few ρ^0 events (5 events), and we attribute 59 ± 10 ρ^0's to the η' decay. The resulting $\rho^0\gamma/\pi^+\pi^-\gamma$ branching fraction of 0.94 ± 0.20 as given in Table VIII is in excellent agreement with the world data[7] (1.0); however, the ratio $\pi^+\pi^-\gamma/\eta_N\pi^+\pi^- = 0.54 \pm 0.10$, also given in this table, is significantly smaller than that quoted by Rittenberg[8] (1.05 ± 0.16), whose data make up a significant part of the world statistics.

As a final comment on the η' branching ratio, we now proceed to examine the broad structure in the 1.0-GeV region observed in the MM distribution of Fig. 3 from reaction 1, ΛMM. We expect that this enhancement, which is similar in appearance to the 1.0-GeV enhancement observed in Fig. 8, is composed of two resonances: the $\eta'(\to \eta_N\pi^0\pi^0)$ and the $\phi(\to K_2^0K_1^0(\to \pi^0\pi^0))$. If we assume the $I = 0$ assignment for the η' then the branching ratio $\eta' \to \eta_N\pi^0\pi^0/\eta_N\pi^+\pi^- = \frac{1}{2}$; using the averaged 3.9- and 4.6-GeV/c $\eta_N\pi^+\pi^-$ cross section given in Table VII, and employing the zero-prong-plus-vee microbarn equivalent given in Table I, we predict the existence of 38 ± 4 $\eta' \to \eta_N\pi^0\pi^0$ events in the missing-mass spectrum of reaction 1. In addition, we expect 27 ± 3 $\phi \to K_1^0K_2^0(\to \pi^0\pi^0)$ events based on the cross section for the mode $\phi \to K_2^0K_1^0$ ($\to \pi^+\pi^-$) observed in the multistrange topology (which will be discussed in Sec. III B 3). We estimate a signal of 90 ± 18 events in the 1.0-GeV region of Fig. 3 compared to the 65 ± 5 events expected from the combined η' and ϕ neutral decay modes. Therefore to ~1.5 standard deviations, the MM signal is consistent with η' and ϕ production.

b. Total and differential cross sections; polarization. In Table VII are given the total $K^-p \to \Lambda\eta'$ cross sections at 3.9 and 4.6 GeV/c, which were obtained by correcting the observed number of $\eta_N\pi^+\pi^-$ events by the $\pi^+\pi^-\gamma$ branching fraction quoted in Table VIII. The differential cross sections obtained by normalizing the number of $\eta' \to \eta_N\pi^+\pi^-$ events [$0.90 \leq M(\pi^+\pi^-\text{MM}) \leq 1.0$ GeV; $0.27 \leq MM^2 \leq 0.33$ GeV^2] plus the $\eta' \to \rho^0\gamma$ events [$0.93 \leq M(\pi^+\pi^-\text{“}\pi^0\text{”}) \leq 0.98$ GeV; $0.64 \leq M(\pi^+\pi^-) \leq 0.84$ GeV] to the total cross section quoted in Table VII are given in Table IX and Fig. 35(a) [35(b)]. We have fitted these distributions to the form $d\sigma/d|t'| \sim e^{At'}$ and extracted the slope parameter A at each momentum:

$$3.9 \text{ GeV}/c\text{: } A = 5.9 \pm 0.9 \text{ GeV}^{-2},$$

$$4.6 \text{ GeV}/c\text{: } A = 5.3 \pm 0.5 \text{ GeV}^{-2}$$

(for $|t'| \leq 1.0$ GeV^2), which shows the extreme peripherality of η' production. At 3.9 (4.6) GeV/c there are 7 ± 3 (1 ± 1) $\eta' \to \eta_N\pi^+\pi^-$ events produced in the backward direction ($\cos\theta^* < 0.0$) correspond-

TABLE IX. Differential cross sections for reaction $K^-p \to \Lambda\eta'$.

$\lvert t'\rvert$ interval (GeV^2)	3.9 GeV/c No. of events	3.9 GeV/c Corrected $d\sigma/dt'$ (μb/GeV^2)	4.6 GeV/c No. of events	4.6 GeV/c Corrected $d\sigma/dt'$ (μb/GeV^2)
0.0–0.1	28 ± 5	143 ± 27	38 ± 6	144 ± 24
0.1–0.2	22 ± 5	113 ± 24	37 ± 6	140 ± 23
0.2–0.3	10 ± 3	25. ± 8.2	16 ± 4	60 ± 15
0.3–0.4			13 ± 4	49 ± 14
0.4–1.0	8 ± 3	6.8 ± 2.4	10 ± 3	6.3 ± 2.0
1.0–2.0	7 ± 3	3.6 ± 1.3	8 ± 3	3.1 ± 1.1
2.0–3.0	4 ± 2	2.0 ± 1.0	3 ± 2	1.1 ± 0.7
3.0–4.0	4 ± 2	2.0 ± 1.0	0	0
4.0–5.0	5 ± 2	2.6 ± 1.1	4 ± 2	1.5 ± 0.8
5.0–6.0	...	...	4 ± 2	1.5 ± 0.8

ing to a total corrected cross section of 5.6 ± 2.1 μb (0.56 ± 0.56 μb).

The Λ polarization is given in Table X and is shown in Fig. 36 as a function of t'; it is consistent with being positive and similar to that observed in the $K^-p \to \Lambda\pi^0$ reaction.

c. Spin-parity analysis. We now present the spin-parity analysis on the $\eta_N\pi^+\pi^-$ decay mode of the η'. Our sample, which is essentially free of background contamination, consists of 109 events [see shaded histogram of Fig. 29(a)] with the following selections: $\cos\theta^* > 0.8$, $0.27 \leq \mathrm{MM}^2 \leq 0.33$ GeV^2, and $0.93 \leq M(\pi^+\pi^-\mathrm{MM}) \leq 0.98$ GeV. A Dalitz-plot analysis (production-independent) and a production-dependent analysis of the normal to the $\eta_N\pi^+\pi^-$ decay plane are presented.

We have performed maximum-likelihood fits on the η' Dalitz plot using the following form for the likelihood:

$$L = \prod_{i=1}^{109} \frac{|m_i|^2}{\int |m_i|^2 d\phi_i},$$

where $d\phi_i$ is the phase-space element for the ith event and m_i is the simplest matrix element corresponding to the decay of a J^{PC} particle. To conform with previous studies, we use the same matrix elements as given in Rittenberg,[8] and which are listed in Table XI. The likelihood function given above is normalized on an event-by-event basis which allows us to take into account the fact that, because of the finite experimental resolution, the η' signal is not a δ function. The $M(\pi^+\pi^-)$ and $\cos(\pi^+, \eta)$ projections[13] of the Dalitz plot are shown in Fig. 37. The results of the analysis are given in Table XI. We reach the same conclusions as have previous investigations with the 0^{-+} (simple matrix element or with $1 + \alpha y$ dependence) strongly favored over all other J^{PC} simple matrix elements; however, the coherent (or incoherent) mixture of the two simplest 2^{-+} amplitudes provides a good description of the experimental data. Oglievetsky *et al.*[9] have shown, based on Adler consistency conditions, that one expects the mixing parameter $|a/b| = 4$, which is in good agreement with our value of $3.09^{+0.47}_{-0.39}$ and previous determinations of 3.23 ± 0.31,[8] 4.1 ± 0.51,[14] and ~3.[15] As this discussion demonstrates, it is not in general possible to distinguish between 0^- and 2^- by means of a Dalitz-plot analysis alone. In addition, it is by no means absolutely clear that the other J^{PC} states are ruled out by this investigation; it may be possible that other more complicated matrix elements, possibly with interfering partial waves, could describe the data as well as the favored J^{PC} states.

We now turn to an investigation of the production-dependent η' decay angular distribution. We show in Table XII the results of a moment analysis on

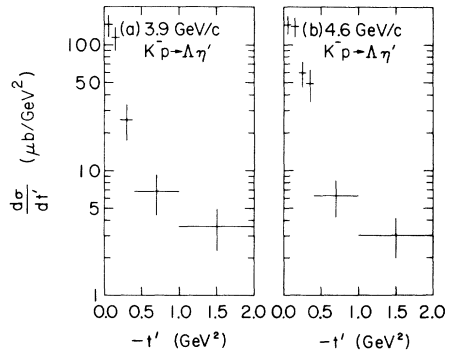

FIG. 35. Differential cross section for reaction $K^-p \to \Lambda\eta'$: (a) at 3.9 GeV/c, (b) at 4.6 GeV/c.

TABLE X. Λ polarization from reaction $K^-p \to \Lambda\eta'$.

$\lvert t'\rvert$ interval (GeV^2)	No. of events	P_Λ
0.0–0.1	66	0.24 ± 0.33
0.1–0.2	59	0.17 ± 0.32
0.2–1.0	57	0.23 ± 0.34

the decay correlations of the normal to the $\eta_N\pi^+\pi^-$ decay plane in the Jackson and helicity frames. The $NH(LM)$'s represent the values of the unnormalized moments in the η' region (defined as above) where

$$H(LM)=\langle D^L_{M0}(\phi,\theta,0)\rangle$$
$$=\left(\frac{4\pi}{2l+1}\right)^{1/2}\langle Y^L_M{}^*(\theta,\phi)\rangle\,.$$

Note that $NH(00)$ represents the mass spectrum. We observe no statistically significant (greater than 2σ) moments up to $L=4$, which implies that if the η' has $J^P=2^-$ its production mechanism conspires to produce no observable correlations. The absence of significant correlations has now been observed over the momentum range 2–5 GeV/c. This strongly favors the 0^- hypothesis (for which no alignments should be found) over 2^- for which, unlike all other resonances with spin produced off Λ's and observed in this experiment, no decay correlations exist. It should also be noted that, if $J^P=2^-$ and $\rho_{22}=0.0$, decay correlations must exist.

We have performed a similar moment analysis on the normal to the decay plane for the $\rho^0\gamma$ decay mode of the η'. The results are shown in Table XII, and again no significant deviations from zero for any of the moments are observed. In addition, we have looked for and found no statistically significant correlation between the $\rho^0\gamma$ decay of the η' (using the ρ^0 as analyzer in the η' rest frame) and the ρ^0 helicity decay angular distribution. The only observed statistically significant correlation for

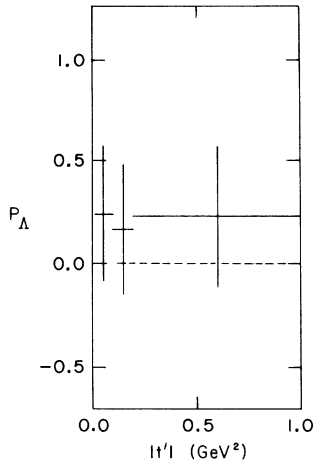

FIG. 36. Λ polarization for reaction $K^-p\to\Lambda\eta'$.

TABLE XI. Results of the Dalitz-plot analysis of the $\eta'\to\eta_N\pi^+\pi^-$ decay.

J^{PC}	l_η [a]	$l_{\pi\pi}$ [b]	Squared matrix element summed over spins [c]	$\ln L$ (109 events)
0^{-+}	0	0	1	470.46
0^{-+}	0	0	$1+\alpha y$ [d]	472.44
1^{++}	1	0	K^2	435.97
1^{-+}	2	2	$q^2K^4\cos^2\theta\sin^2\theta$	398.75
2^{++}	1	2	$q^4K^2\sin^2\theta$	422.59
2^{-+}	0	2	q^4	425.29
2^{-+}	2	0	K^4	378.57
2^{-+}	Mix of (0,2)+(2,0)		$K^4+\lvert a/b\rvert^2q^4$ $+3\lvert a/b\rvert\cos\Phi K^2q^2(\cos^2\theta-\frac{1}{3})$	471.67 [e]
0^{--}	1	1	$q^2K^2\cos^2\theta$	391.64
1^{+-}	0	1	q^2	461.18
1^{--}	1	1	$q^2K^2\sin^2\theta$	433.41
2^{+-}	2	1	$q^2K^4\sin^2\theta$	400.53
2^{--}	1	1	$q^2K^2(3+\cos^2\theta)$	459.40

[a] l_η: orbital angular momentum of η in η' rest frame.
[b] $l_{\pi\pi}$: relative orbital angular momentum of two pions in dipion rest frame.
[c] $q(K)$ is the momentum of the pion (η) in the dipion (η') rest frame; θ is the angle between the outgoing π^+ and η in the dipion rest frame.
[d] $y=[(M_\eta+2M_\pi)/M_\pi]\,T_\eta/Q-1$, where $M_\eta(M_\pi)$ is the mass of the η(pion); T_η is the η kinetic energy in the η' rest frame, and $Q=M_{\eta'}-M_\eta-2M_\pi$. The fit gave $\alpha=-0.34^{+0.17}_{-0.15}$.
[e] The results of the fit gave $|a/b|=3.09^{+0.47}_{-0.39}$ with $\cos\Phi=0.57\pm0.33$.

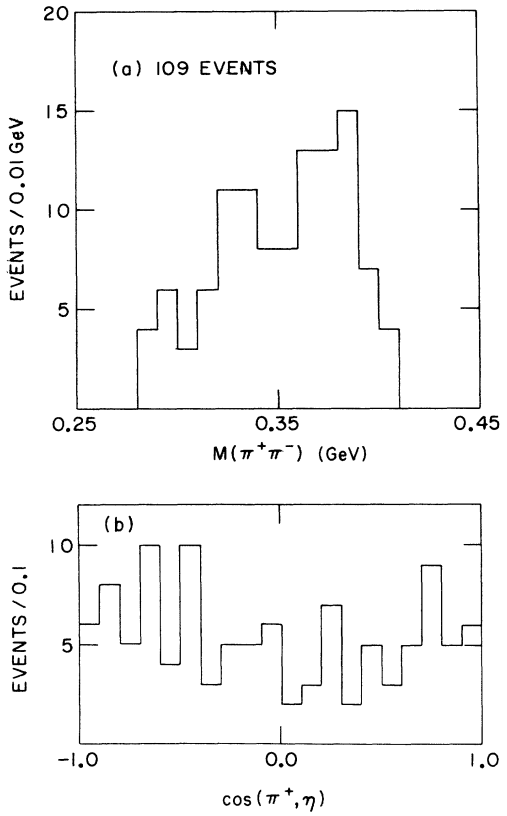

FIG. 37. (a) $M(\pi^+\pi^-)$ projection of the $\eta' \to \eta_N\pi^+\pi^-$ Dalitz plot. (b) $\cos(\pi^+, \eta)$ for events in the η' region.

this decay mode is in the $NH(20)$ moment of the ρ^0 helicity decay angular distribution. The unnormalized moment along with the corresponding $NH(00)$ moment (the mass spectrum) is shown as a function of $\rho^0\gamma$ effective mass in Fig. 38.

The ρ^0 helicity decay angular distribution, $W(\cos\theta)$, can be written

$$W(\cos\theta) \sim \frac{2\rho_{00}}{(1-3\rho_{00})} + \sin^2\theta \,,$$

where ρ_{00} is the ρ^0 density-matrix element in the helicity frame and is related to the normalized resonance $H_R(20)$ moment by[16]

$$\rho_{00} = \tfrac{1}{3}[1 + 5H_R(20)] \,.$$

From Fig. 38 we have determined $H_R(20)$ from an estimate of the number of η' events and the corresponding amount of $NH(20)$ associated with the resonance (a linear form in mass was used as the background representation). The value of ρ_{00} so obtained was

$$\rho_{00} = 0.05 \pm 0.10 \,,$$

which is $\frac{1}{2}$ standard deviation from the value $\rho_{00} = 0.0$ [i.e., $W(\cos\theta) \sim \sin^2\theta$] expected for a 0^- decay.

TABLE XII. Results on analysis of η' decay angular distribution (normal to decay plane).

	$\eta_N\pi^+\pi^-$ (109 events)		$\rho^0\gamma$ (64 events)	
Moment	Jackson frame	Helicity frame	Jackson frame	Helicity frame
$NH(20)$	0.5±4.6	−0.5±4.6	−2.4±3.7	1.2±3.7
$N\,\mathrm{Re}H(21)$	6.4±3.5	−1.6±3.4	−1.6±2.4	−0.9±2.4
$N\,\mathrm{Re}H(22)$	5.4±3.4	5.8±3.4	−1.0±2.6	−2.5±2.6
$NH(40)$	−1.4±3.4	−0.5±3.7	2.9±3.0	1.3±2.9
$N\,\mathrm{Re}H(41)$	1.5±2.5	−3.8±2.1	0.8±1.7	−0.6±1.8
$N\,\mathrm{Re}H(42)$	−0.2±2.5	−1.0±2.7	0.1±1.8	0.1±1.8
$N\,\mathrm{Re}H(43)$	1.4±2.6	−1.3±2.5	−1.6±1.9	1.2±2.0
$N\,\mathrm{Re}H(44)$	2.0±2.6	−0.3±2.6	0.4±2.1	1.0±1.9

Recently, Oglievetsky *et al.*[9] proposed a 2^- matrix element of the form $W(\cos\theta) \sim 1.48 + \sin^2\theta$ which leads to a predicted $\rho_{00} = 0.23$, a value which is 1.8 standard deviations from that obtained in our experiment.

4. *The M(953) Meson*

We now digress from our study of mesons produced recoiling from the Λ and discuss the evi-

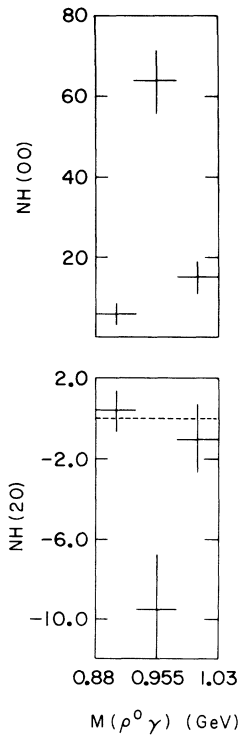

FIG. 38. (a) $NH(00)$ moment (mass spectrum) for "$\rho^0\gamma$" events. (b) $NH(20)$ moment for the same events.

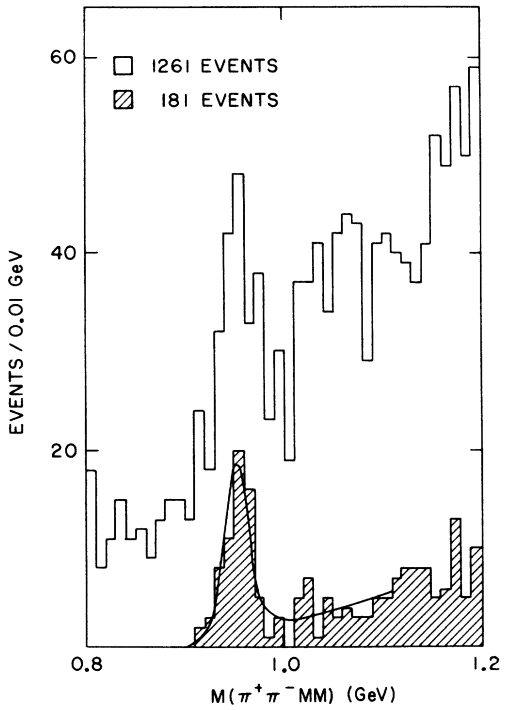

FIG. 39. $\pi^+\pi^-$MM distribution from the reaction $K^-p \to K^-p\pi^+\pi^-$MM after a $\cos\theta^* > 0.0$ selection. The shaded area is the same mass spectrum but after a η_N selection.

dence for the possible existence of a new meson in the 955-MeV mass region, which we call the $M(953)$ and which we have previously reported.[17] We present an investigation which parallels the analysis of the preceding section on the η' meson.

a. Mass, width, decay modes, and branching ratios. Figure 39 shows the $\pi^+\pi^-$ MM effective-mass spectrum from the reaction

$$K^-p \to K^-p\pi^+\pi^-\text{MM} \qquad \text{(a)}$$

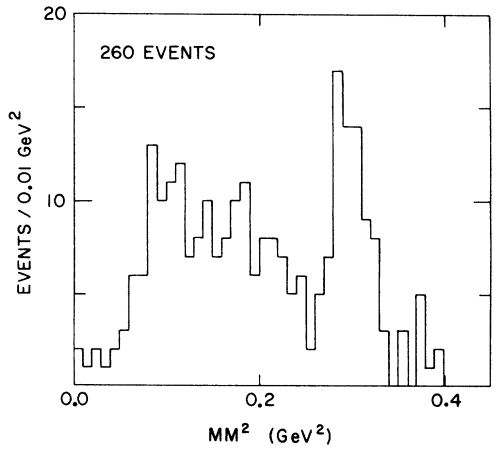

FIG. 40. MM^2 distribution for reaction $K^-p \to K^-p\pi^+\pi^-$MM for events in the region $0.9 \leq M(\pi^+\pi^-\text{MM}) \leq 1.0$ GeV.

for the combined data at 3.9 and 4.6 GeV/c after a $\cos\theta^* > 0.0$ selection (θ^* is the angle between the target proton and the outgoing K^-p system in the over-all center-of-mass system) in which a clear signal in the 955-MeV region is observed. The shaded area represents the same mass spectrum, but after a η_N selection (η_N: $0.27 \leq MM^2 \leq 0.33$ GeV^2), in which a large enhancement is observed over a small background. We show in Fig. 40 the MM^2 projection of the region $0.9 \leq M(\pi^+\pi^-\text{MM}) \leq 1.0$ GeV, in which a prominent η_N signal is seen which is not observed in the MM^2 spectrum of the adjacent background regions. The relative uncertainty in the estimate of the amount of η_N in Fig. 40 to be contrasted with the clear signal observed in Fig. 39 (shaded histogram) caused us to alter the method employed in the last section and to fit here the latter mass spectrum. The tails of the η_N are not included in our MM^2 selection so that the number of $\eta_N\pi^+\pi^-$ events will be underestimated by ~5–10% (based on similar treatment of the η' data and assuming the width of the η_N is similar in $\Lambda\pi^+\pi^-\eta_N$ and $K^-p\pi^+\pi^-\eta_N$). Fitting a Breit-Wigner function with resolution folded in plus a polynomial

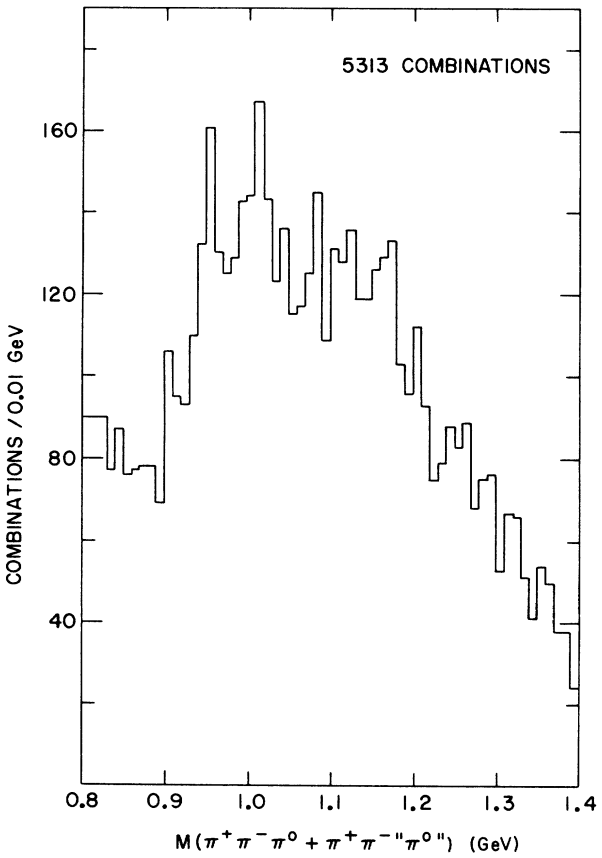

FIG. 41. Unfitted $\pi^+\pi^-\pi^0$ effective-mass spectrum from reaction $K^-p \to K^-p\pi^+\pi^-\pi^0$ for events with $\cos\theta^* > 0.0$.

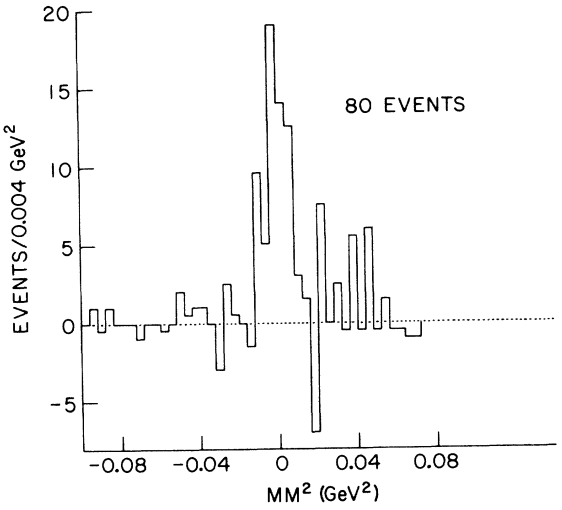

FIG. 42. Background-subtracted missing-mass-squared spectrum for events in the region $0.940 \leq M(\pi^+\pi^-\pi^0 + \pi^+\pi^-\text{“}\pi^0\text{”}) \leq 0.970$ GeV.

background, we obtain 58 ± 7 resonance events, a mass $M = 951 \pm 4$ MeV, and a width $\Gamma < 15$ MeV (95% confidence level).

We now discuss the evidence for the $\pi^+\pi^-\gamma$ enhancement in the 955-MeV mass region. For this purpose, all events that fitted the $K^-p\pi^+\pi^-\pi^0$ final state, with probability greater than 0.1% and which were consistent with ionization, were retained. In Fig. 41 we show the $\pi^+\pi^-\pi^0$ unfitted mass spectrum for the combined 3.9- and 4.6-GeV/c data after a $\cos\theta^* > 0.0$ selection. We observe two clear narrow enhancements: one above 1.0 GeV which we attribute to the $\phi(1019)$,[18] and the other in the 955-MeV mass region. To show that the observed 955-MeV signal is consistent with $\pi^+\pi^-\gamma$ events we give in Fig. 42 the background-subtracted MM^2 distribution for events in the signal region minus events in the adjacent background regions; a clear γ signal peaking at $MM^2 \simeq 0.0$ GeV^2 is observed. The separation of $\pi^+\pi^-\gamma$ from the $\pi^+\pi^-\pi^0$ events is apparent from the comparison of the $\pi^+\pi^-\text{“}\pi^0\text{”}$ ($MM^2 < 0.01$ GeV^2) and $\pi^+\pi^-\pi^0$ ($MM^2 > 0.01$ GeV^2) effective-mass spectra as shown in Figs. 43 and 44, respectively. A significant enhancement is observed in the γ-favored spectrum at ~955 MeV and not in the π^0-favored spectrum, indicating that the peak seen in Fig. 41 is not due to $\pi^+\pi^-\pi^0$ events. An investigation of other possible hypotheses has shown that the peak cannot be due to contamination from any other channels. In addition, there is no evidence for any loss of γ events [with a peak at $M(\pi^+\pi^-\gamma) \sim 1$ GeV] into the reactions $K^-p \to K^-p\pi^+\pi^-$ and $K^-p\pi^+\pi^-$MM.

To sharpen the mass resolution of the $\pi^+\pi^-\gamma$ system, we have refitted all events in Fig. 43 having a $\pi^+\pi^-\text{“}\pi^0\text{”}$ effective mass between 0.8 and 1.1 GeV adding to our normal kinematic hypotheses the 1c-γ hypotheses:

$$K^-p \to K^-p\pi^+\pi^-\gamma\,. \qquad \text{(b)}$$

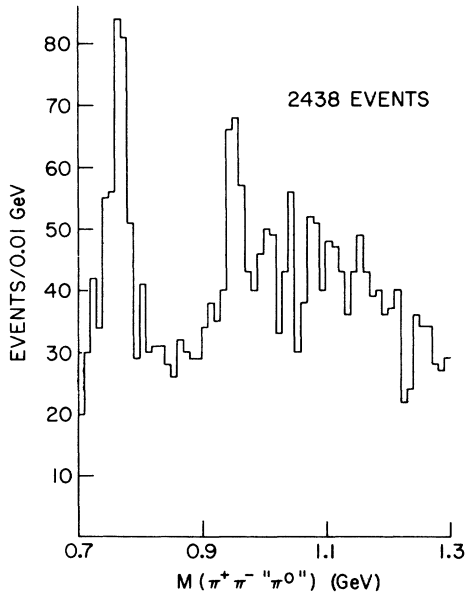

FIG. 43. Unfitted $\pi^+\pi^-\text{“}\pi^0\text{”}$ effective-mass spectrum for events with $MM^2 < 0.01$ GeV^2.

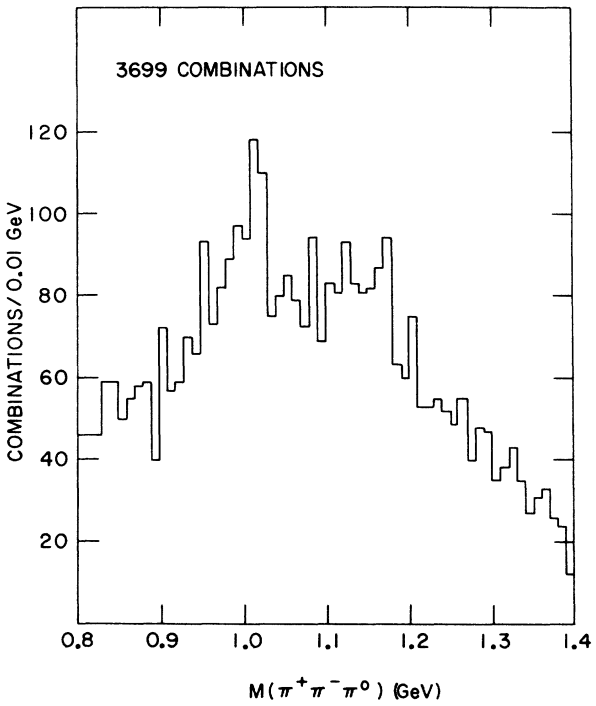

FIG. 44. Unfitted $\pi^+\pi^-\pi^0$ effective-mass spectrum for events with $MM^2 > 0.01$ GeV^2.

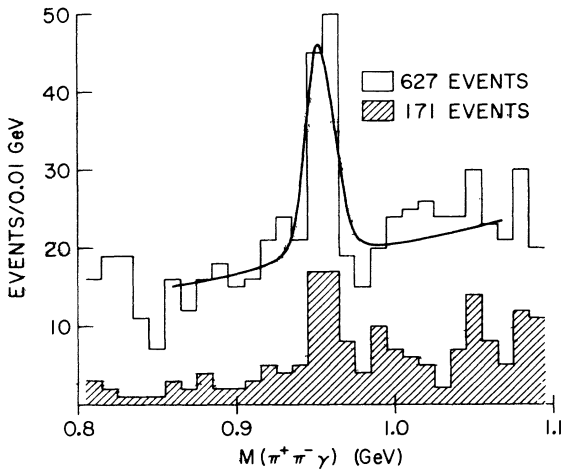

FIG. 45. $\pi^+\pi^-\gamma$ effective-mass spectrum for events that fitted the reaction $K^-p \to K^-p\pi^+\pi^-\gamma$. The shaded area is the same mass spectrum but for events with $\pi^+\pi^-$ effective mass in the ρ^0 region.

We then repeated the fit-selection procedure using ionization estimates and kinematic-fit χ^2 probabilities. In Fig. 45 we plot the fitted $\pi^+\pi^-\gamma$ mass spectrum for only those events with reaction (b) as the best[19] hypothesis and kinematic χ^2 probability greater than 5%. The peak at 955 MeV persists (the number of resonance events is within errors the same in Figs. 45 and 43) and becomes narrower, strengthening our belief that it decays into $\pi^+\pi^-\gamma$. The curve shown is the result of a maximum-likelihood fit using a Breit-Wigner shape with resolution folded in plus a second-order polynomial background shape and yields a mass 953 ± 2 MeV and an intrinsic width of <10 MeV. The statistical significance of the peak is more than 5 standard deviations, corresponding to an excess of 68 ± 12 events.

We now discuss the difference between the structure of the $\pi^+\pi^-\gamma$ signal in the reaction $K^-p \to K^-p\pi^+\pi^-\gamma$ and that observed in the reaction $K^-p \to \Lambda\eta'$ ($\to \pi^+\pi^-\gamma$) which was presented in the last section. The shaded histogram of Fig. 45 shows the $\rho^0_{\text{in}}\gamma$ effective mass spectrum from reaction (b) where the ρ^0_{in} selection is defined, as in the η' analysis, by

$$0.64 \leq M(\pi^+\pi^-) \leq 0.82 \text{ GeV}.$$

We observe that the number of events in the 955-MeV enhancement is much reduced. In fact, the number of events observed above background is consistent with the number expected from phase space. To make this effect even more transparent we show in Fig. 46(a) the $\pi^+\pi^-\gamma$ effective mass spectrum for events of reaction (b), with $\pi^+\pi^-$ effective mass *not* in the ρ slice; 37 ± 10 resonance

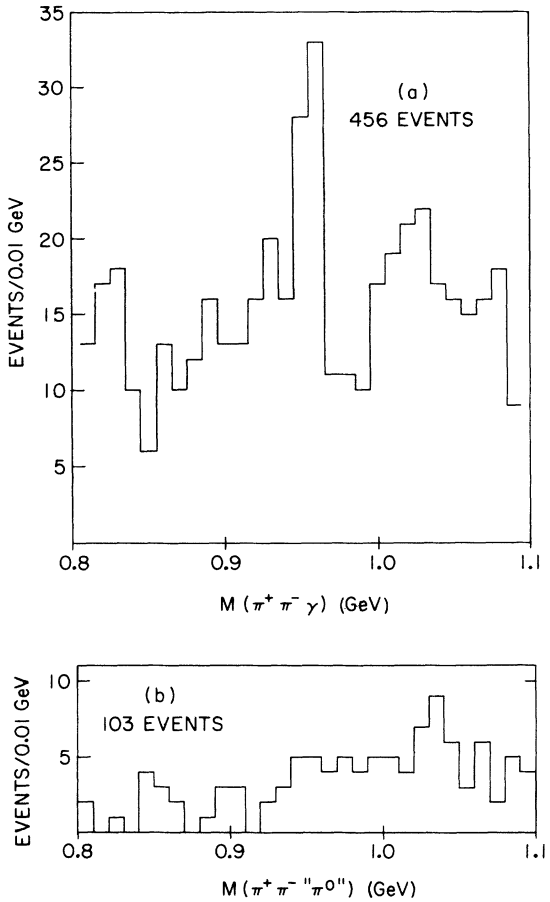

FIG. 46. Comparison of $\pi^+\pi^-\gamma$ effective-mass spectrum for events whose $\pi^+\pi^-$ effective mass is not in the ρ^0 region: (a) reaction $K^-p \to K^-p\pi^+\pi^-\gamma$, (b) reaction $K^-p \to \Lambda\pi^+\pi^-$"$\pi^0$".

events were obtained from a fit to this mass spectrum. The corresponding $\rho_{\text{out}}\gamma$ effective-mass spectrum for the reaction $K^-p \to \Lambda\pi^+\pi^-$"$\pi^0$" ($\cos\theta^* > 0.8$) is shown in Fig. 46(b); no statistically significant resonance signal is observed with only 6 ± 5 events associated with η' production. It is this intrinsic difference between the $\rho^0\gamma$ decay mode of the η' and the $\pi^+\pi^-\gamma$ decay mode of the enhancement in reaction (b) which lends belief that the later enhancement, which we called the M,[17] is an object different from the η'. In order to obtain a more quantitative estimate of the essential difference between the η' and M we have fitted the $\pi^+\pi^-$ mass projection of the M region shown in Fig. 47, in which no apparent ρ^0 peak at 0.730 GeV is observed, with a maximum-likelihood technique using phase space plus a ρ Breit-Wigner function modified by a matrix element corresponding to a decay of a 0^{-+} particle into $\rho^0\gamma$ (as was done for the η'). The results of the fit give 3 ± 6 ρ^0 events so that the M branching ratio is found to be

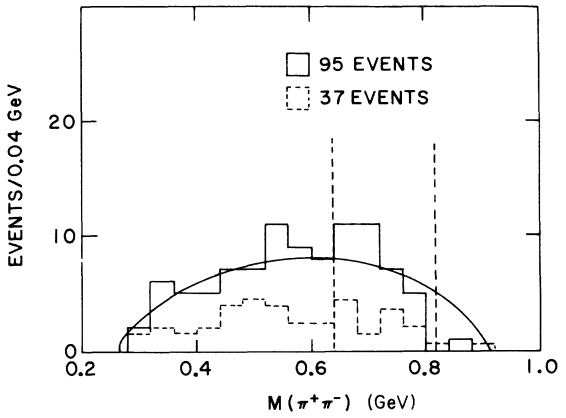

FIG. 47. $\pi^+\pi^-$ effective-mass spectrum for events in the M region. The dotted curve represents the $\pi^+\pi^-$ mass spectrum for the adjacent background region.

$$\frac{M \to \rho^0\gamma}{M \to \pi^+\pi^-\gamma} = \frac{3 \pm 6}{58 \pm 7}$$
$$= 0.05 \pm 0.10,$$

which is 3.5σ from the value obtained for the η'. (The world average value of the η' is constrained to be 1.0.[7]) We stress that we have assumed that the background under the M is phase-space distributed, as seems to be indicated from the suitably adjusted $\pi^+\pi^-$ mass projection of the regions adjacent to the M (dashed histogram in Fig. 47). It is apparent that distortions of the background under the $\pi^+\pi^-\gamma$ enhancement can alter the number of ρ^0's obtained through our simple matrix-element fit;

TABLE XIII. Results of the Dalitz-plot analysis[a] of the $M \to \eta_N\pi^+\pi^-$ decay.

J^{PC}	$\ln L$ (60 events)
0^{-+}	260.84
0^{-+}	262.80[b]
1^{++}	242.78
1^{-+}	200.15
2^{++}	243.15
2^{-+}	242.80
2^{-+}	212.11
2^{-+} (mix)	261.31[c]
0^{--}	190.99
1^{+-}	259.14
1^{--}	245.69
2^{+-}	228.51
2^{--}	258.64

[a]For definition of matrix elements used in the fits see Table XI. (The J^{PC} order here is the same as in Table XI.)

[b]The fitted value for α was $-0.46^{+0.22}_{-0.19}$.

[c]The results of the fit gave $|a/b| = 3.68^{+0.86}_{-0.65}$ and $\cos\Phi = 0.26^{+0.42}_{-0.40}$.

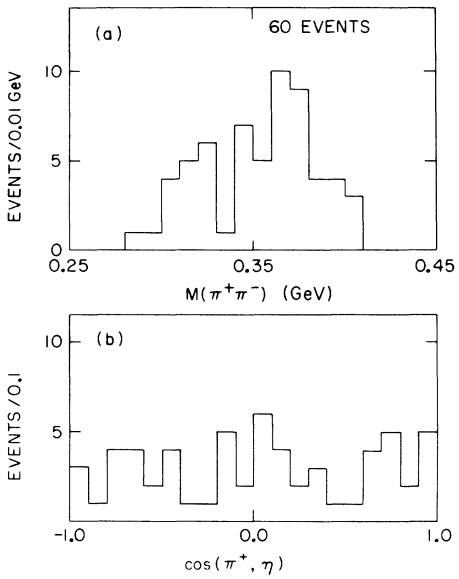

FIG. 48. (a) $M(\pi^+\pi^-)$ projection of the $\eta_N\pi^+\pi^-(M$ region) Dalitz plot from the reaction $K^-p \to K^-p\eta_N\pi^+\pi^-$. (b) $\cos(\pi^+, \eta)$ for events in the M region.

however, one would assume that the sideband technique would provide a reasonable estimate of the background for this observed narrow enhancement. Finally, the $\rho_{\text{out}}\gamma$ spectrum clearly demonstrates that less than 50% of the observed $\pi^+\pi^-\gamma$ enhancement can be attributed to a $\rho^0\gamma$ decay, no matter how severely the background deviates from that of the sidebands.

b. Spin-parity analysis. We now present a Dalitz-plot analysis of the $\eta_N\pi^+\pi^-$ 955-MeV enhancement and then comment upon its association with the observed signal in the $\pi^+\pi^-\gamma$ mode and with the η'. For this investigation our sample consists of 60 events with selections $0.27 \leq \text{MM}^2 \leq 0.33$ GeV^2, $0.93 \leq M(\pi^+\pi^-\text{MM}) \leq 0.98$ GeV, and $\cos\theta^* > 0.0$. The method of analysis follows that outlined in the η' section. The results of the J^{PC} likelihood analysis are given in Table XIII; the $\pi^+\pi^-$ and $\cos(\pi^+, \eta)$ projections are shown in Fig. 48. We observe that the results of this study are very similar to those of the η' section: 0^{-+} and 2^{-+} (mix) are favored. However, the J^{PC} assignment, 1^{+-}, is here only 1.7 times the log of the likelihood units less than 0^{-+} and, considering the small statistics and our inability to properly take the background, although small, into account, cannot be ruled out. We therefore conclude that the results of the $\eta_N\pi^+\pi^-$ Dalitz-plot analysis in the reaction $K^-p \to K^-p\pi^+\pi^-\eta_N$ are very similar to that of the η'; however, we cannot here rule out the 1^{+-} (or in fact the 2^{--}) hypothesis. As was noted in the η' section, other J^{PC} states are, in principle, not ruled out by this

analysis; it may be possible that more complicated matrix elements (with interfering waves) could provide as good description of the data as do the favored J^{PC} states.

Another experimental quantity that could shed light on the η'-M question is the helicity angular distribution of the outgoing π^+ in the $\pi^+\pi^-$ rest frame for the $\pi^+\pi^-\gamma$ system. We reiterate that for a 0^{-+} object which decays into $\rho^0\gamma$ we expect to observe a $\sin^2\theta$ angular distribution which leads to a value of $-0.2N_R$ (N_R is the number of resonance events) for the $NH(20)$ moment in the region of the enhancement. In Figs. 49(a) and 49(b) we show the $\pi^+\pi^-\gamma$ effective-mass spectrum [$NH(00)$] and the corresponding $NH(20)$ moment without any selection on the $\pi^+\pi^-$ effective mass; in the region of the 5σ enhancement in the effective-mass spectrum we observe no statistically significant deviation of the $NH(20)$ moment. In Figs. 49(c)–49(f) the "ρ_{in}"γ and "ρ_{out}"γ moments are presented; in the $NH(20)$ moment of the "ρ_{in}"γ sample we observe about a 3σ deviation in the enhancement region, whereas in the "ρ_{out}"γ region no deviation from isotropy is observed. So whereas no ρ^0 signal is observed in the $\pi^+\pi^-$ effective-mass spectrum, the deviation of $NH(20)$ for the $\rho^0_{in}\gamma$ events suggests that some ρ^0 events may be buried in the $\pi^+\pi^-$ effective-mass distribution of Fig. 47, which in turn implies the presence of some $\eta'(\to\rho^0\gamma)$ production in reaction (b).

c. Conclusions. All the relevant experimental observations that bear on the η'-M question are summarized in Table XIV. It is clear that the $\pi^+\pi^-\gamma$ decay mode of the M seems to be intrinsically different (by $\sim 3\sigma$) from that of the η'; however, the question remains if or to what extent the η' is

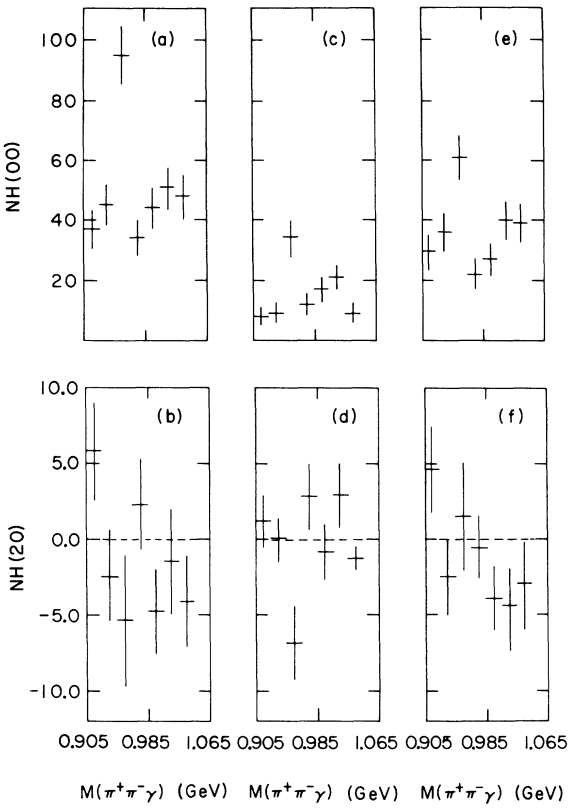

FIG. 49. (a) $NH(00)$ moment (effective-mass spectrum) for events with no selection on $\pi^+\pi^-$ effective mass. (b) $NH(20)$ moment for events with no selection on $\pi^+\pi^-$ effective mass. (c) Same as (a), but for events with $M(\pi^+\pi^-)$ in the ρ^0 region. (d) Same as (b), but for events with $M(\pi^+\pi^-)$ in the ρ^0 region. (e) Same as (a), but for events with $M(\pi^+\pi^-)$ not in the ρ^0 region. (f) Same as (b), but for events with $M(\pi^+\pi^-)$ not in the ρ^0 region.

TABLE XIV. Summary of the experimental information for the η'-M comparison.

	K^-p sample	Λ sample
$\frac{\pi^+\pi^-\gamma}{\eta_N\pi^+\pi^-}$	1.20 ± 0.30	0.54 ± 0.10[a] 1.05 ± 0.16[b]
$\frac{\rho_{out}\gamma}{\rho_{in}\gamma}$	1.12 ± 0.38	0.10 ± 0.08
$\frac{\rho^0\gamma}{\pi^+\pi^-\gamma}$ from Dalitz plot fit	0.05 ± 0.10	0.94 ± 0.20
$\eta_N\pi^+\pi^-$ Dalitz plot	0^{-+} and 2^{-+} (mix) favored but 1^{+-} not ruled out	All J^{PC} except 0^{-+} and 2^{-+} (mix) ruled out
$\pi\pi$ helicity decay angular distribution	ρ_{out} is flat. ρ_{in} has $\sim 3\sigma$ for $\sin^2\theta$	Consistent with $\sin^2\theta$ in ρ region

[a]This experiment.
[b]Reference 8, p. 95.

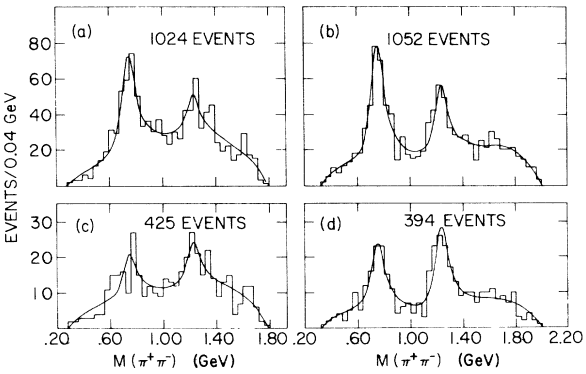

FIG. 50. $\pi^+\pi^-$ effective-mass distribution from the reaction $K^-p \to \Lambda\pi^+\pi^-$: (a) at 3.9 GeV/$c$; (b) at 4.6 GeV/$c$; (c) at 3.9 GeV/$c$ for events with $\cos\theta^* < 0.0$; (d) at 4.6 GeV/c for events with $\cos\theta^* < 0.0$. The curves are the results of the fits described in the text.

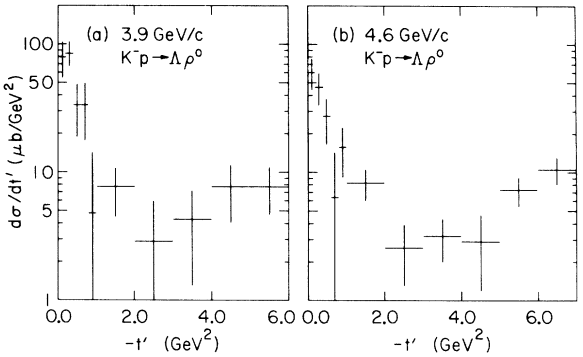

FIG. 51. Differential cross section for reaction $K^-p \to \Lambda\rho^0$: (a) at 3.9 GeV/c, (b) at 4.6 GeV/c.

produced in the $K^-p\pi^+\pi^-\gamma$ and $K^-p\pi^+\pi^-\eta_N$ final states. The similarity of the $\eta_N\pi^+\pi^-$ Dalitz plots in the Λ and K^-p reactions as well as the evidence for a $\sin^2\theta$ helicity decay angular distribution of the $\rho_{in}\gamma$ events in reaction (b) would suggest that the η' is produced in these channels. Whether or not all the $\eta_N\pi^+\pi^-$ signals could be associated with the η' would critically depend on the $\eta' \to \rho^0\gamma/\eta_N\pi^+\pi^-$ branching fraction. If this branching ratio is between the world average and the number that we have obtained, then we cannot rule out both η' and M coexisting in the $K^-p \to K^-p$ ($\eta_N\pi^+\pi^-$ and $\pi^+\pi^-\gamma$) final states. As we have previously stressed,[17] more experimental investigations are needed, both in πp and Kp interactions, to look into the possible existence of mesons in the 955-MeV region. As a point of fact, a search of the literature has revealed that the η' via its $\rho\gamma$ decay mode has only been reported in the reaction $K^-p \to \Lambda\eta'$.

B. Vector Mesons

1. *Reaction* $K^-p \to \Lambda\rho^0$

The ρ^0 meson represents the first of the members of the 1^- nonet which we investigate in the present analysis. The ρ^0 produced in the reaction

$$K^-p \to \Lambda\rho^0$$

shows very different properties than observed in the very extensive studies of its production in π^-p interactions. In particular in the K^-p reaction, we observe significantly smaller (larger) values of the ρ_{00} ($\rho_{1\,-1}$) density-matrix element (evaluated in the Jackson frame) consistent with a larger natural-parity exchange. In addition, no strong forward-backward asymmetry is observed in the ρ^0 decay angular distribution as is the case in all the studies of ρ^0 production in πN interactions.

a. Total and differential cross sections. The data for this channel come from reaction 2, $\Lambda\pi^+\pi^-$. The $\pi^+\pi^-$ effective-mass distribution for the 3.9 [4.6] GeV/c sample is shown in Fig. 50(a) [50(b)] in which clear signals from the ρ^0 and f^0 mesons are observed.[20] We have fitted these mass spectra with a polynomial in the mass as background plus an energy-dependent width Breit-Wigner shape multiplying simple phase space. The weighted averaged ρ^0 mass and width so obtained are

$$M = 757 \pm 5 \text{ MeV},$$

$$\Gamma = 120 \pm 20 \text{ MeV}.$$

The number of events and the total cross section for $K^-p \to \Lambda\rho^0$ are

3.9 GeV/c: 249 ± 32 events; $\sigma = 78 \pm 10$ μb,

4.6 GeV/c: 305 ± 26 events; $\sigma = 66 \pm 6$ μb.

The differential cross sections for the two momenta are shown in Figs. 51(a) and 51(b) and listed in Table XV, and were obtained by normalizing the background-subtracted events in the ρ^0 region defined as $0.64 \leq M(\pi^+\pi^-) \leq 0.88$ GeV to the cross sections listed above. We have fitted the forward region ($|t'| < 1.0$ GeV^2) of the differential cross section to the form $d\sigma/d|t'| \sim e^{At'}$ and obtained the slope parameter A:

3.9 GeV/c: $A = 2.4 \pm 0.6$ GeV^{-2},

4.6 GeV/c: $A = 2.2 \pm 0.6$ GeV^{-2}.

As shown in Figs. 50(c) and 50(d), there exists at both energies significant production of backward ($\cos\theta^* < 0.0$) ρ^0's. The number of backward events (cross sections) at 3.9 and 4.6 GeV/c is estimated to be 49 ± 15 (15.3 ± 4.7 μb) and 98 ± 16 (21.0 ± 3.4 μb), respectively.

b. Decay distributions and polarization. We first present the method we have employed to extract the density-matrix elements as a function of mo-

TABLE XV. Differential cross sections for reaction $K^-p \to \Lambda\rho^0$.

$\lvert t'\rvert$ interval (GeV^2)	3.9 GeV/c No. of ρ [a] events	3.9 GeV/c Corrected $d\sigma/d\lvert t'\rvert$ [b] (μb/GeV^2)	4.6 GeV/c No. of ρ [a] events	4.6 GeV/c Corrected $d\sigma/d\lvert t'\rvert$ [b] (μb/GeV^2)
0.0–0.2	33 ± 10	79.7 ± 25	38 ± 10	60.5 ± 16.4
0.2–0.4	35 ± 9	84.5 ± 21	29 ± 8	46.2 ± 12.9
0.4–0.6	14 ± 6	33.8 ± 15	17 ± 7	27.1 ± 10.5
0.6–0.8	14 ± 6	33.8 ± 16	4 ± 5	6.4 ± 8.1
0.8–1.0	2 ± 4	4.8 ± 10	10 ± 4	15.9 ± 6.7
1.0–2.0	16 ± 7	7.7 ± 3.2	26 ± 7	8.3 ± 2.2
2.0–3.0	6 ± 6	2.9 ± 3.0	8 ± 4	2.6 ± 1.3
3.0–4.0	9 ± 6	4.3 ± 3.0	10 ± 4	3.2 ± 1.2
4.0–5.0	16 ± 8	7.7 ± 3.7	9 ± 5	2.9 ± 1.7
5.0–6.0	16 ± 6	7.7 ± 3.0	23 ± 6	7.3 ± 1.9
6.0–7.0	...	...	33 ± 8	10.5 ± 2.5

[a] Number of background-subtracted events in the region $0.64 \le M(\pi^+\pi^-) \le 0.88$ GeV.
[b] Normalized to the total cross sections listed in text.

mentum transfer. The investigation of the behavior of the unnormalized moments through the ρ^0 region shows that an S-wave background and a P-wave resonance are sufficient to describe these distributions [after removal of the $Y^{*+}(1385)$ events and repopulating the Y^* region with conjugate events].[21] However, the form of the $NH(10)$ unnormalized moment (evaluated in the Jackson frame) shown in Fig. 52 for the forward momentum transfer region ($\lvert t'\rvert < 1.0$ GeV^2) is strikingly different from that observed in πp collisions[22]: No strong forward-backward asymmetry across the ρ^0 region is observed. In the πp case this asymmetry has been attributed to the interference between a possible 0^+ ϵ^0 and the 1^- ρ^0 meson, both produced by pseudoscalar exchange. The simplest explanation of the lack of asymmetry in our data is that pseudoscalar exchange is not the dominant mechanism in the ρ^0 region in[23] reaction 2 (all other J^P exchanges do not couple to 0^+ ϵ^0 production). As shown below, the values of the ρ^0 density-matrix elements are also strikingly different from those expected from pseudoscalar exchange and observed in $\pi^- p \to \rho^0 n$.[24]

The relatively large background in the ρ^0 region precluded our using the simple method of slicing the $\pi^+\pi^-$ mass spectrum and fitting the "ρ^0" events so obtained to a simple P-wave angular distribution, and then extracting the relevant density-matrix elements.[25] Instead, we followed the method we have previously proposed[26] and parametrized the mass-dependent angular distribution using an S-wave background, a P-wave resonance, and the interference between the two waves:

$$\frac{d\sigma(\cos\theta,\phi)}{dw\,d\Omega} = \left.\frac{d\sigma}{dw\,d\Omega}\right|_{S\text{ wave}} + \left.\frac{d\sigma}{dw\,d\Omega}\right|_{P\text{ wave}} + \left.\frac{d\sigma}{dw\,d\Omega}\right|_{SP},$$

where

$$\left.\frac{d\sigma}{dw\,d\Omega}\right|_{S\text{ wave}} = \frac{1}{4\pi}\epsilon_S^2 \lvert f_S(w)\rvert^2,$$

$$\left.\frac{d\sigma}{dw\,d\Omega}\right|_{P\text{ wave}} = \frac{1}{4\pi}\left[1 + \sum_{M=0}^{2} H_P(2M) B_M^2(\Omega)\right] \epsilon_P^2 \lvert f_P(w)\rvert^2,$$

$$\left.\frac{d\sigma}{dw\,d\Omega}\right|_{SP} = \frac{1}{2\pi}\epsilon_P\epsilon_S \mathrm{Re}\left[\sum_{M=0}^{1} f_P(w) f_S^*(w) H_{SP}(1M)\right] B_M^1(\Omega),$$

and

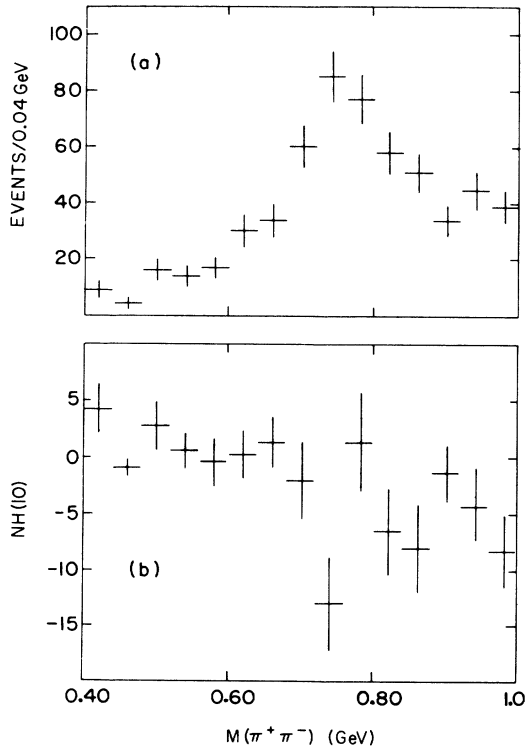

FIG. 52. (a) $NH(00)$ moment (mass spectrum) for events in the ρ^0 region after a $\lvert t'\rvert < 1.0$ GeV^2 selection. (b) $NH(10)$ moment for the same events as in (a).

$$B_M^L(\Omega) = (2-\delta_{M0})(2L+1)d_{M0}^L(\theta)\cos M\phi\,,$$

where ϵ_S^2 (ϵ_P^2) is the fraction of S wave (resonant P wave) in the ρ^0 region [defined as $0.56 \leq w(\pi^+\pi^-) \leq 0.96$ GeV]. $|f_S(w)|^2$ is the mass dependence of the S-wave background (assumed to be linear over the chosen mass interval) and $f_P(w)$ is the ρ^0 Breit-Wigner amplitude. The normalizations

$$\int |f_S(w)|^2 dw = 1 \quad \text{and} \quad \int |f_P(w)|^2 dw = 1$$

(where the integral extends over the mass region defined above) have been used so that $\epsilon_S^2 + \epsilon_P^2 = 1$. The $H(LM)$ are related to the familiar density-matrix elements as shown below. The values of the $d_{MM'}^L(\theta)$ can be found in Berman and Jacob.[27] Since we are not interested in the values of the interference density-matrix elements [or correspondingly the $H_{PS}(LM)$] we add to $d\sigma(\cos\theta, \phi)/dw d\Omega$ the distribution $d\sigma(-\cos\theta, \pi-\phi)/dw d\Omega$ to cancel out the interference term, and we are left with a symmetrized distribution function,

$$\left.\frac{d\sigma}{dw\,d\Omega}\right|_{\text{sym}} = \left.\frac{d\sigma}{dw\,d\Omega}\right|_{S\text{ wave}} + \left.\frac{d\sigma}{dw\,d\Omega}\right|_{P\text{ wave}},$$

which explicitly takes into account the form of the background through the ρ^0 region. Excellent fits as a function of momentum transfer were obtained with this parametrization. The values of the ρ^0 density-matrix elements are related to the $H_P(LM)$ moments by

$$\rho_{00} = \tfrac{1}{3}[1 + 5H_P(20)],$$

$$\rho_{11} = \tfrac{1}{3}[1 - \tfrac{5}{2}H_P(20)],$$

$$\rho_{1-1} = -\frac{5}{\sqrt{6}}H_P(22),$$

$$\mathrm{Re}\rho_{10} = \frac{5}{2\sqrt{3}}H_P(21),$$

and are shown in both the helicity and Jackson frames in Figs. 53(a)–53(f) for the combined 3.9- and 4.6-GeV/c sample and are listed in Table XVI. We observe in the forward region ($|t'| < 1.0$ GeV^2)

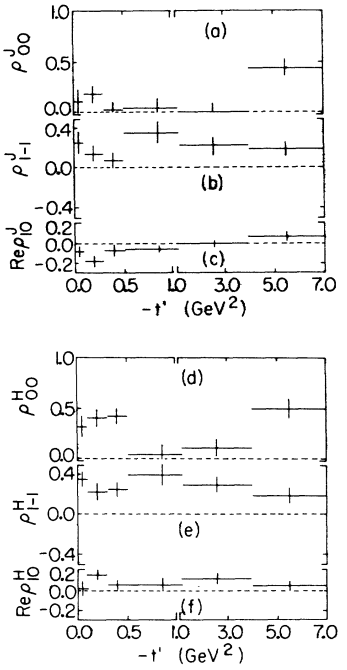

FIG. 53. Density-matrix elements of the ρ^0 produced in the reaction $K^-p \to \Lambda\rho^0$: (a)–(c) Jackson frame, (d)–(f) helicity frame.

the small (large) values of the ρ_{00} (ρ_{1-1}) density matrix in both frames compared to the large (small) values observed in $\pi^-p \to \rho^0 n$ interactions.[24] These observations suggest the presence of a larger natural-parity[28] t-channel exchange mechanism in the production of ρ^0 in the reaction $K^-p \to \Lambda\rho^0$.

Again, due to the large background under the ρ^0, the extraction of the Λ polarization cannot be accomplished following traditional approaches. Instead, we have parametrized the mass dependence of the $N\langle\cos\theta\rangle$ moment ($\cos\theta$ is the angle between the normal to the production plane and the outgoing proton in the Λ rest frame) using the form

$$\frac{d}{dw}[N\langle\cos\theta\rangle] = C[(1-\beta)f(w) + \beta|f_P(w)|^2]$$

TABLE XVI. ρ^0 density-matrix elements in reaction $K^-p \to \Lambda\rho^0$.

$\lvert t'\rvert$ interval (GeV^2)	No. of events[a]	No. of resonance events[a]	Jackson frame ρ_{00}	Jackson frame $\mathrm{Re}\rho_{10}$	Jackson frame ρ_{1-1}	Helicity frame ρ_{00}	Helicity frame $\mathrm{Re}\rho_{10}$	Helicity frame ρ_{1-1}
0.0–0.1	89	55 ± 9	0.11 ± 0.12	−0.08 ± 0.05	0.25 ± 0.11	0.31 ± 0.10	0.01 ± 0.07	0.34 ± 0.07
0.1–0.3	119	84 ± 11	0.18 ± 0.08	−0.18 ± 0.05	0.14 ± 0.08	0.40 ± 0.08	0.15 ± 0.05	0.22 ± 0.08
0.3–0.5	86	57 ± 10	0.02 ± 0.08	−0.07 ± 0.05	0.07 ± 0.08	0.41 ± 0.08	0.05 ± 0.05	0.24 ± 0.08
0.5–1.2	137	60 ± 13	0.04 ± 0.10	−0.06 ± 0.02	0.35 ± 0.11	0.03 ± 0.10	0.05 ± 0.06	0.39 ± 0.10
1.2–4.0	156	94 ± 16	0.00 ± 0.08	0.00 ± 0.03	0.21 ± 0.09	0.10 ± 0.08	0.11 ± 0.05	0.29 ± 0.08
4.0–7.0	212	119 ± 21	0.44 ± 0.08	0.07 ± 0.04	0.18 ± 0.07	0.49 ± 0.09	0.04 ± 0.04	0.19 ± 0.07

[a] Events in the region $0.56 \leq M(\pi^+\pi^-) \leq 0.96$ GeV.

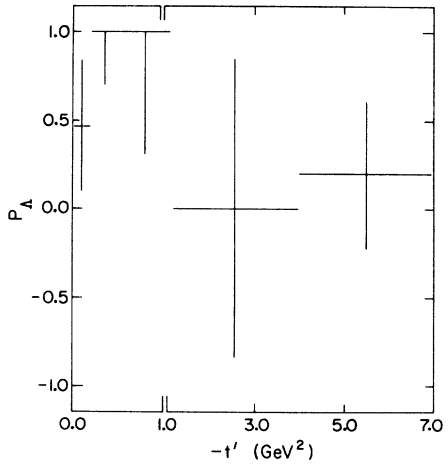

FIG. 54. Λ polarization for reaction $K^-p \to \Lambda\rho^0$.

and

$$C = \sum_{i=1}^{N} \cos\theta_i ,$$

where β is the fraction of the $N\langle\cos\theta\rangle$ moment associated with the ρ^0 resonance and $f(w)$ is the normalized mass dependence of the moment associated with the background (assumed linear across the ρ region), and N is the total number of events in the $\pi\pi$ mass region. From the results of χ^2 fits to the $N\langle\cos\theta\rangle$ moments (not shown), as a function of momentum transfer, we obtained the magnitudes of this moment (βC) associated with the ρ^0. Using the number of ρ^0's, N_ρ, obtained from fits to the mass spectrum in this region, we then obtained the Λ polarization from

$$P_\Lambda = 3\beta C/\alpha_\Lambda N_\rho ,$$

which is shown in Fig. 54 and listed in Table XVII. The data show a large positive polarization in the forward region of momentum transfer ($|t'|<1.0$ GeV^2). The errors for $|t'|>1.0$ GeV^2 are too large to make any definitive statement on the possibility of structure in the shape of P_Λ as a function of the momentum transfer.

TABLE XVII. Λ polarization for reaction $K^-p \to \Lambda\rho^0$.

$-t'$ interval (GeV^2)	P_Λ
0.0–0.2	0.47 ± 0.37
0.2–0.5	$1.00^{+0.00}_{-0.30}$
0.5–1.2	$1.00^{+0.00}_{-0.70}$
1.2–4.0	0.00 ± 0.84
4.0–7.0	0.19 ± 0.42

2. *Reaction $K^-p \to \Lambda\omega$*

a. Branching ratios, total and differential cross sections. In Fig. 8 we have shown the $\pi^+\pi^-\pi^0$ effective-mass spectrum for reaction 3, $\Lambda\pi^+\pi^-\pi^0$, for the combined 3.9- and 4.6-GeV/c data. A large ω signal over a small background is observed. Using a subsample of these events (consisting of 418 ± 18 ω's) with best resolution ($\sigma_{av} = 6.7$ MeV) we have fitted the $\pi^+\pi^-\pi^0$ effective-mass spectrum with a linear background plus a Breit-Wigner shape with the experimentally determined resolution folded in, and obtained the following values for the mass and width of the ω:

$$M = 782.5 \pm 0.8 \text{ MeV},$$

$$\Gamma = 13.3 \pm 2.0 \text{ MeV}.$$

Using these values we have fitted the individual mass spectra at the two momenta which are shown in Figs. 55(a) and 55(b). The results of the fit gave

3.9 GeV/c: 272 ± 12 events, $\sigma = 89 \pm 8$ μb,

4.6 GeV/c: 260 ± 13 events, $\sigma = 59 \pm 5$ μb,

where the quoted cross sections have been corrected for probability cuts, and Λ visibility and losses. We have measured the neutral/$\pi^+\pi^-\pi^0$ branching ratio of the ω from a comparison of the MM spectrum of reaction 1 (Fig. 3) and the combined $\pi^+\pi^-\pi^0$ spectrum (Fig. 8). Fits to the $\pi^+\pi^-\pi^0$ spectrum yielded a corrected cross section (averaged over momenta) of 71 ± 3 μb (the error is

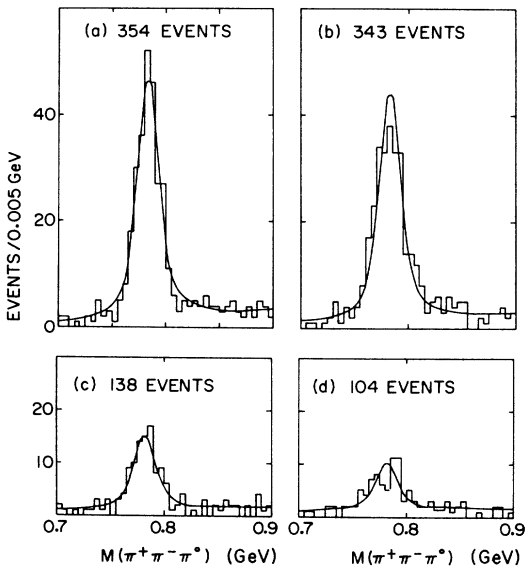

FIG. 55. $\pi^+\pi^-\pi^0$ effective mass distribution from the reaction $K^-p \to \Lambda\pi^+\pi^-\pi^0$: (a) at 3.9 GeV/$c$; (b) at 4.6 GeV/$c$; (c) at 3.9 GeV/$c$ for events with $\cos\theta^* < 0.0$; (d) at 4.6 GeV/c for events with $\cos\theta^* < 0.0$. The curves are the results of the fits described in the text.

statistical). We estimate 46 ± 13 ω events in the neutral mode corresponding to a corrected cross section of 11 ± 3 μb. We therefore find

$$\frac{\omega \to \text{neutrals}}{\omega \to \pi^+\pi^-\pi^0} = 0.15 \pm 0.04,$$

in good agreement with the world-averaged value of 0.104 ± 0.009.[7] Using this value we obtain the following total cross sections for ω production:

3.9 GeV/c: $\sigma = 98 \pm 9$ μb,

4.6 GeV/c: $\sigma = 65 \pm 6$ μb.

The differential cross sections shown in Figs. 56(a) and 56(b) and listed in Tables XVIII(a) and XVIII(b) were obtained by normalizing the background-subtracted number of events in the ω region defined as

$$0.76 \leq M(\pi^+\pi^-\pi^0) \leq 0.805 \text{ GeV}$$

to the total $K^-p \to \Lambda\omega$ ($\to \pi^+\pi^-\pi^0$) cross sections given above. We have fitted the peripheral region $|t'| < 1.4$ GeV^2 to a form $d\sigma/d|t'| \sim e^{At'}$ and obtained the values

3.9 GeV/c: $A = 1.8 \pm 0.4$ GeV^{-2},

4.6 GeV/c: $A = 2.0 \pm 0.3$ GeV^{-2}.

In addition, in the same figure we observe evidence for strong backward ω production. To get a quantitative estimate of the number of events produced with $\cos\theta^* < 0.0$ we have fitted the $\pi^+\pi^-\pi^0$ mass spectra after this selection has been imposed [Figs. 55(c) and 55(d)] with a linear background in the mass plus a Breit-Wigner shape. We obtained 85 ± 8 events (56 ± 8 events) at 3.9 (4.6) GeV/c corresponding to a corrected $\Lambda\omega(\to \pi^+\pi^-\pi^0)$ cross section of 31 ± 4 μb (14 ± 2 μb), similar to but slightly larger than that observed for ρ^0 production.

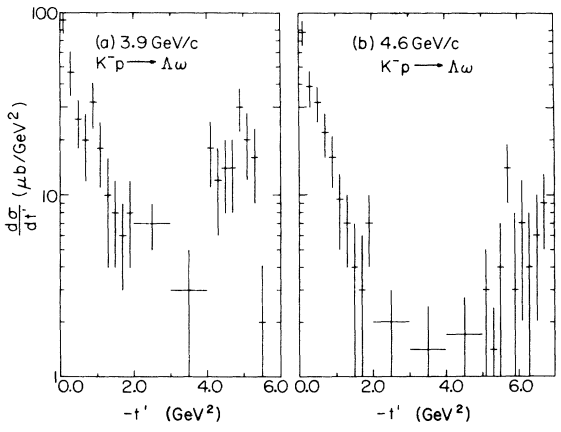

FIG. 56. Differential cross section for reaction $K^-p \to \Lambda\omega$: (a) at 3.9 GeV/c; (b) at 4.6 GeV/c.

TABLE XVIII. Differential cross section for reaction $K^-p \to \Lambda\omega(\to \pi^+\pi^-\pi^0)$.

$\lvert t'\rvert$ interval (GeV^2)	No. of ω [a] events	Corrected[b] $d\sigma/d\lvert t'\rvert$ (μb/GeV^2)
	(a) 3.9 GeV/c	
0.00–0.20	45 ± 7	91 ± 14
0.20–0.40	23 ± 7	47 ± 12
0.40–0.60	13 ± 4	26 ± 8
0.60–0.80	10 ± 4	20 ± 8
0.80–1.00	16 ± 4	32 ± 9
1.00–1.20	9 ± 3	18 ± 7
1.20–1.40	5 ± 3	10 ± 6
1.40–1.60	4 ± 2	8 ± 4
1.60–1.80	3 ± 2	6 ± 3
1.80–2.00	4 ± 2	8 ± 4
2.00–3.00	16 ± 5	7 ± 2
3.00–4.00	8 ± 5	3 ± 2
4.00–4.20	9 ± 3	18 ± 7
4.20–4.40	6 ± 3	12 ± 6
4.40–4.60	7 ± 3	14 ± 6
4.60–4.80	7 ± 3	14 ± 6
4.80–5.00	15 ± 4	30 ± 8
5.00–5.20	10 ± 4	20 ± 8
5.20–5.40	8 ± 3	16 ± 7
5.40–5.60	1 ± 1	2 ± 2
	(b) 4.6 GeV/c	
0.00–0.20	54 ± 8	78 ± 12
0.20–0.40	27 ± 6	39 ± 9
0.40–0.60	22 ± 5	32 ± 7
0.60–0.80	15 ± 4	22 ± 6
0.80–1.00	11 ± 4	16 ± 5
1.00–1.20	6 ± 2	9 ± 4
1.20–1.40	5 ± 2	7 ± 3
1.40–1.60	3 ± 2	4 ± 3
1.60–1.80	2 ± 2	3 ± 3
1.80–2.00	5 ± 2	7 ± 3
2.00–3.00	7 ± 3	2 ± 1
3.00–4.00	5 ± 3	1.4 ± 1
4.00–5.00	6 ± 3	1.7 ± 1
5.00–5.20	2 ± 1	3 ± 2
5.20–5.40	1 ± 1	1.4 ± 1
5.40–5.60	3 ± 2	4 ± 3
5.60–5.80	10 ± 4	14 ± 5
5.80–6.00	2 ± 3	3 ± 5
6.00–6.20	5 ± 3	7 ± 5
6.20–6.40	3 ± 3	4 ± 4
6.40–6.60	4 ± 3	6 ± 4
6.60–6.80	6 ± 3	9 ± 4

[a] Number of events in $0.760 \leq M(\pi^+\pi^-\pi^0) \leq 0.805$ GeV after background subtraction.

[b] Number of ω events normalized to total $\omega \to \pi^+\pi^-\pi^0$ cross section. Cross sections have been corrected for Λ visibility and losses as well as for probability cuts.

TABLE XIX. ω density matrices and Λ polarization from reaction $K^-p \to \Lambda\omega$.

$\lvert t'\rvert$ interval (GeV^2)	No. of events[a]	Jackson frame ρ_{00}	Jackson frame $Re\rho_{10}$	Jackson frame ρ_{1-1}	Helcity frame ρ_{00}	Helcity frame $Re\rho_{10}$	Helcity frame ρ_{1-1}	Λ polarization
0.0–0.1	43	0.63±0.10	−0.22±0.06	0.05±0.07	0.78±0.13	0.10±0.05	0.12±0.07	0.18±0.39
0.1–0.3	96	0.14±0.07	−0.08±0.04	0.26±0.06	0.21±0.07	0.05±0.04	0.29±0.06	0.27±0.26
0.3–0.5	50	0.32±0.08	−0.20±0.07	0.05±0.10	0.27±0.10	0.20±0.07	0.02±0.08	$1.00^{+0.00}_{-0.20}$
0.5–0.8	46	0.06±0.06	−0.05±0.05	0.44±0.06	0.00±0.06	0.04±0.05	0.40±0.07	$1.00^{+0.00}_{-0.37}$
0.8–2.0	81	0.17±0.07	−0.04±0.04	0.29±0.06	0.10±0.06	0.07±0.04	0.25±0.07	0.40±0.30
2.0–4.0	49	0.35±0.10	−0.09±0.06	0.11±0.09	0.19±0.10	−0.08±0.06	0.02±0.10	−0.40±0.37
4.0–5.0	56	0.21±0.10	−0.13±0.06	−0.17±0.08	0.15±0.09	−0.05±0.06	−0.21±0.08	$-1.00^{+0.20}_{-0.00}$
5.0–6.8	73	0.09±0.06	−0.02±0.05	−0.11±0.08	0.09±0.06	0.02±0.04	−0.11±0.08	−0.36±0.31

[a]In the region $0.760 \leq M(\pi^+\pi^-\pi^0) \leq 0.805$ GeV.

b. Decay correlations and polarization. Due to the large resonance signal relative to noise in the ω region (~10:1) and from an investigation of the moments across the ω region which revealed only a resonant P wave to be important, we performed maximum-likelihood fits with the standard P-wave decay angular distribution to determine the $\rho_{mm'}$ as a function of momentum transfer. The density-matrix elements so obtained in the Jackson and helicity frames are given in Table XIX and are shown in Figs. 57(a)–57(f). Except for the first momentum transfer bin ($|t'|<0.1$ GeV^2), the data (for the peripheral sample) are consistent with small values of ρ_{00} (<0.5) as in the $\Lambda\rho^0$ reaction.

The Λ polarization is shown in Fig. 58 and listed in Table XIX. The momentum transfer behavior in the peripheral region is similar to that observed in $K^-p \to \Lambda\rho^0$, being large and positive. There is also evidence for a change of the sign of the polarization at $|t'| \approx 2.0$ GeV^2 and large negative polarization in the backward direction.

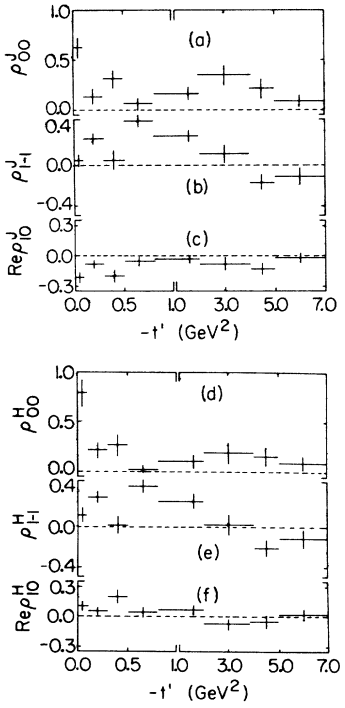

FIG. 57. Density-matrix elements of the ω produced in the reaction $K^-p \to \Lambda\omega$: (a)–(c) Jackson frame; (d)–(f) helicity frame.

3. Reaction $K^-p \to \Lambda\phi$

a. Mass, width, decay modes, and branching ratios. In this section we discuss the reaction $K^-p \to \Lambda\phi$. We present a new determination of the ϕ mass and width as well as its branching ratios. The production properties of this resonance are found to be different from the ω and ρ mesons previously discussed.

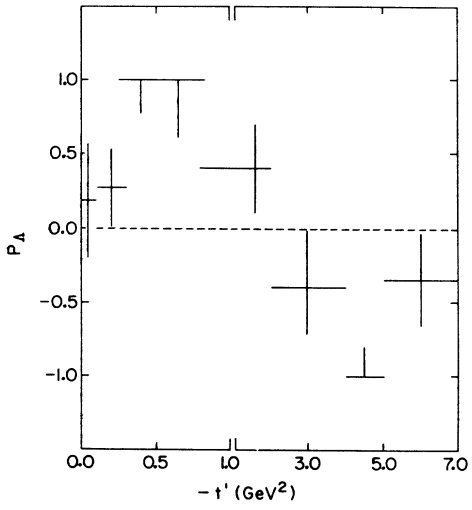

FIG. 58. Λ polarization for reaction $K^-p \to \Lambda\omega$.

The mass and width of the ϕ were determined from our best resolution sample of reaction 5, ΛK^+K^-, for the combined data at 3.9 and 4.6 GeV/c. A maximum-likelihood fit was performed on the events in the region $1.010 \leq M(K^+K^-) \leq 1.03$ GeV with the matrix element

$$|M|^2 = \epsilon |M_\phi|^2 + (1-\epsilon)|M_B|^2 ,$$

where ϵ is the fraction of ϕ events. For the background, $|M_B|^2$, we assume a linear dependence on the $K\bar{K}$ effective mass, and for the resonance term we used

$$|M_\phi|^2 = \frac{|f_{BW}|^2}{\sum \int |f_{BW}|^2 dm} ,$$

where $\sum \int dm$ implies integration over the $K\bar{K}$ effective mass distribution (in the region defined above) plus sum over events. A relativistic energy-dependent width Breit-Wigner with the pertinent phase-space factors and experimental resolution folded in was used for $|f_{BW}|^2$. The form of the distribution function given above allowed us to take into account the experimental resolution and the different center-of-mass energy on an event-per-event basis.

The resonance parameters so obtained are

$$M = 1019.6 \pm 0.3 \text{ MeV} ,$$

$$\Gamma = 4.6^{+1.0}_{-0.8} \text{ MeV} .$$

An excellent representation of the experimental mass distribution was obtained ($\chi^2 = 7.8$ for 10 bins). The solid line of Fig. 59(a) corresponds to the parameters quoted above and was obtained using the average experimental mass resolution ($\sigma = 1.16$ MeV).

In addition we have determined the ϕ mass and width from the reaction

$$K^-p \to K^-pK^+K^-$$

using an identical approach as described above. The mass and width so obtained are[29]

$$M = 1019.9 \pm 0.4 \text{ MeV} ,$$

$$\Gamma = 4.7^{+1.3}_{-1.0} \text{ MeV} ,$$

in excellent agreement with the values obtained above as well as the world value of $M = (1019.5 \pm 0.60)$ MeV and $\Gamma = (4.00 \pm 0.27)$ MeV.[7] The result of this fit is shown as the solid curve in Fig. 59(b). The quality of the fit is, again, very good ($\chi^2 = 10.6$ for 10 bins).

The ϕ branching fraction, $K_1^0K_2^0/K^+K^-$, was obtained from an estimate of the number of events in the ϕ region, defined as

$$1.0 \leq M(K\bar{K}) \leq 1.04 \text{ GeV}$$

from reactions 5 and 12. The $K\bar{K}$ effective-mass spectra at 3.9 and 4.6 GeV/c are shown in Figs. 60(a)–60(d), in which clean ϕ signals are observed.

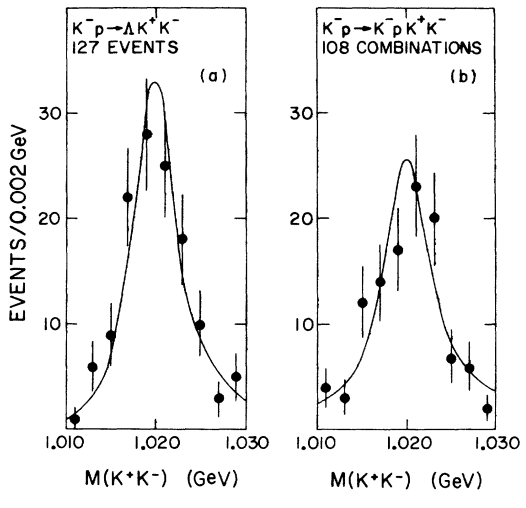

FIG. 59. K^+K^- effective-mass spectrum: (a) from reaction $K^-p \to \Lambda K^+K^-$; (b) from reaction $K^-p \to K^-pK^+K^-$. The curves are the results of the maximum-likelihood fits described in the text.

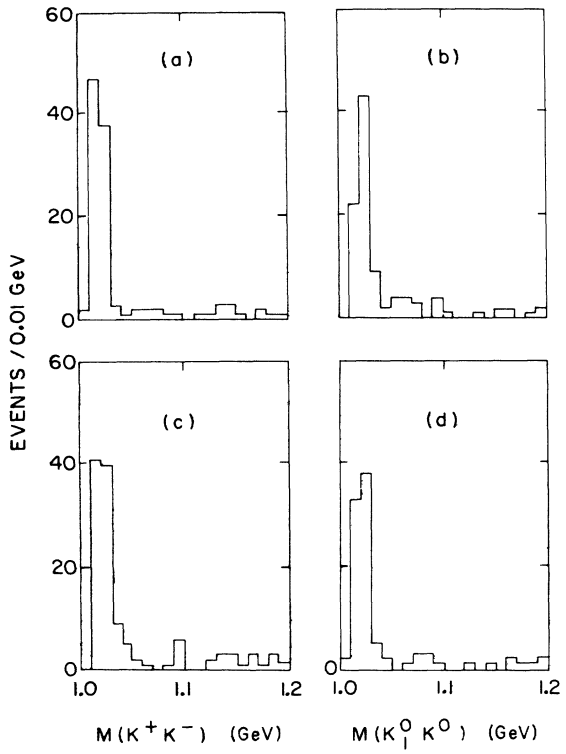

FIG. 60. (a) K^+K^- effective-mass spectrum from reaction 5 at 3.9 GeV/c. (b) $K_1^0K_2^0$ effective-mass spectrum from reaction 12 at 3.9 GeV/c. (c) Same as (a) but at 4.6 GeV/c. (d) Same as (b) but at 4.6 GeV/c.

TABLE XX. ϕ branching ratios.

Final state	No. of observed events 3.9 GeV/c	No. of observed events 4.6 GeV/c	Corrected[a] cross sections (μb) 3.9 GeV/c	Corrected[a] cross sections (μb) 4.6 GeV/c
ΛK^+K^- [b]	84 ± 9.4	85 ± 9.5		
ΛK^+K^- [c]	6 ± 2.4	5 ± 2.2	27.5 ± 3.0	19.0 ± 2.0
$\Lambda K_1^0 K_2^0$	72 ± 8.6	72 ± 8.7	24.8 ± 2.9	17.0 ± 2.1
$\Lambda \pi^+\pi^-\pi^0$ [d]	34 ± 11		5.8 ± 1.9	
$\Lambda \pi^+\pi^+\pi^-\pi^-\pi^0$ [e]	2 (2σ)		0.38 (2σ)	

Branching ratios

$\frac{K_1^0 K_2^0}{K^+K^-}$ [f] $= 0.89 \pm 0.10$; $\frac{\pi^+\pi^-\pi^0}{K^+K^-}$ [g] $= 0.28 \pm 0.09$; $\frac{5\pi}{K^+K^-} = 0.02$ (2σ)

[a] Corrected for probability cuts and V^0 losses; $\pi^+\pi^-\pi^0$ has been corrected for MM^2 cut as described in text.

[b] Reaction 5.

[c] From vee + kink topology.

[d] Observed events: 3.9 + 4.6 GeV/c $|t'| < 1.2$ GeV^2 and $MM^2 > 0.01$ GeV^2.

[e] Observed events, 3.9 and 4.6 GeV/c, in region 1.0–1.04 GeV and $|t'| < 1.2$ GeV^2.

[f] Weighted average over the two momenta.

[g] Corrected cross section for $\Lambda^0 K^+K^-$ with $|t'| < 1.2$ GeV^2 is 20.7 ± 1.7 μb for 3.9 and 4.6 GeV/c combined.

The number of events and the corrected cross sections obtained from these figures are listed in Table XX. In addition to $\phi \to K^+K^-$ events from reaction 5, the number of resonance events obtained from the multistrange channel (vee + kink topology) is also indicated. The weighted branching ratio over the two momenta[30] of 0.89 ± 0.10, given in Table XX, is in good agreement with the world-averaged value of 0.76 ± 0.10.[7]

We now investigate the $\pi^+\pi^-\pi^0$ decay mode of the ϕ. As noted in the η' section, the total fitted $\pi^+\pi^-\pi^0$ effective-mass spectrum shows a large enhancement in the 1.0-GeV region; however, it is difficult to resolve the η' and ϕ signals. In order to circumvent this problem, we examine the $\pi^+\pi^-\pi^0$ effective-mass spectrum for events with $MM^2 > 0.01$ GeV^2; as previously mentioned, the $\pi^+\pi^-\gamma$ signal of the η' is antiselected by this cut. With this selection and for $|t'| < 1.2$ GeV^2 (this momentum transfer region encompasses most of the ϕ events), we show in Fig. 61 the $\pi^+\pi^-\pi^0$ effective-mass spectrum for the combined data at 3.9 and 4.6 GeV/c, in which a signal is observed in the mass region above 1.0 GeV. A fit to this mass spectrum with a Breit-Wigner[31]-plus-polynomial background gives 34 ± 11 resonance events with a mass $M = 1009 \pm 8$ MeV. Associating this observed signal with the ϕ, we then obtain $\phi \to \pi^+\pi^-\pi^0/\phi \to K^+K^-$ branching ratio[32] of 0.28 ± 0.09 which is given in Table XX.

We have also sought and found no evidence for a 5π decay of the ϕ. The 2-standard-deviation upper limit for this mode is indicated in Table XX.

b. Total and differential cross sections. The total cross section for ϕ production (including K^+K^-, $K_1^0K_2^0$, and $\pi^+\pi^-\pi^0$) is then

3.9 GeV/c: $\sigma = 60 \pm 7$ μb,

4.6 GeV/c: $\sigma = 41 \pm 4$ μb.

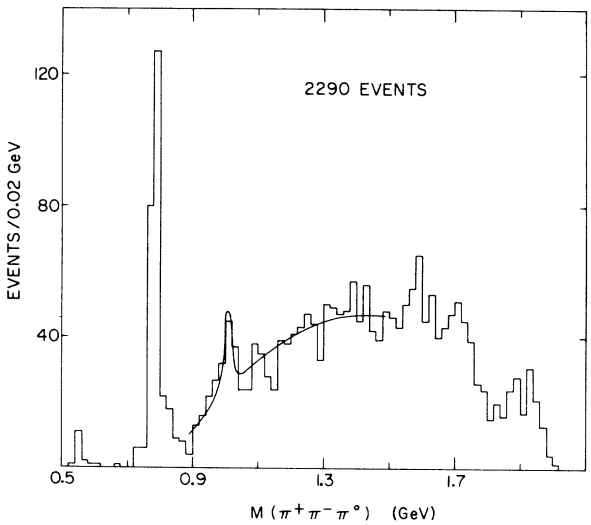

FIG. 61. $\pi^+\pi^-\pi^0$ effective-mass spectrum from reaction 3 for events with $|t'| < 1.2$ GeV^2 and $MM^2 > 0.01$ GeV^2. The curve is the result of the fit described in the text.

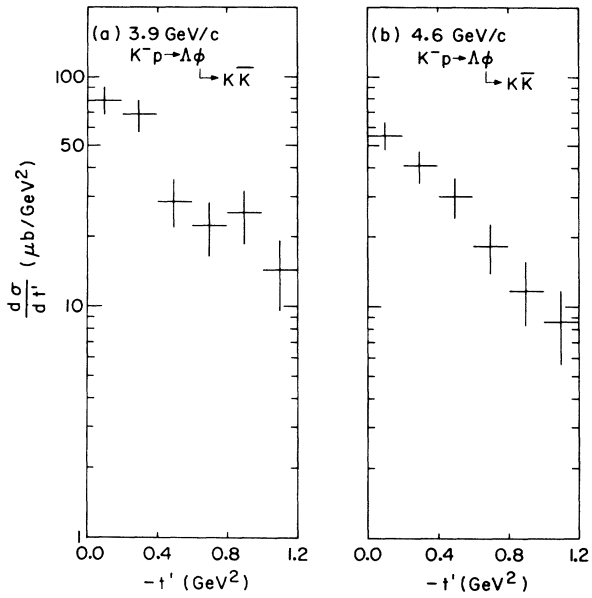

FIG. 62. Differential cross section for reaction $K^-p \to \Lambda\phi(\to K\bar{K})$: (a) at 3.9 GeV/$c$; (b) at 4.6 GeV/$c$.

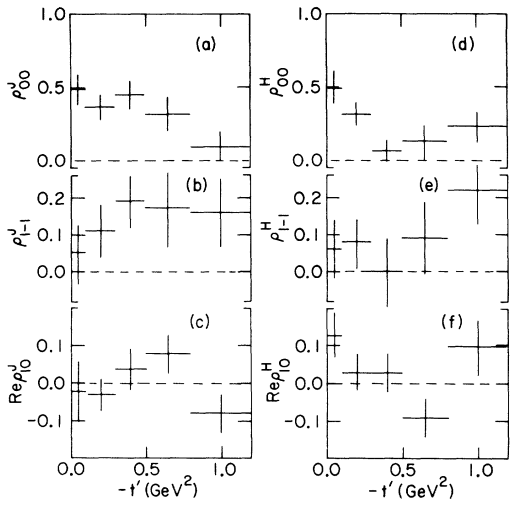

FIG. 63. Density-matrix elements of the ϕ produced in the reaction $K^-p \to \Lambda\phi$: (a)–(c) Jackson frame; (d)–(f) helicity frame.

The differential cross sections obtained for the reaction $K^-p \to \Lambda\phi$ $(\to K\bar{K})$ is shown in Figs. 62(a) and 62(b) and listed in Table XXI. As has been previously observed at other energies[33] there is very little evidence for ϕ production in the backward hemisphere in which we observe 4 ± 2 events (2 ± 1.4 events) corresponding to a total cross section of 1.5 ± 0.7 μb (0.5 ± 0.4 μb) at 3.9 (4.6) GeV/c. The slope parameter describing the differential cross sections of Figs. 62(a) and 62(b) was found to be ($|t'| \leq 1.2$ GeV^2)

TABLE XXI. Differential cross sections for reaction $K^-p \to \Lambda\phi$ $(\to K\bar{K})$.

$\lvert t'\rvert$ interval (GeV^2)	3.9 GeV/c No. of events	3.9 GeV/c Corrected $\frac{d\sigma}{d\lvert t'\rvert}\left(\frac{\mu b}{GeV^2}\right)$	4.6 GeV/c No. of events	4.6 GeV/c Corrected $\frac{d\sigma}{d\lvert t'\rvert}\left(\frac{\mu b}{GeV^2}\right)$
0.0–0.2	50 ± 7	79.7 ± 11.3	52 ± 7	55.7 ± 7.7
0.2–0.4	43 ± 7	68.6 ± 10.5	38 ± 6	40.7 ± 6.6
0.4–0.6	18 ± 4	28.7 ± 6.7	28 ± 5	30.0 ± 5.7
0.6–0.8	14 ± 4	22.3 ± 5.9	17 ± 4	18.2 ± 4.4
0.8–1.0	16 ± 4	25.5 ± 6.4	11 ± 3	11.8 ± 3.5
1.0–1.2	9 ± 3	14.4 ± 4.8	8 ± 3	8.6 ± 3.0
1.2–1.4	4 ± 2	6.4 ± 3.2	4 ± 2	4.3 ± 2.1
1.4–1.6	2 ± 1	3.2 ± 2.2	2 ± 1	2.1 ± 1.5
1.6–1.8	2 ± 1	3.2 ± 2.2	4 ± 2	4.3 ± 2.1
1.8–2.0	1 ± 1	1.6 ± 1.6	0	0
2.0–3.0	2 ± 1	0.6 ± 0.5	1 ± 1	0.2 ± 0.2
3.0–4.0	2 ± 1	0.6 ± 0.5	0	0
4.0–5.0	1 ± 1	0.3 ± 0.3	2 ± 1	0.4 ± 0.3
5.0–6.0	•••	•••	1 ± 1	0.2 ± 0.2

3.9 GeV/c: $A = 1.9 \pm 0.2$ GeV^{-2},

4.6 GeV/c: $A = 2.0 \pm 0.2$ GeV^{-2}.

c. Decay correlations and polarization. The ϕ density-matrix elements obtained by maximum-likelihood fits, using the P-wave angular distribution[34] and the events in the ϕ region [$1.0 \leq M(K\bar{K}) \leq 1.04$ GeV] for the combined 3.9- and 4.6-GeV/c data (K^+K^- plus $K_1^0K_2^0$ events combined) as a function of momentum transfer, are shown in Fig. 63 and listed in Table XXII, in both the Jackson and helicity frames. There appears to be evidence for a larger amount of unnatural-parity exchange than in either the $\Lambda\rho$ or $\Lambda\omega$ reactions as exhibited by the larger value of ρ_{00}^J as a function of momentum transfer (average ~0.4 compared to <0.2 for t' < 1.0 GeV^2). The form of the P_Λ distribution as shown in Fig. 64 also differs from that observed in the $\Lambda\omega$ and $\Lambda\rho$ reactions. Here we find values of P_Λ which are consistent with being negative as a function of momentum transfer, which is in contrast to the large positive polarization found in the ω and ρ reactions.

C. Tensor Mesons

1. Reaction $K^-p \to \Lambda f^0$

a. Total and differential cross sections; branching ratios. The data for this study come from reaction 2, $\Lambda\pi^+\pi^-$, which was previously discussed in the $\Lambda\rho^0$ section. The $\pi^+\pi^-$ effective-mass distributions have already been shown [Figs. 50(a) and 50(b)] at the two momenta in which the $Y^{*+}(1385)$ band has been removed and then repopulated with conjugate events.[20] Whereas this pro-

TABLE XXII. ϕ density matrices and Λ polarization from reaction $K^-p \to \Lambda\phi$.

$\lvert t'\rvert$ Interval (GeV^2)	No. of events	Jackson frame ρ_{00}	Jackson frame $\mathrm{Re}\rho_{10}$	Jackson frame ρ_{1-1}	Helicity frame ρ_{00}	Helicity frame $\mathrm{Re}\rho_{10}$	Helicity frame ρ_{1-1}	Λ polarization
0.0–0.1	46	0.49±0.10	−0.02±0.08	0.05±0.08	0.49±0.11	0.13±0.06	0.06±0.08	0.37±0.42
0.1–0.3	96	0.37±0.08	−0.03±0.04	0.11±0.07	0.31±0.07	0.03±0.05	0.08±0.07	−0.26±0.25
0.3–0.5	67	0.45±0.09	0.04±0.05	0.19±0.07	0.07±0.06	0.03±0.05	0.00±0.09	−0.13±0.35
0.5–0.8	51	0.32±0.11	0.08±0.05	0.17±0.10	0.13±0.11	−0.09±0.05	0.09±0.10	−0.33±0.37
0.8–1.2	44	0.09±0.10	−0.08±0.05	0.16±0.09	0.23±0.09	0.10±0.07	0.22±0.09	−0.58±0.37

cedure has no significant effect on the number of ρ^0's at each energy, it must be employed for an estimate of the f^0 cross section, since the estimated number of f^0's is severely affected by the $Y^{*+}(1385)$ reflection (especially at 3.9 GeV/c). The average mass and width obtained from fits to these mass spectra are

$$M = 1242 \pm 15 \text{ MeV},$$

$$\Gamma = 116 \pm 30 \text{ MeV}.$$

It should be noted that the value of the f^0 mass at 4.6 GeV/c is 2σ lower than the world-averaged value of 1268.9±1.8 MeV, which we can only attribute to a statistical fluctuation. This width is also lower than the world average but well within the spread of reported widths.

The number of f^0 events and the corrected cross sections obtained from these fits are

3.9 GeV/c: 99±26 events, $\sigma = 47 \pm 12$ μb,

4.6 GeV/c: 185±25 events, $\sigma = 60 \pm 8$ μb.

As shown in Figs. 50(c) and 50(d) there is evidence for significant backward f^0 production at our energies. The number of events obtained from fits to these mass spectra is 55±15 (109±17) at 3.9 (4.6) GeV/c, corresponding to a corrected cross section of 26±7 μb (35±6 μb). We observe that f^0 backward is as strong as the forward production for the two momenta, a property only observed for the f^0 meson in our study of resonances produced recoiling off Λ's.

The differential cross sections obtained by normalizing the number of background-subtracted resonance events in the f^0 region,

$$1.12 \leq M(\pi^+\pi^-) \leq 1.36 \text{ GeV},$$

to the total cross sections quoted above are shown in Fig. 65 and listed in Table XXIII. Unlike the previously described $K^-p \to \Lambda$ + vector meson reactions, a less apparent forward peak is observed in f^0 production.

We now discuss an investigation of the f^0 branching ratios. We use the observed strong backwardly-produced ($\cos\theta^* \leq 0.0$) f^0 sample at 4.6 GeV/c in the $\pi^+\pi^-$ decay mode as the standard and look for f^0 backward production in the channels listed

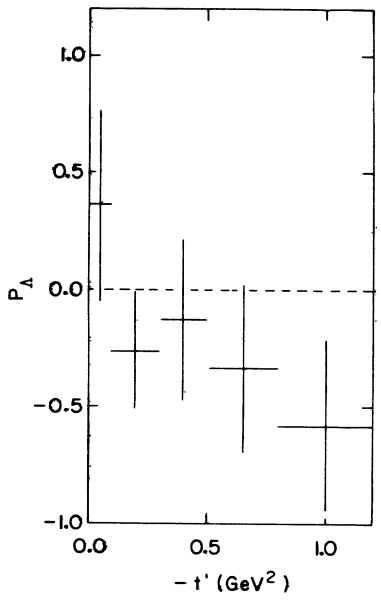

FIG. 64. Λ polarization for reaction $K^-p \to \Lambda\phi$.

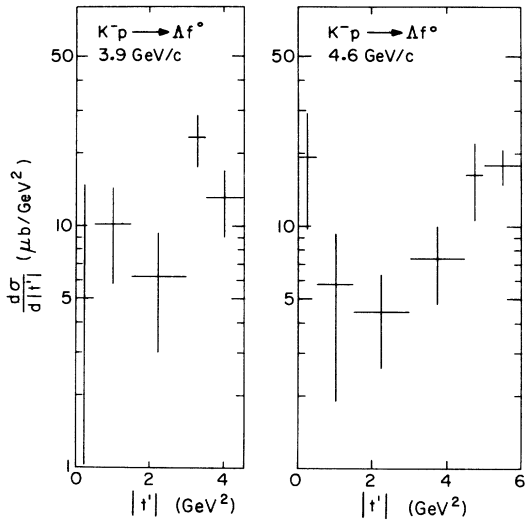

FIG. 65. Differential cross section for reaction $K^-p \to \Lambda f^0$: (a) at 3.9 GeV/c; (b) at 4.6 GeV/c.

TABLE XXIII. Differential cross sections for reaction $K^-p \to \Lambda f^0(\to \pi\pi)$.

$\lvert t' \rvert$ interval (GeV^2)	3.9 GeV/c No. of f^0 [a] events	3.9 GeV/c Corrected [b] $d\sigma/d\lvert t' \rvert$ (μb/GeV^2)	4.6 GeV/c No. of f^0 [a] events	4.6 GeV/c Corrected [b] $d\sigma/d\lvert t' \rvert$ (μb/GeV^2)
0.0–0.5	5 ± 10	4.9 ± 9.8	20 ± 10	19.4 ± 9.7
0.5–1.5	21 ± 9	10.2 ± 4.4	12 ± 8	4.8 ± 3.9
1.5–3.0	19 ± 10	6.2 ± 3.2	14 ± 6	4.5 ± 1.9
3.0–3.5	24 ± 6	23.4 ± 5.9	23 ± 8	7.5 ± 2.6
3.5–4.5	27 ± 8	13.2 ± 3.9		
4.5–5.0			17 ± 6	16.5 ± 5.8
5.0–6.0			37 ± 6	18.0 ± 2.9

[a] In the region $1.12 \leq M(\pi^+\pi^-) \leq 1.36$ GeV.
[b] Normalized to the total cross sections quoted in text.

in Table XXIV. We observe no statistically significant signal in the f^0 region in the following modes: $\pi^+\pi^+\pi^-\pi^-$, $K\bar{K}$ (K^+K^- plus $K_1^0K_1^0$), $\pi^+\pi^-$MM ($0.27 \leq \mathrm{MM}^2 \leq 0.33$ GeV^2), and $K_1^0K^\pm\pi^\mp$. The effective-mass spectra for all the reactions studied are shown in Figs. 66(a)–66(e). The 2-standard-deviation upper limits for these decay modes relative to $\pi^+\pi^-$ are given in Table XXIV. It should be noted that we observe no significant $A_2 \to \rho\pi$ signal (see next section) so that little if any $A_2 \to K\bar{K}$ is expected in Fig. 66(c).

b. Decay correlations. The extraction of the f^0 density matrix elements was carried out following the procedure outlined in a separate publication.[26] We will not discuss all the details of this method, which can be found in this reference. We have found that the only significant moments in the region $1.0 \leq M(\pi^+\pi^-) \leq 1.6$ GeV are due to the presence of D-wave resonance and S- and P-wave backgrounds, which we included in a mass-dependent analysis. From the values of the $H(LM)$ resonance moments the f^0 density-matrix elements were obtained. In the present approach, we have not included interference effects between any of the waves, and we obtain physically acceptable values for the resonance density-matrix elements. We stress that this does not imply that interference effects are not present; they are just not needed to explain the data. We fitted the forward and backward regions[35] separately for the combined data at

TABLE XXIV. f^0 decay modes.

Decay mode	No. of events observed [a]	Corrected cross sections (μb) [b]
$f^0 \to \pi\pi$	84 ± 14	27.4 ± 4.6
$f^0 \to K\bar{K}$	7[c]	1.9[c]
$f^0 \to \eta\pi\pi$	12[c]	5.3[c]
$f^0 \to \pi^+\pi^+\pi^-\pi^-$	12[c]	3.2[c]
$f^0 \to K^0K^-\pi^+ + \bar{K}^0K^+\pi^-$	4[c]	1.9[c]
f^0 branching ratios		
$\frac{K\bar{K}}{\pi\pi} < 0.07$; $\frac{\eta\pi\pi}{\pi\pi} < 0.19$; $\frac{\pi^+\pi^+\pi^-\pi^-}{\pi\pi} < 0.12$; $\frac{K^0K^-\pi^+ + \bar{K}^0K^+\pi^-}{\pi\pi}$		< 0.07

[a] Events in region 1.12–1.36 GeV.
[b] Corrected for unseen resonance decays, Λ and K^0 visibility and losses and probability cuts.
[c] Two-standard-deviation upper limits.

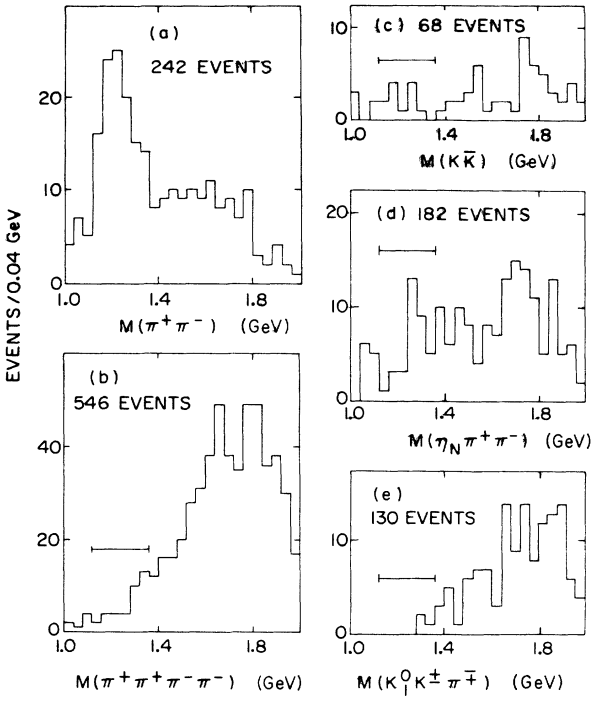

FIG. 66. Effective-mass spectra for events produced with $\cos\theta^* < 0.0$ at 4.6 GeV/c: (a) reaction 2; (b) reaction 9; (c) reactions 5, 11, and 12; (d) reaction 4 with $0.27 \leq \mathrm{MM}^2 \leq 0.33$ GeV^2; (e) reaction 13.

TABLE XXV. Density-matrix elements (Jackson frame) of the f^0 from reaction $K^-p \to \Lambda f^0$ at 3.9 and 4.6 GeV/c.

Density-matrix elements[a]	selection $\cos\theta^* > 0.0$	$\cos\theta^* < 0.0$
ρ_{00}	0.33 ± 0.12	0.18 ± 0.10
ρ_{11}	0.28 ± 0.08	0.29 ± 0.05
ρ_{22}	0.06 ± 0.06	0.12 ± 0.07
$\mathrm{Re}\rho_{10}$	-0.15 ± 0.06	0.10 ± 0.05
ρ_{1-1}	0.09 ± 0.08	-0.08 ± 0.06
$\mathrm{Re}\rho_{20}$	0.02 ± 0.06	-0.11 ± 0.05
$\mathrm{Re}\rho_{21}$	$-0.16^{+0.04}_{-0.07}$	-0.01 ± 0.05
$\mathrm{Re}\rho_{2-1}$	-0.02 ± 0.06	0.02 ± 0.04
ρ_{2-2}	$0.06^{+0.06}_{-0.09}$	0.05 ± 0.05

[a]Under assumption of no interference between the D-wave resonance and the S- and P-wave background.

3.9 and 4.6 GeV/c with $Y^{*+}(1385)$ removed and then repopulated with conjugate events.[21] The values of the density matrix elements as obtained from the $H(LM)$ moments are given in Table XXV. Within 1 standard deviation they were found to satisfy the spin-two positivity conditions.[26] The small value of the ρ_{00} density-matrix element obtained in the forward direction is consistent with a large natural-parity exchange mechanism similar to that observed in the previously discussed 1^- reactions. It is interesting to note that in the $\pi^-p \to f^0n$ reaction[24] a significantly negative value of ρ_{22} was found as well as evidence for strong S-D-wave interferences which are not observed in the present experiment.

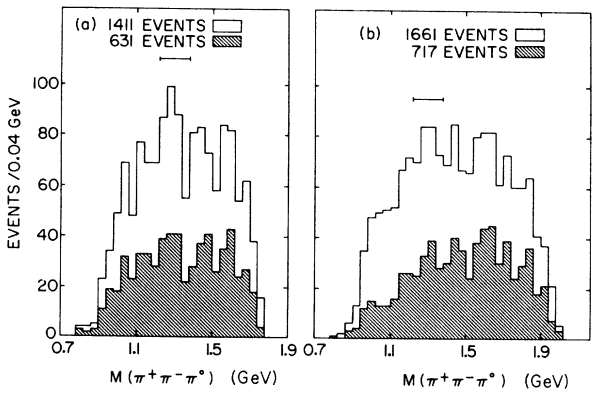

FIG. 67. $\pi^+\pi^-\pi^0$ effective-mass distribution from reaction 3 for events with $\pi^-\pi^0$ or $\pi^+\pi^0$ effective mass in the ρ^0 region [$0.64 \leq M(\pi\pi) \leq 0.89$ GeV] after removal of the $Y^{*+}(1385)$ band: (a) at 3.9 GeV/c; (b) at 4.6 GeV/c. The shaded area is the same mass spectrum, but after a $\cos\theta^* < 0.0$ selection.

2. *Reaction* $K^-p \to \Lambda A_2$

We have searched for production of the A_2 meson in reaction 3. Figures 67(a) and 67(b) show the $\pi^+\pi^-\pi^0$ effective-mass spectrum at 3.9 and 4.6 GeV/c, respectively, for events in which either the $\pi^-\pi^0$ or $\pi^+\pi^0$ effective mass is in the ρ region [$0.64 \leq M(\pi\pi) \leq 0.89$ GeV], and for which events in the $Y^{*+}(1385)$ region have been removed. Very weak if any indication for A_2 production is observed. In order to obtain an estimate of the A_2 cross section we have performed a simple background subtraction on the events in the A_2 region [$1.22 \leq M(\rho\pi) \leq 1.38$ GeV] minus events in the adjacent control region and obtained[36]

3.9 GeV/c: 27 ± 25 events;

$\sigma(K^-p \to \Lambda A_2) = 23 \pm 21$ μb,

4.6 GeV/c: 40 ± 24 events;

$\sigma(K^-p \to \Lambda A_2) = 23 \pm 14$ μb.

We have previously observed that there is evidence at both momenta for strong backward production of the f^0 meson; however, as shown in the shaded areas of Fig. 67(a) [67(b)], there is no significant signal for the production of its octet partner, the A_2, in the backward hemisphere at both momenta. The background subtraction technique gives the following number of events[36] for backward A_2 production:

3.9 GeV/c: 0 ± 17 events; $\sigma = 0 \pm 14$ μb,

4.6 GeV/c: 9 ± 16 events; $\sigma = 5 \pm 9$ μb.

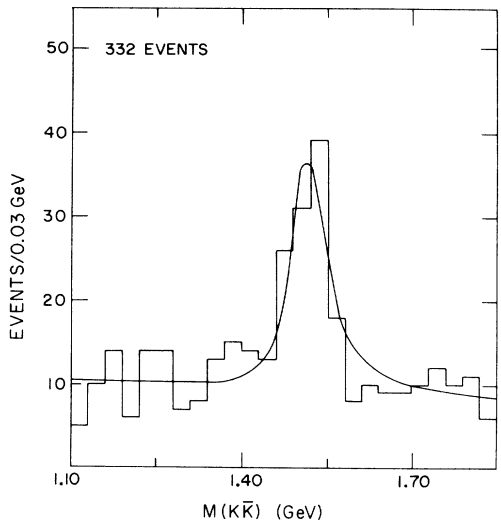

FIG. 68. $K\bar{K}$ effective distribution at 4.6 GeV/c from reactions 5, 8, 11, 12, and 14. The curve is the result of the fit described in the text.

3. *Reaction* $K^-p \to \Lambda f'$

The discovery of the $I=0$ member of the 2^+ nonet, the f' meson, was first reported in this experiment.[37] Here, we discuss the properties of the f' meson using additional data to that previously reported.

a. Mass, width, decay modes, and branching ratios. To obtain the mass and width of the f' we have added the data from reactions 5, 8, 11, 12, and 14 at 4.6 GeV/c (there is no significant evidence for f' production at 3.9 GeV/c). This total mass spectrum is shown in Fig. 68. A maximum-likelihood fit was performed on the events in this mass distribution using a matrix element containing a D-wave Breit-Wigner multiplying phase space plus a linear form in the mass for the background. The result so obtained is

$$M = 1519 \pm 7 \text{ MeV},$$

$$\Gamma = 69 \pm 22 \text{ MeV}.$$

Other f' decay modes were searched for in the final states listed in Table XXVI at 4.6 GeV/c ($\cos\theta^* > 0.0$). The mass spectra associated with these final states are shown in Fig. 69(a)–69(e). The shaded area in the $K_1^0 K^\pm \pi^\mp$ effective-mass distribution corresponds to events in which at least one $K\pi$ combination is in the $K^*(890)$ region. Except in the $K\bar{K}$ mass spectrum, no statistically significant signal is observed in any of the mass spectra shown in the figure. Two-standard-deviation upper limits corresponding to the decay modes listed in Table XXVI are also given therein.

TABLE XXVI. f' Decay modes.

Decay mode	No. of events observed[a]	Corrected cross sections (μb)[b]
$f' \to K\bar{K}$	40 ± 8	10.8 ± 2.2
$f' \to \pi\pi$	12[c]	3.9[c]
$f' \to \eta\pi\pi$	10[c]	4.4[c]
$f' \to \pi^+\pi^+\pi^-\pi^-$	13[c]	3.5[c]
$f' \to K^0 K^- \pi^+$		
$f' \to K^0 K^- \pi^+ + \bar{K}^0 K^+ \pi^-$	8[c]	3.8[c]

f' branching ratios

$$\frac{\pi\pi}{K\bar{K}} < 0.36; \quad \frac{\eta\pi\pi}{K\bar{K}} < 0.41; \quad \frac{\pi^+\pi^+\pi^-\pi^-}{K\bar{K}} < 0.32; \quad \frac{K^0K^-\pi^+ + \bar{K}^0K^+\pi^-}{K\bar{K}} < 0.35$$

[a] Events in region 1.48–1.56 GeV.

[b] Corrected for unseen resonance decays, Λ and K^0 visibility and losses and probability cuts.

[c] Two-standard-deviation upper limit.

We now turn to an investigation of f' production as observed in reactions 5, 11, and 12. The number of f' events obtained from fits to the combined mass spectra at each energy is

3.9 GeV/c: 17 ± 11 events; $\sigma = 7 \pm 4$ μb,

4.6 GeV/c: 70 ± 14 events; $\sigma = 19 \pm 4$ μb.

The cross sections quoted above have been corrected for unseen resonance decays, Λ^0 and K^0 visibility, and losses and probability cuts.

b. Total and differential cross sections. The differential cross section for f' production at 4.6 GeV/c is shown in Fig. 70 and listed in Table XXVII. There is no evidence for a sharp forward peak in the differential cross section (this situation is similar to that observed in the $K^-p \to \Lambda f^0$ reaction), but the small statistics preclude the extraction of the slope parameter. There is no significant evidence for f' backward production with a 2-standard-deviation upper limit of 2 μb (at 4.6 GeV/c). The lack of backward production was also a feature in ϕ production. This similar behavior

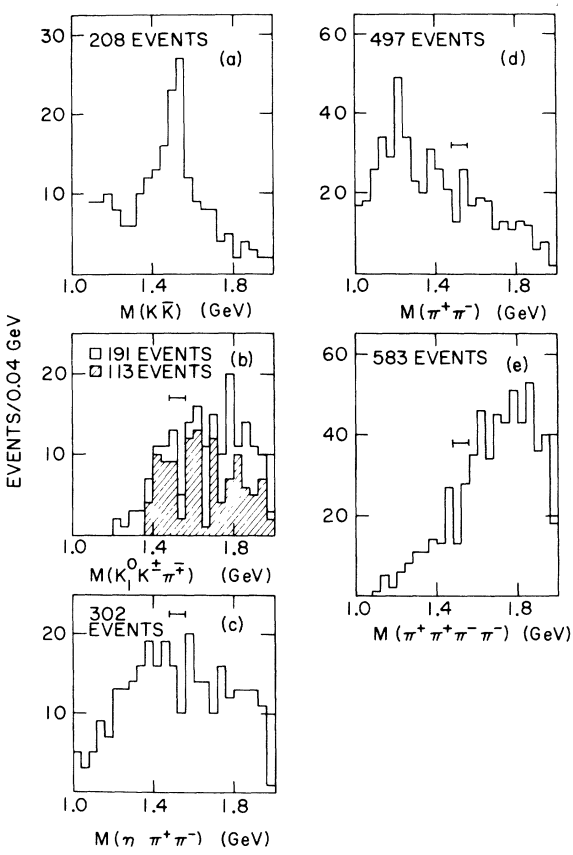

FIG. 69. Effective-mass spectra for events produced with $\cos\theta^* > 0.0$ at 4.6 GeV/c: (a) reactions 5, 11, and 12; (b) reaction 13; (c) reaction 4 with $0.27 \leq MM^2 \leq 0.33$ GeV^2; (d) reaction 2; (e) reaction 9.

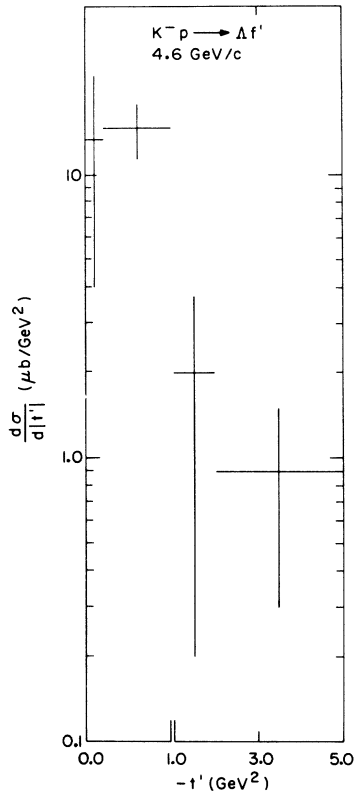

FIG. 70. Differential cross section for reaction $K^-p \to \Lambda f'$ at 4.6 GeV/c.

is expected from simple quark-model arguments; both ϕ and f' are mainly built up of strange quark-antiquark pairs and do not couple to the $N\bar{N}$ system, in contrast to the other resonances discussed in this paper which in turn do show some backward production.

c. Decay correlations. The f' density-matrix elements (in the Jackson frame) were obtained for the 4.6-GeV/c sample after a $\cos\theta^* > 0.0$ selection. The method employed is that of Ref. 26 (already discussed in the Λf^0 section) which is a mass-dependent partial-wave analysis containing S, P, and D waves. For this study we only use the $K_1^0K_1^0$ events which have a significantly better f' signal-to-noise ratio than the K^+K^- sample. We have carried out this analysis assuming both no interference and also maximum S-D-wave interference. The latter method does not give unique values of the density-matrix elements but, instead, gives upper and lower limits as determined by the phase of the interference between resonance and background. The results are given in Table XXVIII for these two cases. It should be noted that the no-interference assumption produces physically acceptable 2^+ density-matrix elements, which satisfy the spin-2 positivity conditions, but it is obvious that interference effects cannot be ruled out. We note in passing that an investigation of the moments in the K^+K^- sample, in contrast to the $K_1^0K_1^0$ case, indicates that interference between S-wave background and the D-wave resonance produces a negative value of ρ_{22}. The effect in this channel is similar to that observed in the reaction $K^-p \to K^{*0}(1420)n$,[1] in which a similar effect is found. The limited statistics on the $f' \to K^+K^-$ mode, which is produced on a large background (see Fig. 16), precludes any further quantitative investigation.

Finally we note that the f' density-matrix elements with $m=0$ or 1 given in Table XXVIII are similar to those obtained for ϕ production and can be interpreted as evidence for both unnatural- and natural-parity exchange in the reaction $K^-p \to \Lambda f'$.

TABLE XXVII. Differential cross section for reaction $K^-p \to \Lambda f'$ at 4.6 GeV/c.

$\lvert t'\rvert$ interval (GeV²)	No. of f' [a] events	Corrected[b] $d\sigma/d\lvert t'\rvert$ (μb/GeV²)
0.0–0.2	8 ± 6	13.3 ± 3.3
0.2–1.0	35 ± 8	14.6 ± 3.3
1.0–2.0	6 ± 5	2.0 ± 1.8
2.0–5.0	8 ± 5	0.9 ± 0.6

[a] In the region $1.48 \leq M(K\bar{K}) \leq 1.56$ GeV.
[b] Normalized to the total cross section quoted in the text.

IV. STUDY OF REACTIONS $K^-p \to \Sigma^0$ + MESON

A. Reaction $K^-p \to \Sigma^0\rho^0$

There is clear evidence in Fig. 71 for production of the ρ^0 meson in reaction 7, $\Sigma^0\pi^+\pi^-$, at 3.9 and 4.6 GeV/c. The fit to the combined data gives the

TABLE XXVIII. f' density-matrix elements from reaction $K^-p \to \Lambda f'$ at 4.6 GeV/c (for $\cos\theta^* > 0.0$).

No interference	Interference
$\rho_{00} = 0.45 \pm 0.13$	$0.29 \pm 0.12 \leq \rho_{00} \leq 0.46 \pm 0.12$
$\rho_{11} = 0.27^{+0.03}_{-0.08}$	$0.18 \pm 0.06 \leq \rho_{11} \leq 0.27 \pm 0.06$
$\rho_{22} = 0.00 \pm 0.09$	$0.00 \leq \rho_{22} \leq 0.17 \pm 0.07$
$\mathrm{Re}\rho_{10} = 0.00^{+0.06}_{-0.10}$	$-0.10 \pm 0.08 \leq \mathrm{Re}\rho_{10} \leq 0.05 \pm 0.08$
$\rho_{1-1} = 0.21 \pm 0.09$	$0.07 \pm 0.10 \leq \rho_{1-1} \leq 0.27 \pm 0.06$
$\mathrm{Re}\rho_{20} = 0.00^{+0.07}_{-0.05}$	$-0.11 \pm 0.06 \leq \mathrm{Re}\rho_{20} \leq 0.13 \pm 0.06$
$\mathrm{Re}\rho_{21} = 0.00^{+0.07}_{-0.04}$	$-0.13 \pm 0.04 \leq \mathrm{Re}\rho_{21} \leq 0.15 \pm 0.04$
$\mathrm{Re}\rho_{2-1} = 0.00^{+0.05}_{-0.08}$	$\mathrm{Re}\rho_{2-1} = 0.00 \pm 0.06$
$\rho_{2-2} = 0.00 \pm 0.07$	$\rho_{2-2} = 0.00 \pm 0.07$

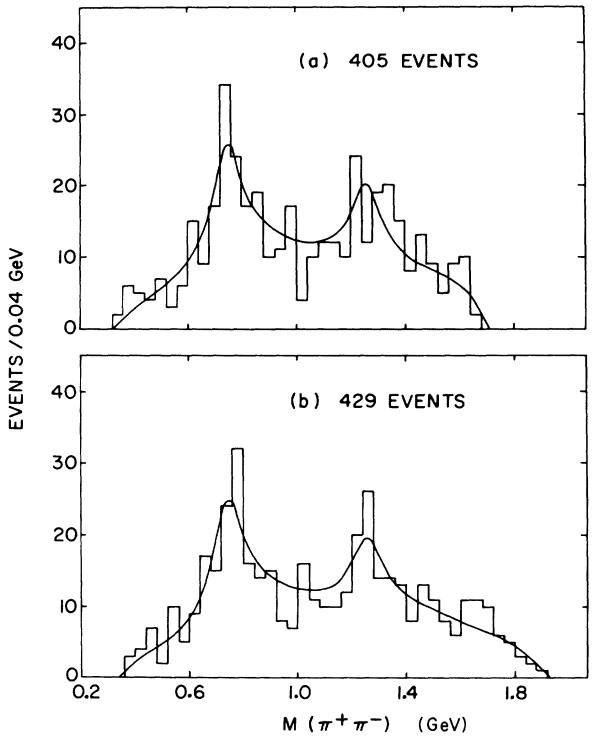

FIG. 71. $\pi^+\pi^-$ effective-mass distribution from the reaction $K^-p \to \Sigma^0\pi^+\pi^-$: (a) at 3.9 GeV/$c$; (b) at 4.6 GeV/$c$.

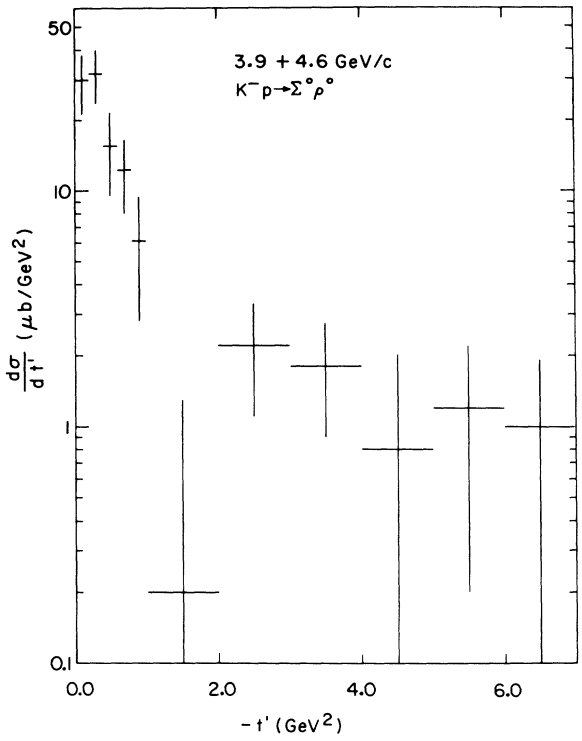

FIG. 72. Differential cross section for reaction $K^-p \to \Sigma^0\rho^0$ for the combined data at 3.9 and 4.6 GeV/c.

following values for the mass and width of the ρ:

$M = 756 \pm 9$ MeV,

$\Gamma = 157 \pm 22$ MeV.

The number of ρ^0 events and the corrected cross section obtained from fits to the $\pi^+\pi^-$ effective-mass spectrum at each momentum are

3.9 GeV/c: 96 ± 18 events; $\sigma = 32 \pm 6$ μb,

4.6 GeV/c: 100 ± 18 events; $\sigma = 23 \pm 4$ μb.

The differential cross section for the combined 3.9- and 4.6-GeV/c data is shown in Fig. 72 and listed in Table XXIX and was obtained by normalizing the number of background-subtracted events in the ρ^0 region to the weighted average of the 3.9- and 4.6-GeV/c cross sections quoted above. We observe evidence of a forward slope in the $d\sigma/d(t')$ distribution with a fitted slope parameter of

3.9+4.6 GeV/c: $A = 1.9 \pm 0.5$ GeV^{-2},

in good agreement with the corresponding value obtained in the $K^-p \to \Lambda\rho^0$ reaction. As observed in Fig. 72 there is no significant evidence for backward ρ^0 production recoiling off the Σ^0. Fits to the backward ($\cos\theta^* < 0.0$) mass spectrum at 3.9 (4.6) GeV/c (not shown) give 20 ± 11 events (18 ± 8 events) corresponding to a corrected cross section of 6.6 ± 3.6 μb (4.1 ± 2.5 μb).

The density-matrix elements were obtained in the manner described in Sec. III B 1 b; however, because of the severe reflection of low-lying $\Sigma^0\pi^+$ resonances only half the Dalitz plot was used. The values of the density-matrix elements for the ρ^0 produced with $|t'| < 1.0$ GeV^2 are given in Table XXX for combined data at 3.9 and 4.6 GeV/c.

TABLE XXIX. Differential cross section for reaction $K^-p \to \Sigma^0\rho^0$ at 3.9 and 4.6 GeV/c.

$\lvert t' \rvert$ interval (GeV^2)	No. of ρ^0 events[a]	Corrected[b] $d\sigma/d\lvert t' \rvert$ (μb/GeV^2)
0.0–0.2	29 ± 8	29.5 ± 8.4
0.2–0.4	31 ± 8	31.5 ± 7.9
0.4–0.6	15 ± 6	15.3 ± 5.8
0.6–0.8	12 ± 4	12.2 ± 4.3
0.8–1.0	6 ± 3	6.1 ± 3.3
1.0–2.0	1 ± 5	0.2 ± 1.1
2.0–3.0	11 ± 5	2.2 ± 1.1
3.0–4.0	9 ± 4	1.8 ± 0.9
4.0–5.0	4 ± 6	0.8 ± 1.2
5.0–6.0	6 ± 5	1.2 ± 1.0
6.0–7.0	5 ± 4	1.0 ± 0.9

[a] In the region $0.64 \leq M(\pi^+\pi^-) \leq 0.88$ GeV.

[b] Normalized to the weighted average cross sections as quoted in the text.

TABLE XXX. ρ density-matrix elements from reaction $K^-p \to \Sigma^0\rho^0$ for $|t'| < 1.0$ GeV^2.

	Jackson	Helicity
ρ_{00}	$0.02^{+0.08}_{-0.02}$	0.06 ± 0.07
ρ_{1-1}	0.23 ± 0.05	0.30 ± 0.07
$\mathrm{Re}\rho_{10}$	0.05 ± 0.05	-0.01 ± 0.05

The Σ^0 polarization was obtained by parametrizing the mass dependence of the $N\langle\cos\theta_1 \cos\theta_2\rangle$ moment using a method similar to that employed to extract the Λ polarization in the $K^-p \to \Lambda\rho^0$ reaction. Here, $\cos\theta_1$ is the cosine of the angle between the normal to the production plane (defined as incident proton cross outgoing Σ^0 direction in the over-all center-of-mass system) and the outgoing Λ direction in the Σ^0 rest frame; $\cos\theta_2$ is the cosine of the angle between the outgoing Λ direction in the Σ^0 rest frame and the direction of the outgoing proton in the Λ rest frame. The Σ^0 polarization is related to the magnitude of this moment, C, associated with the ρ^0 [in the region $0.64 \leq M(\pi^+\pi^-) \leq 0.88$ GeV] through the following equation:

$$P_\Sigma = -9C/\alpha_\Lambda N_\rho ,$$

where $\alpha_\Lambda = 0.645$ and N_ρ is the number of ρ events obtained from fits to the mass spectra (in the same mass region as defined above).

We find in the region $|t'| < 1.0$ GeV^2 the value

$$P_\Sigma = 0.03 \pm 0.56$$

whose small value reflects the fact that there is no evidence for a ρ^0 Breit-Wigner shape in the $N\langle\cos\theta_1 \cos\theta_2\rangle$ mass distribution.

In Sec. VII we will further compare the $K^-p \to \Lambda\rho$ and $K^-p \to \Sigma^0\rho$ reactions.

B. Reaction $K^-p \to \Sigma^0\phi$

The K^+K^- mass spectrum from reaction 8, $\Sigma^0K^+K^-$, is shown in Figs. 73(a) [73(b)] for the 3.9- [4.6-] GeV/c data in which clear signals for ϕ-meson production are observed. The insert in Fig. 73(a) shows the distribution of the angle between the normal to the Σ^0 production plane and the outgoing Λ for the events of reaction 8; as expected for Σ^0 events this distribution is consistent with being isotropic and provides evidence for the clean separation between the ΛK^+K^- and $\Sigma^0K^+K^-$ hypothesis.

The number of $\phi \to K^+K^-$ events estimated from the mass spectra of Fig. 73(a) [73(b)] and the corrected $K^-p \to \Sigma^0\phi$ [$\to K^+K^-$] cross sections are

3.9 GeV/c: 46 ± 7 events; 15 ± 3 μb,

4.6 GeV/c: 38 ± 6 events; 9 ± 2 μb.

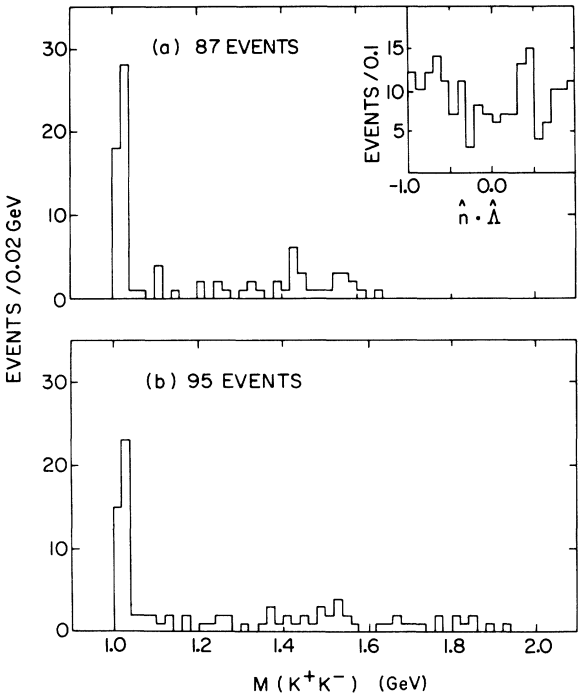

FIG. 73. K^+K^- effective-mass spectrum from the reaction $K^-p \to \Sigma^0K^+K^-$: (a) at 3.9 GeV/c; (b) at 4.6 GeV/c. The insert is the distribution of the angle between the normal to the production plane and the outgoing Λ in the Σ^0 rest frame for the combined 3.9- and 4.6-GeV/c sample.

After correction for the unobserved $K_1^0K_2^0$ and $\pi^+\pi^-\pi^0$ decay modes,[38] the $K^-p \to \Sigma^0\phi$ cross sections were obtained:

3.9 GeV/c: $\sigma = 33 \pm 7$ μb,

4.6 GeV/c: $\sigma = 20 \pm 5$ μb.

The differential cross sections for the reaction $K^-p \to \Sigma^0\phi$ ($\to K\bar{K}$) are listed in Table XXXI and shown in Fig. 74 for the combined 3.9- and 4.6-GeV/c data. The slope parameter A obtained from a fit to the $d\sigma/d|t'|$ distribution of Fig. 74 for the region $|t'| \leq 1.2$ GeV^2 was found to be

TABLE XXXI. Differential cross section for reaction $K^-p \to \Sigma^0\phi$ ($\to K\bar{K}$) for 3.9 and 4.6 GeV/c.

$\lvert t'\rvert$ interval (GeV^2)	No. of ϕ events	Corrected $d\sigma/d\lvert t'\rvert$ (μb/GeV^2)
0.0–0.2	17 ± 4	21.5 ± 5.1
0.2–0.4	15 ± 4	18.9 ± 4.9
0.4–0.6	15 ± 4	18.9 ± 4.9
0.6–0.8	10 ± 3	12.7 ± 4.0
0.8–1.2	12 ± 3	7.6 ± 2.3
1.2–1.6	10 ± 3	6.2 ± 2.1
1.6–2.2	3 ± 2	1.3 ± 0.8

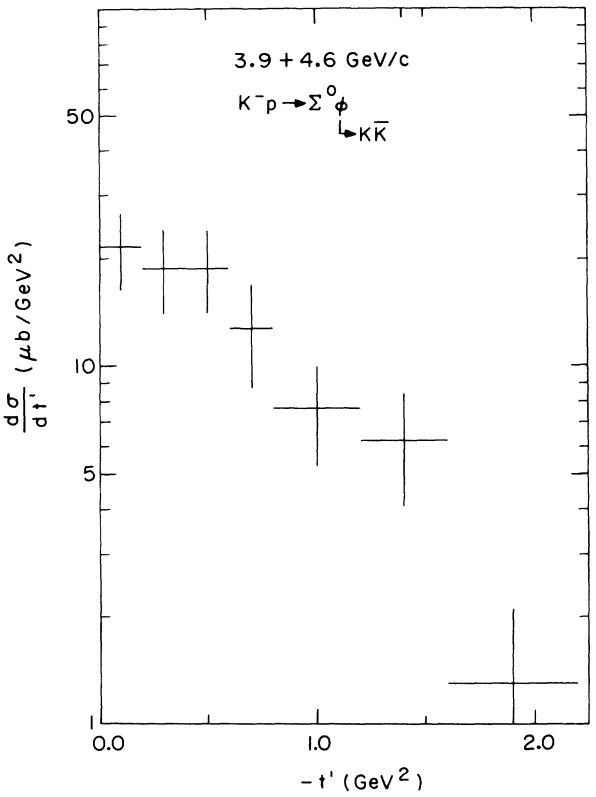

FIG. 74. Differential cross section for reaction $K^-p \to \Sigma^0\phi(\to K\bar{K})$ for the combined data at 3.9 and 4.6 GeV/c.

$$A = 1.1 \pm 0.4 \text{ GeV}^{-2},$$

which is about 2 standard deviations smaller than the values obtained in the reaction $K^-p \to \Lambda\phi$.

The density-matrix elements obtained from a maximum-likelihood fit to the events in the ϕ region employing a simple P-wave decay angular distribution are shown in Fig. 75 and listed in Table XXXII. In the forward momentum transfer region ($|t'| < 0.5$ GeV^2) we observe the dominant contribution of the natural-parity exchange ($\rho_{00} \approx 0.0$; $\rho_{1-1} \approx 0.5$), and, as will be more fully discussed later, the values of the density matrices are different from those obtained in the $K^-p \to \Lambda\phi$ reaction.

The Σ^0 polarization listed in Table XXXII was obtained through a maximum-likelihood fit using the following form for the decay angular distribution:

$$W(\cos\theta_1, \cos\theta_2) \sim 1.0 - \alpha_\Lambda P_\Sigma \cos\theta_1 \cos\theta_2,$$

where $\alpha_\Lambda = 0.645$ and $\cos\theta_1$ and $\cos\theta_2$ are defined as in the $\Sigma^0\rho^0$ section. We observe that the baryon polarization in the reaction $K^-p \to \Sigma^0\phi$ is large and positive in contrast to the negative polarization found in the $K^-p \to \Lambda\phi$ reaction.

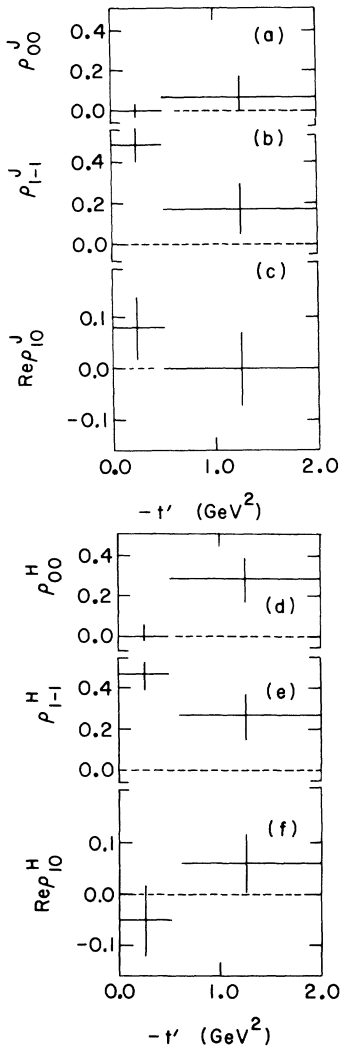

FIG. 75. Density-matrix elements of the ϕ produced in the reaction $K^-p \to \Sigma^0\phi$: (a)–(c) Jackson frame; (d)–(f) helicity frame.

TABLE XXXII. ϕ density-matrix elements and Σ^0 polarization from reaction $K^-p \to \Sigma^0\phi$.

$\lvert t'\rvert$ interval (GeV^2)	No. of ϕ events	Jackson frame			Helicity frame			
		ρ_{00}	ρ_{1-1}	$\mathrm{Re}\rho_{10}$	ρ_{00}	ρ_{1-1}	$\mathrm{Re}\rho_{10}$	P_Σ
0.0–0.5	40	$0.00^{+0.02}_{-0.00}$	$0.48^{+0.02}_{-0.08}$	0.08 ± 0.06	$0.00^{+0.03}_{-0.00}$	$0.46^{+0.04}_{-0.06}$	-0.05 ± 0.07	$1.0^{+0.0}_{-0.45}$
0.5–2.0	40	0.06 ± 0.10	0.16 ± 0.11	0.00 ± 0.07	0.28 ± 0.11	0.26 ± 0.11	0.06 ± 0.06	$1.0^{+0.0}_{-0.50}$

C. Reaction $K^-p \to \Sigma^0 f^0$

The $\pi^+\pi^-$ effective-mass spectrum at 3.9 and 4.6 GeV/c has already been shown (Fig. 71). The fit to these mass spectra, in which clear evidence for f^0 production is observed, gives the following values for the mass and width of the f^0 meson:

$M = 1265 \pm 16$ MeV,

$\Gamma = 141 \pm 35$ MeV.

The number of f^0 events and the corresponding corrected cross sections obtained from the fits are

3.9 GeV/c: 50 ± 18 events; $\sigma = 25 \pm 9$ μb,

4.6 GeV/c: 43 ± 16 events; $\sigma = 15 \pm 5$ μb.

There is no strong evidence for backward f^0 production with the number of events obtained from fits to the appropriate mass spectra being

3.9 GeV/c: 0 ± 12 events; $\sigma = 0 \pm 6$ μb,

4.6 GeV/c: 14 ± 9 events; $\sigma = 5 \pm 3$ μb.

The small statistics in this channel preclude any further investigation of the f^0 production properties.

D. Reaction $K^-p \to \Sigma^0 f'$

From fits to the combined K^+K^- and $K_1^0K_1^0$ effective-mass spectrum of reactions 8 and 14 using a D-wave Breit-Wigner function with mass and width fixed at the values obtained in Sec. III C 3 a, the number of f' events and the corrected cross section were found to be

3.9 GeV/c: 0 ± 7 events; $\sigma = 0 \pm 2.5$ μb,

4.6 GeV/c: 16 ± 6 events; $\sigma = 5.3 \pm 2.0$ μb.

The limited statistics preclude any further studies.

V. STUDY OF REACTIONS $K^-p \to Y^*(1385)$ +MESON

A. Reaction $K^-p \to Y^{*+}(1385)\pi^-$

1. *Mass and Width; Branching Ratios*

The data for this final state come from reaction 3. In Fig. 76 we show the $\Lambda\pi^+$ effective-mass spectrum for a subsample of best resolution events (average $\sigma = 3.1$ MeV). The indicated curve is a fit to this mass spectrum with an energy-dependent width Breit-Wigner shape (resolution folded) multiplying phase space plus a linear form in the mass as background.[39] This yields the following parameters for the $Y^{*+}(1385)$:

$M = 1382.0 \pm 2.0$ MeV,

$\Gamma = 32.5 \pm 6.0$ MeV.

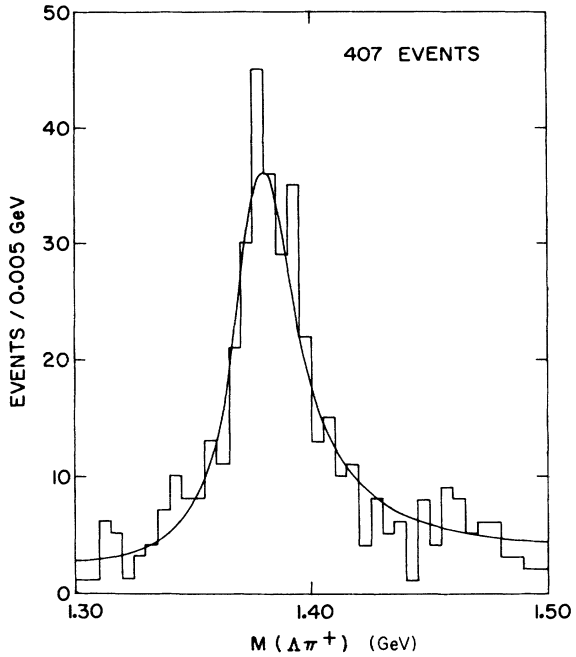

FIG. 76. $\Lambda\pi^+$ effective-mass spectrum for best resolution events from reaction 2. The curve is a result of the fit described in the text.

The total $\Lambda\pi^+$ effective-mass spectra at 3.9 and 4.6 GeV/c are shown in Figs. 77(a) and 77(b), respectively. Performing fits with an energy-dependent width Breit-Wigner form multiplying phase space with mass and width fixed at the values given above, and a polynomial in the mass as background, we have obtained the following number of resonance events:

218 ± 14 at 3.9 GeV/c,

252 ± 18 at 4.6 GeV/c.

The $\Sigma\pi/\Lambda\pi$ branching ratio of the $Y^*(1385)$ was determined from a comparison of the $\Lambda\pi^+$ and $\Sigma^0\pi^+$ mass spectra for the combined sample at 3.9 and 4.6 GeV/c. The latter distribution is shown as an insert in Fig. 77(a) in which a small but significant $Y^{*+}(1385)$ signal is observed. Also apparent is a small contamination of $Y^{*+}(1385) \to \Lambda^0\pi^+$ events into reaction 7, which causes a peak in the $\Sigma^0\pi^+$ mass spectrum around 1.45 GeV. The number of $Y^{*+}(1385) \to \Sigma^0\pi^+$ events obtained from this mass spectrum was found to be 35 ± 15. After correction for the 5% probability selection in reaction 7, the following branching ratio was obtained:

$$\frac{Y^*(1385) \to \Sigma\pi}{Y^*(1385) \to \Lambda\pi} = 0.16 \pm 0.07,$$

which is in good agreement with the world-averaged value of 0.10 ± 0.03.[7]

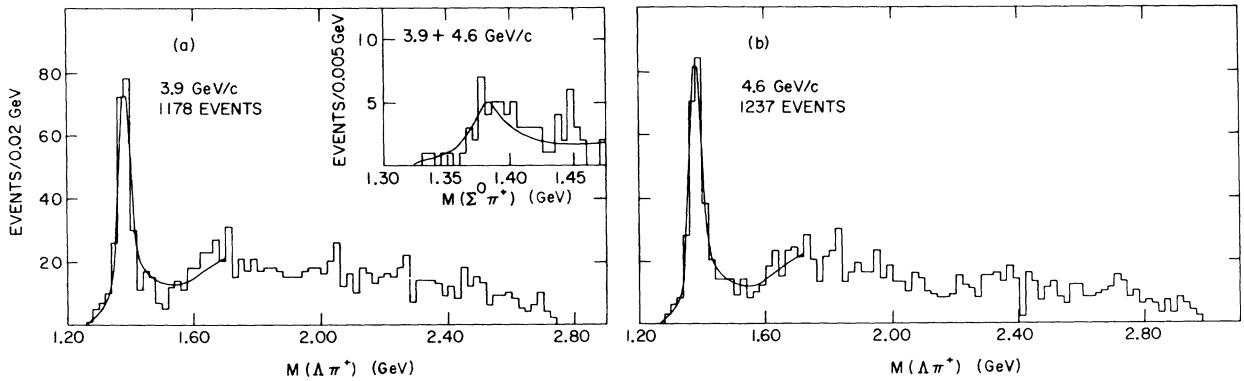

FIG. 77. $\Lambda\pi^+$ effective-mass distribution from the reaction $K^-p \to \Lambda\pi^+\pi^-$: (a) at 3.9 GeV/$c$; (b) at 4.6 GeV/$c$. The insert shows the $\Sigma^0\pi^+$ effective-mass spectrum for the combined data at 3.9 and 4.6 GeV/c from the reaction $K^-p \to \Sigma^0\pi^+\pi^-$.

2. *Total and Differential Cross Sections*

After correction for Λ visibility and losses, and folding in the $\Sigma\pi/\Lambda\pi$ branching fraction, the total cross sections for the reaction $K^-p \to Y^{*+}(1385)\pi^-$ were obtained and are

3.9 GeV/c: $\sigma = 79 \pm 8$ μb,

4.6 GeV/c: $\sigma = 63 \pm 6$ μb.

The differential cross sections were obtained by a background-subtraction technique using events in adjacent control regions from those in the $Y^{*+}(1385)$ region defined as

$$1.34 \leq M(\Lambda\pi^+) \leq 1.42 \text{ GeV}.$$

The numbers of events thus obtained were then normalized to the total $Y^{*+}(1385)$ cross sections given above. The differential cross sections are shown in Figs. 78(a) and 78(b) and are listed in Table XXXIII. At both momenta we observe evidence for a forward dip in the differential cross section. The slope parameters obtained from fits to these distributions excluding the forward dip region were found to be

3.9 GeV/c: $A = 3.0 \pm 0.5$ GeV^{-2},

4.6 GeV/c: $A = 3.9 \pm 0.6$ GeV^{-2}.

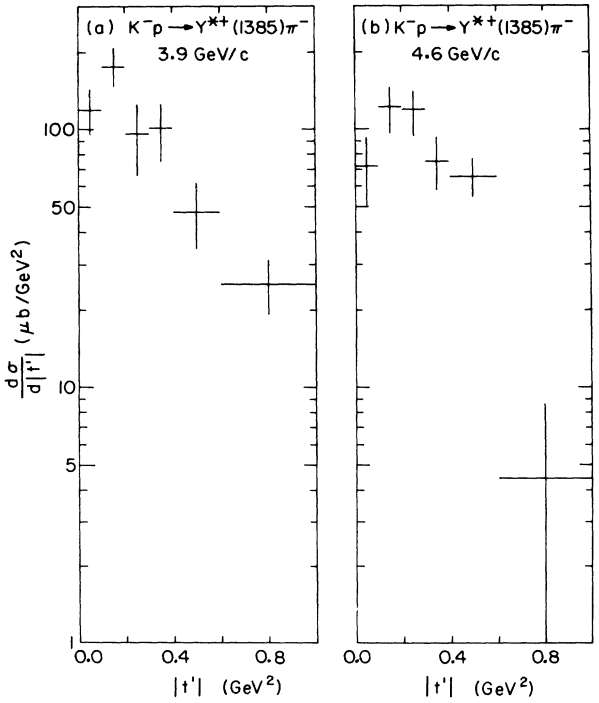

FIG. 78. Differential cross section for reaction $K^-p \to Y^{*+}(1385)\pi^-$: (a) at 3.9 GeV/$c$; (b) at 4.6 GeV/$c$.

3. *Decay Correlations*

We now discuss the method we have employed to extract the $Y^{*+}(1385)$ density-matrix elements. As in the case of ρ^0 production, described previously, we use a mass-dependent analysis which explicitly takes into account the background under

TABLE XXXIII. Differential cross section for reaction $K^-p \to Y^{*+}\pi^-$.

$\lvert t'\rvert$ interval (GeV^2)	3.9 GeV/c No. of $Y(1385)$ events[a]	3.9 GeV/c Corrected $\frac{d\sigma}{dt'}\left(\frac{\mu b}{GeV^2}\right)$	4.6 GeV/c No. of $Y(1385)$ events[a]	4.6 GeV/c Corrected $\frac{d\sigma}{dt'}\left(\frac{\mu b}{GeV^2}\right)$
0.0–0.1	25 ± 5	118 ± 25	20 ± 6	71 ± 21
0.1–0.2	37 ± 7	175 ± 31	34 ± 7	120 ± 26
0.2–0.3	20 ± 6	95 ± 30	33 ± 7	117 ± 24
0.3–0.4	21 ± 5	100 ± 26	21 ± 5	74 ± 18
0.4–0.6	20 ± 6	47 ± 14	37 ± 7	65 ± 12
0.6–1.0	21 ± 5	25 ± 6	5 ± 5	4.4 ± 4.1
1.0–2.0	3 ± 3	1.4 ± 1.4	13 ± 4	1.6 ± 1.4
2.0–3.0	6 ± 4	2.8 ± 1.9	0	0
3.0–4.0	5 ± 3	2.4 ± 1.2	1 ± 1	0.4 ± 0.4
4.0–5.0	2 ± 4	0.9 ± 1.8	3 ± 3	1.1 ± 1.1
5.0–6.0	...	...	3 ± 3	1.1 ± 0.9
6.0–7.0	...	...	2 ± 3	0.7 ± 1.1

[a]In the region $1.34 \leq M(\Lambda\pi^+) \leq 1.42$ GeV.

TABLE XXXIV. Density-matrix elements of $Y^{*+}(1385)$ from reaction $K^-p \to Y^{*+}(1385)\pi^-$.

$\lvert t'\rvert$ Interval (GeV^2)	Events[a]	Resonance events[a]	Jackson frame ρ_{33}	Jackson frame $\mathrm{Re}\rho_{31}$	Jackson frame $\mathrm{Re}\rho_{3-1}$	Helicity frame ρ_{33}	Helicity frame $\mathrm{Re}\rho_{31}$	Helicity frame $\mathrm{Re}\rho_{3-1}$
0.0–0.1	67	60± 5	0.29± 0.07	0.11± 0.08	0.22± 0.07	0.44± 0.06	0.09± 0.05	0.13± 0.09
0.1–0.2	100	91± 5	0.21± 0.06	−0.09± 0.06	0.16± 0.06	0.27± 0.06	0.13± 0.05	0.12± 0.06
0.2–0.3	91	80± 6	0.28± 0.06	−0.05± 0.04	$0.24^{+0.01}_{-0.06}$	0.40± 0.04	0.06± 0.06	0.19± 0.06
0.3–0.4	56	53± 4	0.36± 0.08	0.01± 0.06	$0.22^{+0.03}_{-0.04}$	0.38± 0.07	−0.01± 0.06	$0.22^{+0.03}_{-0.08}$
0.4–0.6	81	75± 5	0.31± 0.06	−0.05± 0.05	$0.23^{+0.02}_{-0.06}$	0.40± 0.05	0.06± 0.06	0.19± 0.06
0.6–1.0	52	41± 5	0.37± 0.06	0.01± 0.08	$0.21^{+0.04}_{-0.06}$	0.39± 0.09	−0.03± 0.07	$0.20^{+0.05}_{-0.09}$

[a]In the region $1.30 \leq M(\Lambda\pi^+) \leq 1.50$ GeV.

the resonance. The probability function used in our maximum-likelihood fit for the 3.9- and 4.6-GeV/c combined data may be written as

$$M(\theta, \phi, m) = \alpha \lvert f_P(m)\rvert^2 W(\cos\theta, \phi) + (1-\alpha)(a + bm),$$

where α is the fraction of resonance events in the fitted region, $1.3 \leq m(\Lambda\pi^+) \leq 1.5$ GeV; $f_P(m)$ is the Breit-Wigner amplitude for the $Y^{*+}(1385)$; a and b are coefficients of the linear background in the fitted region assumed to have no θ, ϕ dependence, and the angular distribution of the $Y^{*+}(1385)$, $W(\cos\theta, \phi)$, evaluated in either the Jackson or helicity frame, is given in terms of the density-matrix elements $\rho_{2m,2m'}$:

$$W(\cos\theta, \phi) = \frac{3}{4\pi}\left[\rho_{33}\sin^2\theta + \rho_{11}(\tfrac{1}{3} + \cos^2\theta) - \frac{2}{\sqrt{3}}\mathrm{Re}\rho_{3-1}\sin^2\theta\cos 2\phi - \frac{2}{\sqrt{3}}\mathrm{Re}\rho_{31}\sin 2\theta\cos\phi\right],$$

where the spin-$\frac{3}{2}$ positivity conditions demand that[40]

$$(\mathrm{Re}\rho_{31})^2 + (\mathrm{Re}\rho_{3-1})^2 \leq \rho_{33}\rho_{11}.$$

A moment analysis across the $Y^{*+}(1385)$ region, extending into the adjacent background regions, revealed no significant evidence for interference or nonresonance moments, which justified our assumption for the background parametrization. The density-matrix elements obtained in this manner were required to satisfy the spin-$\frac{3}{2}$ positivity condition and are listed in Table XXXIV and shown in Figs. 79(a)–79(f), in which we have indicated the predictions of the Stodolsky-Sakurai model[41] (dotted line). The model is seen to give a poor description of the experimentally determined ρ_{33} density-matrix element in the small momentum-transfer region of $Y^{*+}(1385)$ production. In order to investigate the significance of this discrepancy,

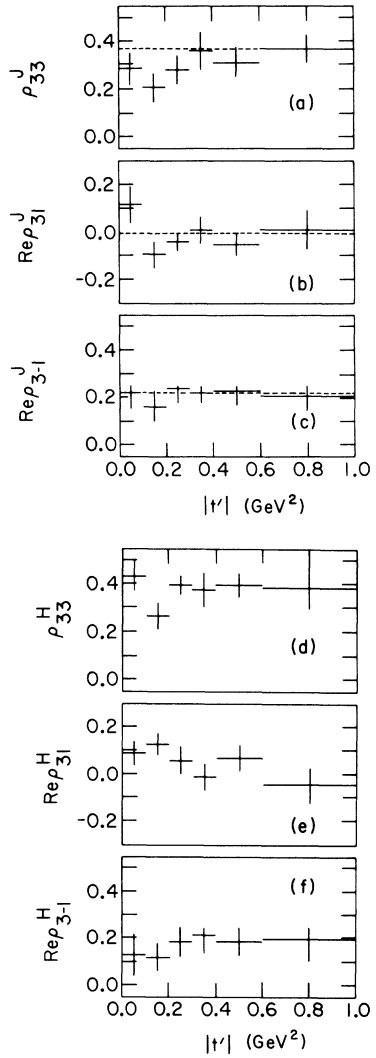

FIG. 79. Density-matrix elements of the $Y^{*+}(1385)$ produced in the reaction $K^-p \to Y^{*+}(1385)\pi^-$: (a)–(c) Jackson frame; (d)–(f) helicity frame. The dotted lines represent the predictions of the Stodolsky-Sakurai model.

we have performed a maximum-likelihood fit on the events for $|t'|<0.3$ GeV^2 and we find

$$\rho_{33}=0.278\pm0.023 \quad (0.375),$$

$$\mathrm{Re}\rho_{3-1}=0.242^{+0.008}_{-0.021} \quad (0.216),$$

$$\mathrm{Re}\rho_{31}=-0.026\pm0.034 \quad (0.00),$$

where the Stodolsky-Sakurai predictions[41] are indicated in parentheses. The resultant χ^2 is 19.9 for 3 degrees of freedom, which represents about a 4-standard-deviation disagreement[42] with theory in the small momentum-transfer region. It should also be noted that the additivity quark model[43] also gives the Stodolsky-Sakurai predictions, so that it seems to be similarly violated.

B. Reaction $K^-p\to Y^{*-}(1385)\pi^+$

The $\Lambda\pi^-$ effective-mass spectrum from reaction 1 is shown in Fig. 80(a) [80(b)] for the 3.9- [4.6-] GeV/c sample in which evidence for $Y^{*-}(1385)$ production is observed. We have fitted these distributions and obtained the number of events of the reaction $K^-p\to Y^{*-}(1385)\pi^+$:

3.9 GeV/c: 40 ± 11 events; $\sigma=14\pm4$ μb,

4.6 GeV/c: 20 ± 8 events; $\sigma=5\pm2$ μb,

where σ includes corrections for probability cuts, and Λ visibility and losses, as well as for the $\Sigma\pi$ decay mode.

The shaded area in Fig. 80(a) [80(b)] represents the $\Lambda\pi^-$ effective mass spectrum for events produced with $\cos(K^-,\pi^+)\geq 0$. For the 3.9-GeV/c sample a small signal from $Y^{*-}(1385)$ production is observed. A simple count of the number of resonance events over a smooth background curve yields

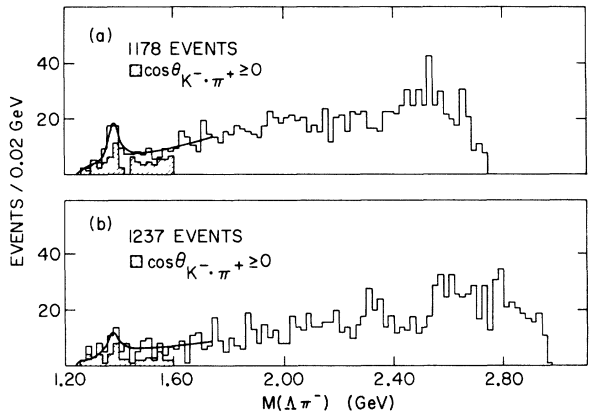

FIG. 80. $\Lambda\pi^-$ effective-mass distribution from the reaction $K^-p\to\Lambda\pi^-\pi^+$: (a) at 3.9 GeV/c; (b) at 4.6 GeV/c. The shaded area is for events in the "exotic" region $\cos\theta(K^-,\pi^+)\geq 0.0$.

3.9 GeV/c: 11 ± 4 events; $\sigma=4.0\pm1.5$ μb,

4.6 GeV/c: 6 ± 3 events; $\sigma=1.5\pm0.8$ μb.

The small number of events in this channel does not allow further investigation which could associate the $Y^{*-}(1385)$ events [produced with $\cos(K^-,\pi^+)\geq 0$] with exotic $Q=2$ t-channel exchange.

C. Reaction $K^-p\to Y^*(1385)\rho$

1. *Total and Differential Cross Sections*

We first investigate the reaction

$$K^-p\to Y^{*+}(1385)\rho^-. \qquad \text{(a)}$$

The $M(\Lambda\pi^+)$-vs-$M(\pi^-\pi^0)$ scatter plot for the combined data at 3.9 and 4.6 GeV/c is displayed in Fig. 11 (after removal of events in the narrow ω band) in which a strong accumulation of events in

TABLE XXXV. Differential cross sections for reaction $K^-p\to Y^{*+}\rho^-$.

$\lvert t'\rvert$ interval (GeV^2)	3.9 GeV/c No. of $Y(1385)\rho^-$ events[a]	3.9 GeV/c Corrected $\frac{d\sigma}{dt'}\left(\frac{\mu\mathrm{b}}{\mathrm{GeV}^2}\right)$[b]	4.6 GeV/c No. of $Y(1385)\rho^-$ events[a]	4.6 GeV/c Corrected $\frac{d\sigma}{dt'}\left(\frac{\mu\mathrm{b}}{\mathrm{GeV}^2}\right)$[b]
0.0–0.1	29± 8	149 ±41	33± 8	130 ±32
0.1–0.2	28± 7	144 ±36	18± 6	71 ±24
0.2–0.4	25± 7	64 ±18	24± 7	47 ±14
0.4–0.6	12± 6	31 ±15	13± 6	26 ±12
0.6–0.8	14± 6	36 ±15	19± 6	38 ±12
0.8–1.0	9± 5	23 ±13	4± 4	7.9± 7.9
1.0–2.0	15± 8	7.7± 4.1	10± 6	3.9± 2.4
2.0–3.0	10± 7	5.1± 3.6	4± 4	1.6± 1.6
3.0–4.0	19± 7	9.8± 3.6	7± 5	2.8± 2.0
4.0–5.0	12± 5	6.2± 2.6	7± 5	2.8± 2.0
5.0–6.0	···		9± 6	3.6± 2.4
6.0–7.0	···		4± 2	1.6± 0.8

[a]Obtained from background-subtraction technique described in text.
[b]Obtained by normalizing number of events to total $Y^{*+}\rho^-$ cross section.

the Y^{*+}-ρ^- overlap region is observed. We now describe the method used to extract the number of events of reaction (a) at the two momenta. The $\Lambda\pi^+$ (or $\pi^-\pi^0$) effective-mass spectrum was divided into 0.04-GeV (or 0.08-GeV) mass slices and the corresponding $\pi^-\pi^0$ (or $\Lambda\pi^+$) effective-mass spectrum was fitted in our usual manner to determine the number of ρ^- (or $Y^{*+}(1385)$) events. The resulting distribution of the number of resonance ρ^- ($Y^{*+}(1385)$) events is shown in Figs. 81(a) and 81(c) [81(b) and 81(d)] for the 3.9- and 4.6-GeV/c samples, respectively. These distributions were then fitted with linear backgrounds in the mass plus $Y^{*+}(1385)$ (ρ^-) Breit-Wigner shapes. The number of events thus obtained from the two methods (i.e., the fit to the $\Lambda\pi^+$ or $\pi^-\pi^0$ spectrum) differed by less than 1 standard deviation. We note that this method adequately takes into account the events in the resonance Y^{*+} and ρ^- tails. The number of events[44] and the corrected cross sections for reaction (a) obtained in this manner are

3.9 GeV/c: 242 ± 22 events; $\sigma = 92 \pm 8$ μb,

4.6 GeV/c: 237 ± 39 events; $\sigma = 62 \pm 10$ μb.

In order to obtain the differential cross sections at the two momenta, where the limited number of events in each $|-t'|$ bin did not allow for the more accurate treatment described above, we have used a background-subtraction technique[45] and normalized the numbers to the total cross sections given above. The differential cross section for reaction (a) at 3.9 [4.6] GeV/c is shown in Fig. 82(a) [82(b)] and listed in Table XXXV. The slope parameters were found to be (in the interval $|t'| < 1.0$ GeV^2)

3.9 GeV/c: 2.7 ± 0.8 GeV^{-2},

4.6 GeV/c: 2.7 ± 0.7 GeV^{-2},

whose values are similar to the slopes found in the reactions $K^-p \to \Lambda\rho^0$ and $K^-p \to \Sigma^0\rho^0$.

2. *Isospin Exchange in the t Channel: Comparison of $Y^{*0}\rho^0$, $Y^{*+}\rho^-$, and $Y^{*-}\rho^+$ Final States*

It is of general interest to investigate the isospin exchange in the reactions $K^-p \to Y^*\rho$. The neces-

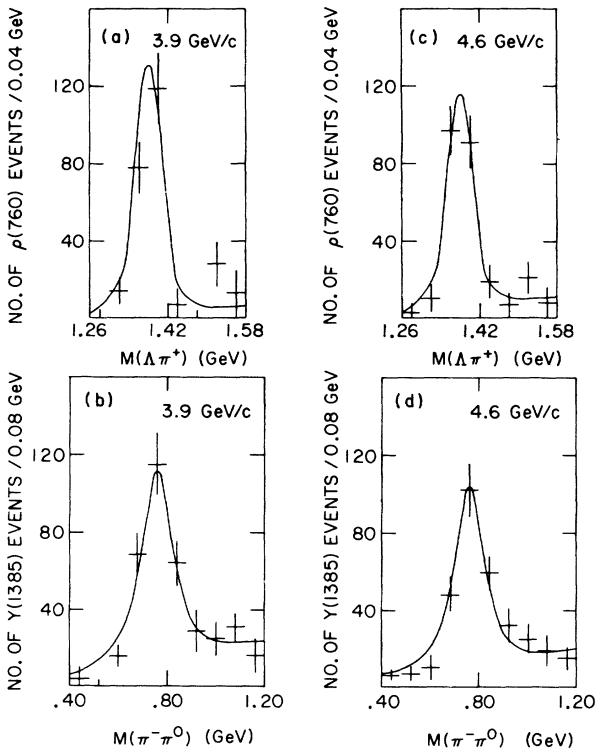

FIG. 81. (a) Distribution of the number of ρ^- events as a function of $\Lambda\pi^+$ effective mass from the reaction $K^-p \to \Lambda\pi^+\pi^-\pi^0$ at 3.9 GeV/c after removal of events in the ω region. (b) Distribution of the number of $Y^{*+}(1385)$ events as a function of $\pi^-\pi^0$ effective mass from the reaction $K^-p \to \Lambda\pi^+\pi^-\pi^0$ at 3.9 GeV/c after removal of events in the ω region. (c) Same as (a) but at 4.6 GeV/c. (d) Same as (b) but at 4.6 GeV/c.

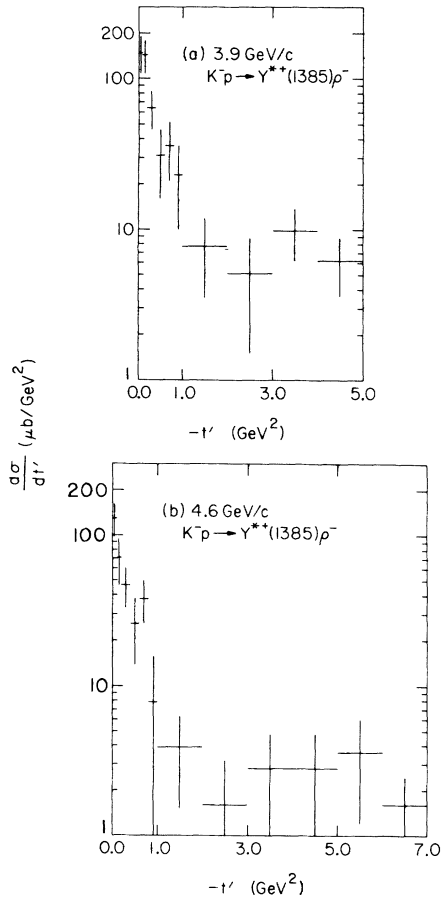

FIG. 82. Differential cross section for reaction $K^-p \to Y^{*+}(1385)\rho^-$: (a) at 3.9 GeV/$c$; (b) at 4.6 GeV/$c$.

TABLE XXXVI. Comparison of number of $Y^*\rho$ events (for $|t'|<1.0$ GeV^2).

Reaction	No. of events[a]	Predicted No. of events[b]
	3.9 GeV/c	
$K^-p\to Y^{*+}\rho^-$	117±16	117±16
$K^-p\to Y^{*0}\rho^0$	16±12	29± 4
$K^-p\to Y^{*-}\rho^+$	−9±10	0
	4.6 GeV/c	
$K^-p\to Y^{*+}\rho^-$	111±16	111±16
$K^-p\to Y^{*0}\rho^0$	14±12	28± 4
$K^-p\to Y^{*-}\rho^+$	9± 9	0

[a] Number of events obtained by background-subtraction technique as described in text.

[b] Based on number of events found in $K^-p\to Y^{*+}\rho^-$ and assuming only $I=\frac{1}{2}$ exchange in the t channel (i.e., no exotic exchange).

sary further information comes from the quasi-two-body reactions

$$K^-p\to Y^{*0}(1385)\rho^0 \qquad \text{(b)}$$

and

$$K^-p\to Y^{*-}(1385)\rho^+ . \qquad \text{(c)}$$

The scatter plot of $M(\Lambda\pi^0)$ vs $M(\pi^+\pi^-)$ is shown in Fig. 12 in which evidence for production of (b) is observed. The number of events obtained from our background-subtraction technique and the cross section corrected for the events lying in the ρ and Y^* tails[46] for reaction (b) was found to be

3.9 GeV/c: 56±17 events; $\sigma=19\pm6$ μb,

4.6 GeV/c: 35±18 events; $\sigma=9\pm5$ μb.

The corresponding scatter plot of $M(\Lambda\pi^-)$ vs $M(\pi^+\pi^0)$ is shown in Fig. 13. No significant evidence for reaction (c) is observed with the background-subtraction technique[46] giving

3.9 GeV/c: 30±17 events; $\sigma=10\pm6$ μb,

4.6 GeV/c: 0±16 events; $\sigma=0\pm4$ μb.

We have introduced reactions (b) and (c) in order to compare their relative cross section with that of reaction (a). We note that if only $I=\frac{1}{2}$ t-channel exchange is allowed we would expect the ratio of these cross sections to be

$$\sigma(a):\sigma(b):\sigma(c)=4:1:0.$$

In Table XXXVI, we have compared the number of events in the peripheral region ($|t'|<1.0$ GeV^2) obtained from our background-subtraction technique for reactions (a)–(c) for the combined 3.9- and 4.6-GeV/c sample. We find that good agreement is obtained between the observed number of events and that expected from only $I=\frac{1}{2}$ (with no $I=\frac{3}{2}$) t-channel exchange.

3. *Decay Distributions*

The method used to extract the $Y^{*+}(1385)$ and ρ^- density-matrix elements follows that described in the $\Lambda\rho^0$ and $Y^{*+}(1385)\pi^-$ sections, in which we tried to take explicitly into account the background under the resonances. This was accomplished here by taking a ρ^- (or Y^{*+}) mass slice defined by $0.66\leq M(\pi^-\pi^0)\leq 0.86$ GeV (or $1.34\leq M(\Lambda\pi^+)\leq 1.42$ GeV) and fitting the resultant $\Lambda\pi^+$ (or $\pi^-\pi^0$) events in the region $1.30\leq M(\Lambda\pi^+)\leq 1.50$ GeV ($0.56\leq M(\pi^-\pi^0)\leq 0.96$ GeV) with a mass-dependent form

$$\frac{d\sigma}{d\Omega\, dm}=\alpha|f(m)|^2W(\theta,\phi)+(1-\alpha)(\text{polynomial in mass}),$$

where α is the fraction of $Y^{*+}(\rho^-)$, $|f(m)|^2$ is the $Y^{*+}(\rho^-)$ Breit-Wigner resonance shape, and $W(\theta,\phi)$ is the angular distribution corresponding to a decay of a $\frac{3}{2}^+$ (1^-) particle. As before, the background was found to be well described by an isotropic distribution in $\cos\theta$ and ϕ. We note that there remains ~10% $\pi^-\pi^0Y^{*+}$ (and $\Lambda\pi^+\rho^-$) events because of our initial ρ^- (or Y^{*+}) mass slice. These events should provide only a small systematic uncertainty (less than 15%) in the values of the density-matrix elements for the events of reaction (a). The values of the Y^{*+} and ρ^- density-matrix elements obtained in both the Jackson and helicity frames are shown in Figs. 83 and 84, respectively, and are listed in Table XXXVII. We observe, in contrast to the $\Lambda\rho^0$ and $\Sigma^0\rho^0$ reactions, the relatively large value of the ρ_{00} density-matrix element of the ρ^- as a function of $|-t'|$. We also note that in the low-momentum-transfer region ($|t'|<0.4$ GeV^2) the values of the $Y^{*+}(1385)$ density-matrix elements do not agree with the K^* exchange predictions of the Stodolsky-Sakurai model[41] (i.e., $\rho_{33}=0.375$; $\mathrm{Re}\rho_{31}=0.0$; $\mathrm{Re}\rho_{3-1}=0.216$). These observations suggest a strong K (unnatural-parity) exchange contribution to reaction (a). From this point of view it is interesting to note that the slope of the differential cross section is similar to that of the $\Sigma^0\rho^0$, $\Lambda\rho^0$, and $Y^{*+}(1385)\pi^-$ reactions, whereas one would naively expect that the stronger pseudoscalar exchange in reaction (a) would result in a more pronounced peripheral production.

4. *Quark-Model Predictons*

a. Class-A predictions. As discussed by Białas and Zalewski,[43] the decay correlations between the Y^* and ρ in reaction (a) represent a vital test of the additivity assumption of the quark model. The predictions of the model are represented by relationships among statistical tensors (or correspondingly density-matrix elements) evaluated in frames with z axis normal to the production plane. Following the notation of Ref. 43 we define

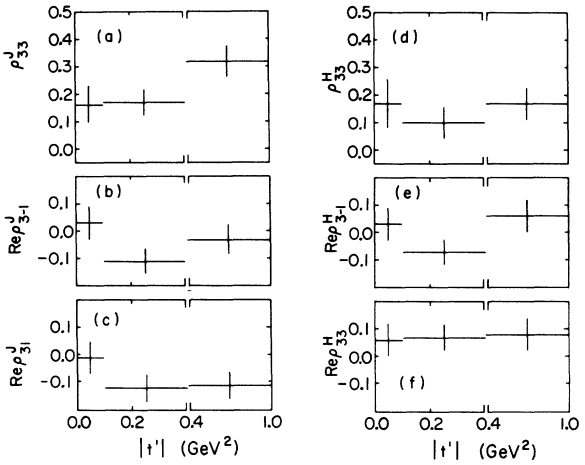

FIG. 83. Density-matrix elements of the $Y^{*+}(1385)$ produced in the reaction $K^-p \to Y^{*+}(1385)\rho^-$: (a)–(c) Jackson frame; (d)–(f) helicity frame.

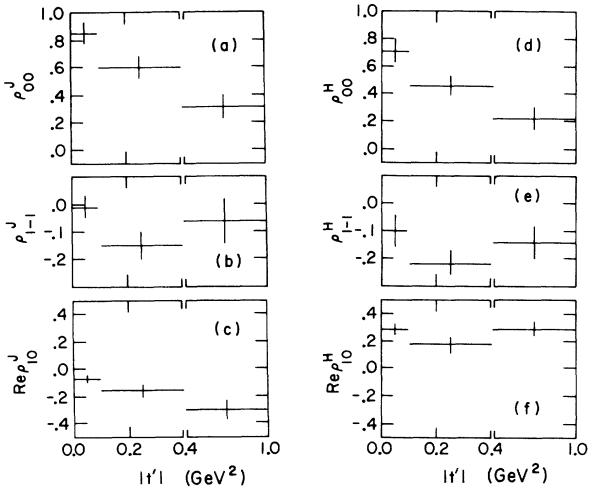

FIG. 84. Density-matrix elements of the ρ^- produced in the reaction $K^-p \to Y^{*+}(1385)\rho^-$: (a)–(c) Jackson frame; (d)–(f) helicity frame.

$$T^{20}_{M0} = \frac{1}{2F(\rho)}\langle Y^2_M(\theta_1, \phi_1)\rangle,$$

$$T^{02}_{0M} = \frac{1}{\sqrt{3}\,F(Y^*)}\langle Y^2_M(\theta_2, \phi_2)\rangle,$$

$$T^{22}_{MN} = \frac{1}{F(Y^*)F(\rho)}\langle Y^2_M(\theta_1, \phi_1)Y^2_N(\theta_2, \phi_2)\rangle,$$

with $F(\rho) = -(3/10\pi)^{1/2}$ and $F(Y^*) = -(1/5\pi)^{1/2}$, and where θ_1, ϕ_1 (θ_2, ϕ_2) are the polar and azimuthal decay angles of the ρ (Y^*), and $Y^L_M(\theta, \phi)$ are the usual spherical harmonics. The class-A quark model then predicts the following six relationships among the statistical tensors:

$$T^{20}_{00} = \sqrt{2}\; T^{02}_{00}, \tag{1}$$

$$\mathrm{Re}T^{22}_{20} = \tfrac{1}{2}\,\mathrm{Re}T^{20}_{20}, \tag{2}$$

$$\mathrm{Im}T^{22}_{20} = \tfrac{1}{2}\,\mathrm{Im}T^{20}_{20}, \tag{3}$$

$$\mathrm{Re}T^{22}_{02} = \frac{1}{\sqrt{2}}\,\mathrm{Re}T^{02}_{02}, \tag{4}$$

$$\mathrm{Im}T^{22}_{02} = \frac{1}{\sqrt{2}}\,\mathrm{Im}T^{02}_{02}, \tag{5}$$

$$T^{22}_{00} = \frac{1}{2\sqrt{6}} - \frac{1}{\sqrt{2}}\,T^{02}_{00}. \tag{6}$$

We have tested these predictions for the reaction $K^-p \to Y^{*+}\rho^-$ using events with $|t'| < 1.0$ GeV^2 and with mass selections [47]

$$0.66 \leq M(\pi^-\pi^0) \leq 0.86 \text{ GeV},$$

$$1.34 \leq M(\Lambda\pi^+) \leq 1.42 \text{ GeV}.$$

The values of the nineteen independent $T^{LL'}_{mm'}$ evaluated in both the transversity and Jackson transversity frames [48] are listed in Table XXXVIII. The

TABLE XXXVII. Density-matrix elements of the $Y^{*+}(1385)$ and ρ^- produced in reaction $K^-p \to Y^{*+}(1385)\rho^-$.

(a) $Y^{*+}(1385)$ density-matrix elements

$\lvert t'\rvert$ interval (GeV^2)	Jackson frame ρ_{33}	Jackson frame $\mathrm{Re}\rho_{3-1}$	Jackson frame $\mathrm{Re}\rho_{31}$	Helicity frame ρ_{33}	Helicity frame $\mathrm{Re}\rho_{3-1}$	Helicity frame $\mathrm{Re}\rho_{31}$
0.0–0.1	0.16± 0.07	0.03± 0.06	−0.01± 0.06	0.17± 0.09	0.03± 0.06	0.06± 0.06
0.1–0.4	0.17± 0.05	−0.11± 0.05	−0.12± 0.05	0.10± 0.06	−0.07± 0.05	0.07± 0.05
0.4–1.0	0.32± 0.06	−0.03± 0.06	−0.11± 0.05	0.17± 0.06	0.06± 0.06	0.08± 0.06

(b) ρ^- density-matrix elements

$\lvert t'\rvert$ interval (GeV^2)	Jackson frame ρ_{00}	Jackson frame ρ_{1-1}	Jackson frame $\mathrm{Re}\rho_{10}$	Helicity frame ρ_{00}	Helicity frame ρ_{1-1}	Helicity frame $\mathrm{Re}\rho_{10}$
0.0–0.1	0.85± 0.08	−0.01± 0.04	−0.07± 0.03	0.71± 0.09	−0.10± 0.06	0.29± 0.04
0.1–0.4	0.60± 0.08	−0.15± 0.05	−0.15± 0.05	0.46± 0.07	−0.22± 0.05	0.18± 0.05
0.4–1.0	0.31± 0.08	−0.06± 0.08	−0.29± 0.07	0.22± 0.08	−0.14± 0.06	0.29± 0.05

TABLE XXXVIII. Test of quark-model predictions for reaction $K^-p \to Y^{*+}(1385)\rho^-$.

(a) Values for $T^{LL'}_{MM'}(\rho, Y^*)$

	Transversity	Jackson transversity		Transversity	Jackson transversity
T^{20}_{00}	0.103 ± 0.025	0.103 ± 0.025	T^{22}_{00}	0.233 ± 0.062	0.233 ± 0.062
T^{02}_{00}	0.062 ± 0.037	0.062 ± 0.037	$\mathrm{Re}T^{22}_{2-2}$	0.057 ± 0.048	0.027 ± 0.049
$\mathrm{Re}T^{22}_{20}$	0.115 ± 0.046	−0.106 ± 0.043	$\mathrm{Im}T^{22}_{2-2}$	0.054 ± 0.049	0.079 ± 0.049
$\mathrm{Im}T^{22}_{20}$	−0.023 ± 0.041	0.045 ± 0.044	$\mathrm{Re}T^{22}_{1-1}$	−0.015 ± 0.044	−0.031 ± 0.044
$\mathrm{Re}T^{20}_{20}$	0.022 ± 0.021	−0.068 ± 0.021	$\mathrm{Im}T^{22}_{1-1}$	0.059 ± 0.041	0.050 ± 0.041
$\mathrm{Im}T^{20}_{20}$	0.125 ± 0.020	−0.094 ± 0.020	$\mathrm{Re}T^{22}_{22}$	−0.074 ± 0.048	−0.044 ± 0.050
$\mathrm{Re}T^{22}_{02}$	−0.066 ± 0.036	−0.002 ± 0.035	$\mathrm{Im}T^{22}_{22}$	−0.100 ± 0.050	0.074 ± 0.047
$\mathrm{Im}T^{22}_{02}$	0.043 ± 0.040	−0.058 ± 0.041	$\mathrm{Re}T^{22}_{11}$	0.085 ± 0.042	−0.011 ± 0.042
$\mathrm{Re}T^{02}_{02}$	−0.048 ± 0.027	−0.006 ± 0.027	$\mathrm{Im}T^{22}_{11}$	−0.036 ± 0.043	0.052 ± 0.043
$\mathrm{Im}T^{02}_{02}$	0.058 ± 0.029	−0.051 ± 0.029			

(b) Test of quark-model class-A predictions

Relation	LHS[a]	RHS[b]	Difference	No. of standard deviations
		Transversity Frame		
(1)	0.103 ± 0.025	0.088 ± 0.052	0.015 ± 0.058	0.26
(2)	0.115 ± 0.046	0.011 ± 0.011	0.104 ± 0.047	2.20
(3)	−0.023 ± 0.041	0.063 ± 0.010	−0.086 ± 0.040	2.15
(4)	−0.066 ± 0.036	−0.034 ± 0.019	0.032 ± 0.041	0.78
(5)	0.043 ± 0.040	0.041 ± 0.020	0.002 ± 0.045	0.04
(6)	0.233 ± 0.062	0.160 ± 0.026	0.073 ± 0.067	1.09
		Jackson Transversity Frame		
(1)	0.103 ± 0.025	0.088 ± 0.052	0.015 ± 0.058	0.26
(2)	−0.106 ± 0.043	−0.034 ± 0.011	−0.072 ± 0.044	1.64
(3)	0.045 ± 0.044	−0.047 ± 0.010	0.092 ± 0.045	2.04
(4)	−0.002 ± 0.035	−0.004 ± 0.019	0.002 ± 0.040	0.05
(5)	−0.058 ± 0.041	−0.036 ± 0.020	−0.022 ± 0.045	0.49
(6)	0.233 ± 0.062	0.160 ± 0.026	0.073 ± 0.067	1.09

(c) Test of quark-model class-B predictions

Relation	LHS[a]	RHS[b]	Difference	No. of standard deviations
		Transversity Frame		
(7)	0.022 ± 0.021	−0.068 ± 0.038	0.090 ± 0.043	2.09
(8)	0.125 ± 0.020	0.082 ± 0.041	0.043 ± 0.046	0.94
(9)	0.115 ± 0.046	−0.066 ± 0.036	0.181 ± 0.058	3.09
(10)	−0.023 ± 0.041	0.043 ± 0.040	−0.066 ± 0.057	1.15
(11)	0.054 ± 0.049	0.0	0.054 ± 0.049	1.10
(12)	0.059 ± 0.041	0.0	0.059 ± 0.041	1.44
		Jackson Transversity Frame		
(7)	−0.068 ± 0.021	−0.008 ± 0.038	−0.060 ± 0.043	1.40
(8)	−0.094 ± 0.020	−0.072 ± 0.040	−0.022 ± 0.044	0.50
(9)	−0.106 ± 0.043	−0.002 ± 0.035	−0.104 ± 0.055	1.87
(10)	0.045 ± 0.044	−0.058 ± 0.041	0.103 ± 0.060	1.72
(11)	0.079 ± 0.049	0.0	0.079 ± 0.049	1.61
(12)	0.050 ± 0.041	0.0	0.050 ± 0.041	1.22

[a] LHS = left-hand side. [b] RHS = right-hand side.

test of the relations (1)–(6) is given in Table XXXVIII in both these frames. We observe adequate agreement between the experimental data and the theoretical predictions. Similar tests have also been performed on the reactions $\bar{p}p \to N^*\bar{N}^*$ and $Kp \to K^*N^*$,[49] with no observed deviation from these quark-model predictions. In addition, we have tested relation (1), as written in terms of the density-matrix elements evaluated in the Jackson frame, as a function of momentum transfer. This relation (A1) as shown in Table XXXIX is also in good agreement with the experimental data for all the $|-t'|$ intervals.

b. Class-B predictions. Under additional assumptions on the quark-quark scattering amplitudes, as shown by Białas and Zalewski,[43] further relationships can be derived among the statistical tensors. The so-called class-B predictions are

$$\mathrm{Re}T^{20}_{20} = \sqrt{2}\ \mathrm{Re}T^{02}_{02}, \tag{7}$$

$$\mathrm{Im}T^{20}_{20} = \sqrt{2}\ \mathrm{Im}T^{20}_{20}, \tag{8}$$

$$\mathrm{Re}T^{22}_{20} = \mathrm{Re}T^{22}_{02}, \tag{9}$$

$$\mathrm{Im}T^{22}_{20} = \mathrm{Im}T^{22}_{02}, \tag{10}$$

$$\mathrm{Im}T^{22}_{2-2} = 0, \tag{11}$$

$$\mathrm{Im}T^{22}_{1-1} = 0. \tag{12}$$

We have tested these relations in the transversity and Jackson transversity frames as shown in Table XXXVIII (c). We observe that, although the predictions are not grossly violated, they are in lesser agreement with the experimental data than were the class-A predictions. Using (7) along with (1), relations (B1)–(B3) in Table XXXIX can be derived. We have tested these predictions as a function of momentum transfer as shown in this table.

TABLE XXXIX. Test of quark-model predictions for reaction $K^-p \to Y^{*+}(1385)\rho^-$.

Class	Density-matrix element relation	Relation No.
A	$\rho_{11}+\rho_{1-1}=\frac{4}{3}\rho_{3/2\,3/2}+(4/\sqrt{3})\rho_{3/2\,-1/2}$	(A1)
B	$\rho_{11}=\frac{4}{3}\rho_{3/2\,3/2}$	(B1)
	$\rho_{1-1}=(4/\sqrt{3})\,\mathrm{Re}\rho_{3/2\,-1/2}$	(B2)
	$\mathrm{Re}\rho_{10}=(4/\sqrt{6})\,\mathrm{Re}\rho_{3/2\,1/2}$	(B3)
C	$\mathrm{Re}\rho_{3/2\,1/2}=0$	(C1)
	$\mathrm{Re}\rho_{10}=0$	(C2)

Relation No.	$\lvert t'\rvert$ interval (GeV^2)	LHS[a]	RHS[b]	Difference	No. of standard deviations
	0.0–0.1	0.065± 0.056	0.283± 0.167	−0.218± 0.176	1.2
(A1)	0.1–0.4	0.050± 0.064	−0.027± 0.133	0.077± 0.148	0.5
	0.4–1.0	0.285± 0.089	0.357± 0.160	−0.072± 0.183	0.4
	0.0–0.1	0.075± 0.040	0.213± 0.093	−0.138± 0.101	1.4
(B1)	0.1–0.4	0.200± 0.040	0.226± 0.067	−0.026± 0.078	0.33
	0.4–1.0	0.345± 0.040	0.427± 0.080	−0.082± 0.089	0.92
	0.0–0.1	−0.010± 0.040	0.069± 0.139	−0.079± 0.145	0.5
(B2)	0.1–0.4	−0.150± 0.050	−0.254± 0.115	0.104± 0.125	0.8
	0.4–1.0	−0.060± 0.080	−0.069± 0.139	0.009± 0.160	0.1
	0.0–0.1	−0.070± 0.030	−0.016± 0.098	−0.054± 0.102	0.5
(B3)	0.1–0.4	−0.150± 0.050	−0.196± 0.082	0.046± 0.096	0.5
	0.4–1.0	−0.290± 0.070	−0.180± 0.082	−0.110± 0.108	1.0

		LHS (Jackson)	LHS (helicity)	RHS	J	H
	0.0–0.1	−0.01± 0.06	0.06± 0.06	0	0.2	1.0
(C1)	0.1–0.4	−0.12± 0.05	0.07± 0.05	0	2.4	1.4
	0.4–1.0	−0.11± 0.05	0.08± 0.06	0	2.2	1.3
	0.0–0.1	−0.07± 0.03	0.29± 0.04	0	2.3	7.3
(C2)	0.1–0.4	−0.15± 0.05	0.18± 0.05	0	3.0	3.6
	0.4–1.0	−0.29± 0.07	0.29± 0.05	0	4.1	5.8

[a] LHS = left-hand side.
[b] RHS = right-hand side.

Good agreement between the predictions and the experimental data were found.

c. Class-C predictions. Class-*C* predictions require stronger additional assumptions on the quark-quark scattering amplitudes. They predict that all the statistical tensors are real and in particular give the relations (C1) and (C2) of Table XXXIX. We observe that there is a strong violation of these predictions with large imaginary values for some statistical tensors found in both the Jackson transversity and transversity frames. In addition, (C1) and (C2) are grossly violated as a function of momentum transfer in both the Jackson and helicity frames.

D. Reaction $K^-p \to Y^{*0}(1385)\phi$

1. *Total and Differential Cross Sections*

In Fig. 18, for the combined 3.9- and 4.6-GeV/c data, the $M(\Lambda\pi^0)$-vs-$M(K^+K^-)$ scatter plot is shown in which evidence for the quasi-two-body process

$$K^-p \to Y^{*0}(1385)\phi \qquad \text{(a)}$$

is observed. In order to obtain a relatively pure sample of reaction (a), we have required $|t'|$ to be

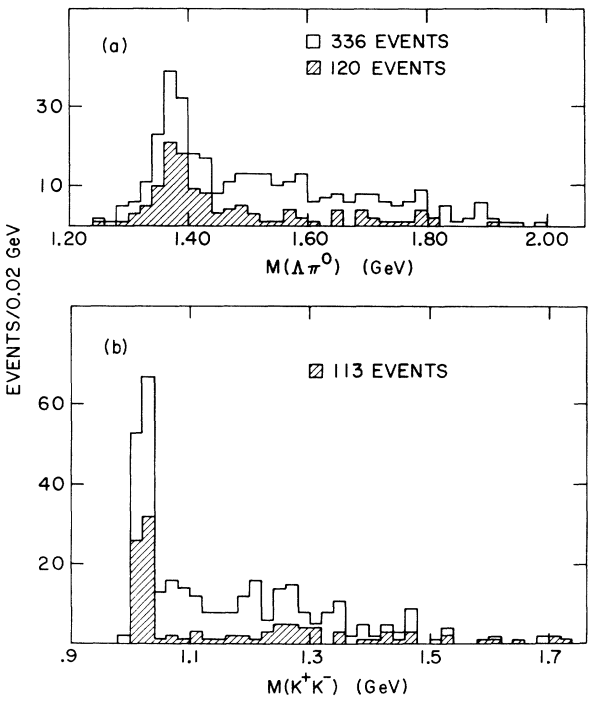

FIG. 85. (a) $\Lambda\pi^0$ effective-mass distribution from the reaction $K^-p \to \Lambda\pi^0K^+K^-$ for events with $|t'| < 1.0$ GeV^2. The shaded area is the same mass spectrum after a ϕ selection on the K^+K^- effective mass. (b) K^+K^- effective-mass distribution with the same selections as in (a). The shaded area is for events with $\Lambda\pi^0$ effective mass in the $Y^{*0}(1385)$ region.

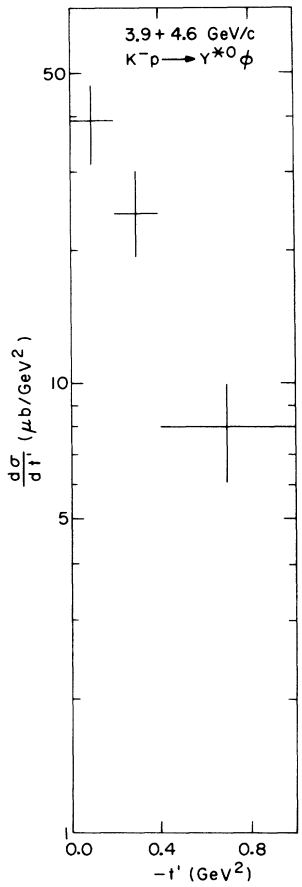

FIG. 86. Differential cross section for reaction $K^-p \to Y^{*0}(1385)\phi$ for the combined data at 3.9 and 4.6 GeV/c.

less than 1.0 GeV^2. The resultant $\Lambda\pi^0$ and K^+K^- effective-mass distributions for the combined 3.9- and 4.6-GeV/c data are shown in Figs. 85(a) and 85(b). The shaded areas in this figure represent the $\Lambda\pi^0(K^+K^-)$ effective-mass distributions after a $\phi(Y^{*0})$ selection has been imposed which was defined by $1.0 \leq M(K^+K^-) \leq 1.04$ GeV $[1.34 \leq M(\Lambda\pi^0) \leq 1.42$ GeV] in which the resonance signals are observed over small backgrounds. Using this selection procedure the number of events for reaction (a) was obtained:

3.9 GeV/c: 24 ± 6 events; $\sigma = 20 \pm 5\mu$b,

4.6 GeV/c: 32 ± 6 events; $\sigma = 18 \pm 4$ μb,

where the σ is corrected for unseen resonance decay modes, probability cuts, and Λ visibility and losses.

In Fig. 86 and in Table XL the average differential cross section for the combined 3.9- and 4.6-GeV/c sample is shown. The slope parameter obtained from a fit to the differential cross section is $A = 2.8 \pm 0.6$ GeV^{-2}.

TABLE XL. Differential cross sections for reaction $K^-p \to Y^{*0}\phi(\to K\bar{K})$ at 3.9 and 4.6 GeV/c.

$\lvert t'\rvert$ interval (GeV^2)	No. of events	Corrected $\frac{d\sigma}{dt'}\left(\frac{\mu b}{GeV^2}\right)$
0.0–0.2	26± 5	34± 7
0.2–0.4	16± 4	21± 5
0.4–1.0	16± 4	7± 2

2. *Decay Distributions*

The $Y^{*0}(1385)$ and ϕ density-matrix elements evaluated for events with $|t'|<0.5$ GeV^2 are listed in Table XLI. We observe that in this case the values of the Y^{*0} density-matrix elements are consistent with the K^* exchange predictions of the Stodolsky-Sakurai model.[41] In addition, the ϕ density-matrix elements (ρ_{00} small, ρ_{1-1} large) are consistent with the hypothesis of a large natural-parity exchange. These observations are in contrast to the already discussed $Y^{*+}\rho^-$ reaction in which evidence for strong unnatural-parity exchange was found.

3. *Quark-Model Predictions*

We have also tested the quark-model predictions of class A (1)–(6) and (A1) listed previously for the reaction $K^-p \to Y^*\rho$. The nineteen independent $T^{LL'}_{mm'}(\phi, Y^*)$ evaluated in both the transversity and Jackson transversity frames are listed in Table XLII. The quark-model predictions in both these frames are again seen to be in good agreement with the experimental data.

In Table XLII(c) and Table XLIII the class-B and -C predictions are tested with the experimental data. Here an almost 3-standard-deviation violation of two class-B predictions [relations (11) and (12)] is found, caused by the observed large values of the $\mathrm{Im}T^{22}_{2-2}$ and $\mathrm{Im}T^{22}_{1-1}$. As in the $Y^{*+}\rho^-$ case, the class-C predictions (i.e., all $\mathrm{Im}T^{LL'}_{mm'}$ =0.0) are violated by the experimental data in both the Jackson transversity and transversity frames.

TABLE XLI. Density-matrix elements for the ϕ and $Y^{*0}(1385)$ from the reaction $K^-p \to Y^{*0}\phi$ at 3.9 and 4.6 GeV/c with $|t'|<0.5$ GeV^2 (48 events).

	Jackson	Helicity
(a) ϕ density-matrix elements		
ρ_{00}	0.15± 0.09	0.23± 0.09
ρ_{1-1}	0.25± 0.08	0.29± 0.07
$\mathrm{Re}\rho_{10}$	−0.01± 0.05	0.02± 0.06
(b) Y^{*0} density-matrix elements		
ρ_{33}	0.31± 0.08	0.23± 0.09
$\mathrm{Re}\rho_{3-1}$	0.09± 0.09	0.13± 0.08
$\mathrm{Re}\rho_{31}$	−0.04± 0.07	−0.05± 0.09

VI. SUMMARY OF EXPERIMENTAL DATA

We proceed to summarize the results of our analysis on mesons produced recoiling off Λ, Σ^0, and $Y^*(1385)$. Here, qualitative remarks about the general behavior of these reactions are made, with more quantitative comparisons reserved for the following sections. As a guide to this study, the results on the total and forward cross sections as well as the slopes of the differential cross sections are summarized in Table XLIV.

The 0^- mesons produced off Λ are observed to have the most peripheral characteristics of all the reactions. The forward cross sections for vector mesons produced off Λ (i.e., ρ, ω, and ϕ) are found to be equal with one another within the experimental errors, as are the forward slopes. (This also holds for ρ and ϕ production off Σ^0.) Similarly the forward cross sections for tensor-meson production (i.e., f^0, A_2, and f') off Λ are found to be equal within the statistical errors.

Strong backward ρ, ω, and f^0 production is found with Λ (the f^0 cross section is at least as large as in the forward direction), while no significant evidence for backward ρ^0 or f^0 is observed with Σ^0. This result can be qualitatively explained by the weak coupling of the exchanged baryon (assumed to be a proton) to the ΣK system compared to its strong ΛK coupling (i.e., $g_{K\Lambda p}{}^2 > g_{K\Sigma p}{}^2$).[50] The weak ΣKp coupling would suggest that the K exchange in the reactions $K^-p \to \Sigma^0\phi$ and $K^-p \to \Sigma^0\rho$ should be smaller than in the Λ reactions consistent with the small unnatural-parity exchange contribution actually observed in these reactions (i.e., ρ_{00} is small, $\rho_{11}+\rho_{1-1}$ is large).

A compilation of the available cross-section data for channels in which sufficient experimental data exist is given in Figs. 87–93 and in Tables XLV–LI in which the appropriate references are included. A fit to these distributions, using the form $\sigma \sim p^{-n}$, was performed and the values of the parameter are listed in Table XLIV (the fit was performed for data with $P_{\mathrm{Lab}} \gtrsim 2$ GeV/c). It should be pointed out that the fit was not good in some cases, and we have attempted to include systematic uncertainties in the quoted error. We have used the total cross sections in our fits so that only qualitative comparisons of the n parameters can be made for the study of meson exchange. This is particularly true for channels in which large backward cross sections are observed (e.g., $K^-p \to \Lambda\omega$) at low momentum (which fall faster than the corresponding forward cross sections). All cross sections listed fall with n values between 2 and 3

TABLE XLII. Test of quark-model predictions for reaction $K^-p \to Y^{*0}(1385)\phi$ for $|t'| < 1.0$ GeV^2.

(a) Values for $T^{LL'}_{MM'}(\phi, Y^*)$

	Transversity	Jackson transversity		Transversity	Jackson transversity
T^{20}_{00}	−0.205± 0.076	−0.205± 0.076	T^{22}_{00}	0.302± 0.190	0.302± 0.190
T^{02}_{00}	−0.102± 0.086	−0.102± 0.086	$\mathrm{Re}T^{22}_{2-2}$	−0.085± 0.085	−0.069± 0.085
$\mathrm{Re}T^{22}_{20}$	−0.091± 0.086	0.066± 0.077	$\mathrm{Im}T^{22}_{2-2}$	−0.222± 0.078	−0.230± 0.077
$\mathrm{Im}T^{22}_{20}$	−0.031± 0.070	−0.040± 0.080	$\mathrm{Re}T^{22}_{1-1}$	−0.065± 0.086	−0.073± 0.086
$\mathrm{Re}T^{20}_{20}$	−0.029± 0.039	−0.013± 0.037	$\mathrm{Im}T^{22}_{1-1}$	0.290± 0.10	0.290± 0.10
$\mathrm{Im}T^{20}_{20}$	−0.002± 0.035	0.017± 0.037	$\mathrm{Re}T^{22}_{22}$	−0.082± 0.089	0.194± 0.079
$\mathrm{Re}T^{22}_{02}$	0.024± 0.108	−0.120± 0.087	$\mathrm{Im}T^{22}_{22}$	0.048± 0.072	0.016± 0.084
$\mathrm{Im}T^{22}_{02}$	0.127± 0.097	−0.069± 0.116	$\mathrm{Re}T^{22}_{11}$	0.103± 0.081	0.073± 0.10
$\mathrm{Re}T^{02}_{02}$	−0.044± 0.059	0.006± 0.054	$\mathrm{Im}T^{22}_{11}$	−0.228± 0.105	0.145± 0.087
$\mathrm{Im}T^{02}_{02}$	0.012± 0.054	−0.040± 0.059			

(b) Test of quark-model class-A predictions

Relation	LHS[a]	RHS[b]	Difference	No. of standard deviations
		Transversity Frame		
(1)	−0.205± 0.076	−0.144± 0.120	−0.061± 0.140	0.43
(2)	−0.091± 0.086	−0.015± 0.020	−0.076± 0.088	0.86
(3)	−0.031± 0.070	−0.001± 0.017	−0.030± 0.070	0.43
(4)	0.024± 0.108	−0.031± 0.042	0.055± 0.116	0.47
(5)	0.127± 0.097	0.008± 0.038	0.119± 0.104	1.14
(6)	0.302± 0.190	0.276± 0.060	0.026± 0.200	0.13
		Jackson Transversity Frame		
(1)	−0.205± 0.076	−0.144± 0.120	−0.061± 0.142	0.43
(2)	0.066± 0.077	−0.007± 0.018	0.073± 0.079	0.92
(3)	−0.040± 0.080	0.009± 0.018	−0.049± 0.080	0.61
(4)	−0.120± 0.087	0.004± 0.038	−0.124± 0.090	1.38
(5)	−0.069± 0.116	−0.028± 0.042	−0.041± 0.123	0.33
(6)	0.302± 0.190	0.276± 0.060	0.026± 0.209	0.13

(c) Test of quark-model class-B predictions

Relation	LHS[a]	RHS[b]	Difference	No. of standard deviations
		Transversity Frame		
(7)	−0.029± 0.039	−0.062± 0.083	−0.033± 0.091	0.36
(8)	−0.002± 0.035	0.017± 0.076	0.019± 0.084	0.23
(9)	−0.091± 0.086	0.024± 0.018	−0.115± 0.088	1.31
(10)	−0.031± 0.070	0.127± 0.097	−0.158± 0.120	1.32
(11)	−0.222± 0.078	0.0	−0.222± 0.078	2.85
(12)	0.290± 0.100	0.0	0.290± 0.100	2.90
		Jackson Transversity Frame		
(7)	−0.013± 0.037	0.008± 0.076	−0.021± 0.085	0.25
(8)	0.017± 0.037	−0.057± 0.083	0.074± 0.090	0.82
(9)	0.066± 0.077	0.120± 0.087	−0.054± 0.116	0.47
(10)	−0.040± 0.080	−0.069± 0.116	0.029± 0.141	0.21
(11)	−0.230± 0.077	0.0	−0.230± 0.077	2.98
(12)	0.290± 0.100	0.0	0.290± 0.100	2.90

[a]LHS = left-hand side. [b]RHS = right-hand side.

TABLE XLIII. Test of quark-model predictions for reaction $K^-p \to Y^{*0}(1385)\phi$.

Relation[a]	$\lvert t' \rvert$ interval (GeV^2)	LHS[b]	RHS[c]	Difference	No. of standard deviations
(A1)	0.0–0.5	0.675± 0.094	0.621± 0.234	0.054± 0.252	0.2
(B1)	0.0–0.5	0.425± 0.045	0.413± 0.107	0.012± 0.116	0.1
(B2)	0.0–0.5	0.250± 0.080	0.208± 0.208	0.042± 0.223	0.2
(B3)	0.0–0.5	−0.010± 0.050	−0.065± 0.114	−0.055± 0.124	0.4

		LHS (Jackson)	LHS (helicity)	RHS	J	H
(C1)	0.0–0.5	−0.04± 0.07	−0.05± 0.07	0	0.6	0.7
(C2)	0.0–0.5	−0.01± 0.05	0.02± 0.06	0	0.2	0.3

[a] See Table XXXIX for definition of relation tested.
[b] LHS = left-hand side.
[c] RHS = right-hand side.

except that of the $K^-p \to \Lambda\phi$ reaction, which has a somewhat smaller slope. The cross section for this reaction, which is much smaller at low energies, is found to approach the $\Lambda\omega$ and $\Lambda\rho$ cross sections in the 4- to 6-GeV/c region. Similarly, the $K^-p \to \Lambda\eta'$ cross section approaches the $K^-p \to \Lambda\pi^0$ cross section in this energy region.

VII. SU(3) COMPARISON OF VECTOR-MESON PRODUCTION

A. Description of Prediction

The SU(3) symmetry scheme has been remarkably successful in describing the spectroscopy of the well-known boson and baryon states. The situation with regard to dynamics, i.e., predicting

TABLE XLIV. Summary of reactions studied.

Reaction	Cross section (μb) 3.9 GeV/c	Cross section (μb) 4.6 GeV/c	Forward cross section[a] (μb) 3.9 GeV/c	Forward cross section[a] (μb) 4.6 GeV/c	Forward slope (GeV^{-2}) 3.9 GeV/c	Forward slope (GeV^{-2}) 4.6 GeV/c	$\sigma \sim p^{-n}$ n
$K^-p \to \Lambda\pi^0$	67± 6	44 ± 5	61 ± 6	41.6± 5	3.1± 0.5	4.6± 0.5	3.1± 0.6
$K^-p \to \Lambda\eta$	26± 6	11 ± 3	26 ± 6[b]	11 ± 3[b]			2.5± 0.4
$K^-p \to \Lambda\eta'$	45± 7	50 ± 6	39.4± 7	49.4± 6	5.9± 0.9	5.3± 0.5	1.9± 0.4
$K^-p \to \Lambda\rho$	78± 10	66 ± 6	62.7± 9	45 ± 5	2.4± 0.6	2.2± 0.6	2.6± 0.6
$K^-p \to \Lambda\omega$	98± 9	65 ± 6	63.7± 8	49.5± 6	1.8± 0.4	2.0± 0.3	2.8± 0.2
$K^-p \to \Lambda\phi$	60± 7	41 ± 4	58.5± 7	40.5± 4	1.9± 0.2	2.0± 0.2	1.3± 0.4
$K^-p \to \Lambda f^0$	46± 12	60 ± 8	20 ± 10	25 ± 5			
$K^-p \to \Lambda A_2$	23± 21	23 ± 14	23 ± 21	18 ± 11			
$K^-p \to \Lambda f'$	7± 4	19 ± 4	7 ± 4[b]	19 ± 4[b]			
$K^-p \to \Sigma^0 p$	32± 6	23 ± 4	25.4± 5	19 ± 3	1.9± 0.5		
$K^-p \to \Sigma^0\phi$	33± 7	20 ± 5	33 ± 7	20 ± 5	1.1± 0.4		
$K^-p \to \Sigma^0 f^0$	25± 9	15 ± 5	25 ± 9	10 ± 4			
$K^-p \to \Sigma^0 f'$	0± 3	5.3± 2	0 ± 3[b]	5.3± 2[b]			
$K^-p \to Y^{*+}\pi^-$	79± 8	63 ± 6	79 ± 8	63 ± 6	3.0± 0.5	3.9± 0.6	2.5± 0.8
$K^-p \to Y^{*-}\pi^+$	14± 4	5 ± 2	4 ± 1.5	1.5± 0.8			
$K^-p \to Y^{*+}\rho^-$	92± 8	62 ± 10	92 ± 8[b]	62 ± 10[b]	2.7± 0.8	2.7± 0.7	
$K^-p \to Y^{*0}\rho^0$	19± 6	9 ± 5					
$K^-p \to Y^{*-}\rho^+$	10± 6	0 ± 4					
$K^-p \to Y^{*0}\phi$	20± 5	18 ± 4	20 ± 5[b]	18 ± 4[b]	2.8± 0.6		

[a] The forward cross section for reaction $K^-p \to MB$ is defined by $\cos\theta^*(p,B) \gtrsim 0$ where $M(B)$ represents the outgoing meson (baryon).
[b] There is no significant evidence for production in the backward direction, so that the forward cross section is essentially equal to the total cross section.

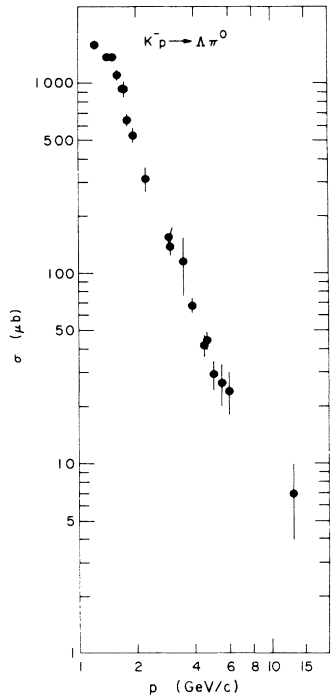

FIG. 87. Cross section vs incident K^- momentum for the reaction $K^-p \to \Lambda\pi^0$.

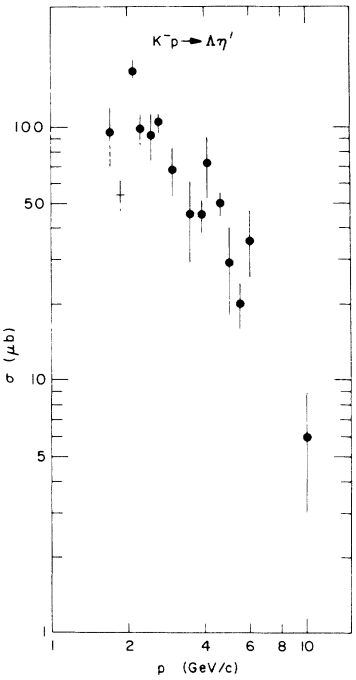

FIG. 89. Cross section vs incident K^- momentum for the reaction $K^-p \to \Lambda\eta'$.

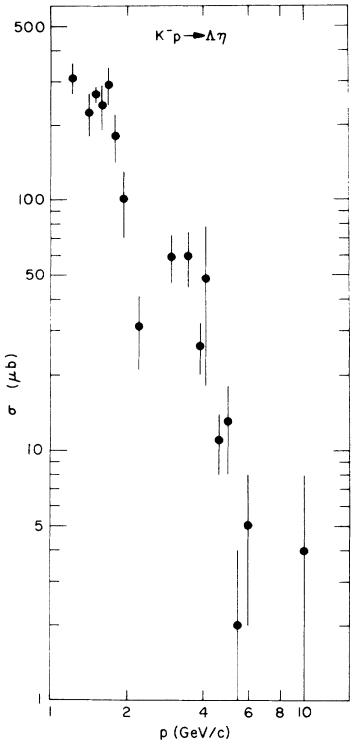

FIG. 88. Cross section vs incident K^- momentum for the reaction $K^-p \to \Lambda\eta$.

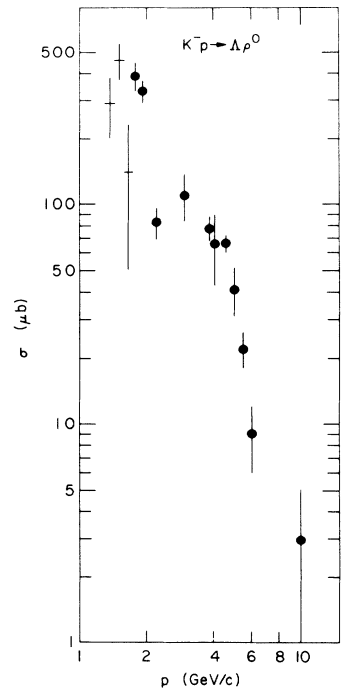

FIG. 90. Cross section vs incident K^- momentum for the reaction $K^-p \to \Lambda\rho$.

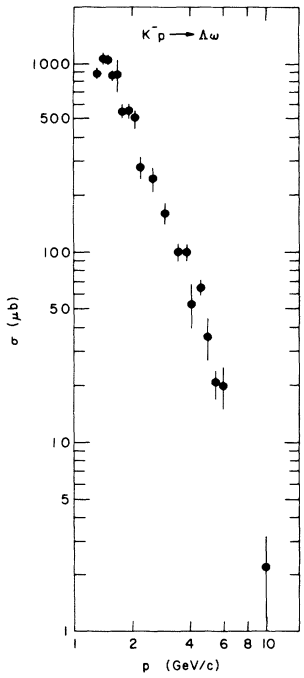

FIG. 91. Cross section vs incident K^- momentum for the reaction $K^-p \to \Lambda\omega$.

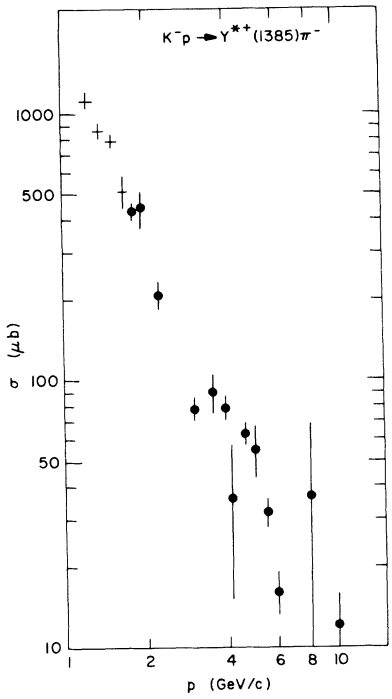

FIG. 93. Cross section vs incident K^- momentum for the reaction $K^-p \to Y^{*+}(1385)\pi^-$.

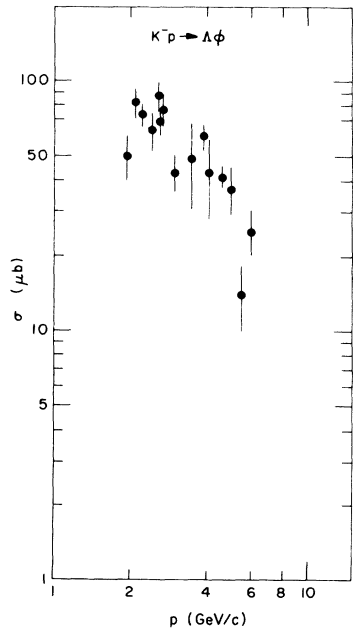

FIG. 92. Cross section vs incident K^- momentum for the reaction $K^-p \to \Lambda\phi$.

TABLE XLV. Cross sections for reaction $K^-p \to \Lambda\pi^0$.

P_{K^-} (GeV/c)	σ (μb)	Reference
1.22	1580± 70	51
1.42	1370± 60	51
1.51	1370± 60	51
1.60	1100± 70	51
1.70	940± 50	51
1.72	930± 80	51
1.80	640± 50	52
1.95	530± 50	52
2.24	315± 47	53
3.0	138± 15	54
3.0[a]	155± 20	55
3.5	115± 40	56
3.9	67± 6	b
4.5[a]	42± 6	57
4.6	44± 5	b
5.0[a]	30± 5	58
5.5[a]	27± 7	59
6.0	24± 6	60
13.0[a]	7± 3	61

[a] These are data for the reaction $K^-n \to \Lambda\pi^-$, and we give (from isotopic spin) $\frac{1}{2}\sigma$ for this reaction.
[b] Present experiment.

TABLE XLVI. Cross sections for reaction $K^-p \to \Lambda\eta$.

P_{K^-} (GeV/c)	σ (μb)	Reference
1.22	310± 45	62
1.42	225± 45	62
1.51	265± 20	62
1.60	240± 50	62
1.70	290± 50	62
1.8	180± 40	52
1.95	100± 30	52
2.24	31± 10	53
3.0	59± 13	54
3.5	59± 15	63
3.9	26± 6	a
4.1	48± 30	64
4.6	11± 3	a
5.0	13± 5	65
5.5	2± 2	64
6.0	5± 3	60
10.1	4± 4	66

[a] Present experiment.

relations among cross sections, has been less clear.[73] In this section we address ourselves to several SU(3) dynamical predictions which satisfy the expected regularities to within the experimental errors. These involve reactions in which vector mesons are produced via a meson exchange process with the baryon vertex remaining the same. Here we compare the differential cross sections,

TABLE XLVII. Cross sections for reaction $K^-p \to \Lambda\eta'$.

P_{K^-} (GeV/c)	σ (μb)	Reference
1.70	95± 25	8
1.80–1.95	54± 8	52
2.10	168± 17	8
2.24	98± 14	53
2.47	93± 20	8
2.65	104± 9	8
3.0	68± 15	63
3.5[a]	45± 16	56
3.9	45± 7	b
4.1	72± 20	64
4.6	50± 6	b
5.0	29± 11	65
5.5	20± 4	64
6.0[a]	36± 11	60
10.1[a]	6± 3	66

[a] From reaction

$$K^-p \to \Lambda\eta' \searrow \eta\pi^+\pi^-$$

and world-average decay rate

$$\eta' \to \eta\pi^+\pi^-/\eta' \to \text{total} = 0.444 \pm 0.024.$$

[b] This experiment.

TABLE XLVIII. Cross sections for reaction $K^-p \to \Lambda\rho^0$.

P_{K^-} (GeV/c)	σ (μb)	Reference
1.15–1.30	0± 70	67
1.30–1.45	290± 90	67
1.45–1.60	460± 90	67
1.60–1.75	140± 30	67
1.8	390± 60	52
1.95	330± 40	52
2.24	83± 14	53
3.0	110± 26	54
3.9	78± 10	a
4.1	66± 23	64
4.6	66± 6	a
5.0	41± 10	65
5.5	22± 4	64
6.0	9± 3	60
10.1	3± 2	66

[a] This experiment.

polarization, and density-matrix elements of ω and ρ produced in the reactions

$$K^-p \to \Lambda\omega, \quad \text{(a)}$$

$$K^-p \to \Lambda\rho, \quad \text{(b)}$$

which have been discussed in Sec. III. In addition, we compare the previously discussed reactions[74]

$$K^-p \to Y\phi \quad \text{(c)}$$

and

$$\pi^-p \to YK(890), \quad \text{(d)}$$

TABLE XLIX. Cross sections for reaction $K^-p \to \Lambda\omega$.

P_{K^-} (GeV/c)	σ (μb)	Reference
1.32[a]	884± 66	68
1.42[a]	1072± 88	68
1.51[a]	1061± 55	68
1.60[a]	862± 55	68
1.70[a]	873± 177	68
1.80	550± 50	52
1.95	560± 50	52
2.1[a]	508± 55	68
2.24	278± 36	53
2.6[a]	243± 33	68
3.0	160± 20	54
3.5[a]	99± 11	56
3.9	98± 9	b
4.1	54± 14	64
4.6	65± 6	b
5.0	36± 9	65
5.5	21± 3	64
6.0	20± 5	60
10.1	2.2± 1.0	66

[a] Using $\omega \to \pi^+\pi^-\pi^0/\omega \to \text{total} = 0.905$.

[b] This experiment.

TABLE L. Cross sections for reaction $K^-p \to \Lambda\phi$.

P_K- (GeV/c)	σ (μb)	Reference
1.95	50 ± 10	52
2.10	82 ± 11	69
2.24	73 ± 8	53
2.43	63 ± 11	69
2.58	87 ± 12	69
2.61	69 ± 9	69
2.68	77 ± 11	69
3.0	43 ± 7	63
3.5[a]	49 ± 18	56
3.9	60 ± 7	c
4.1	43 ± 15	64
4.25[b]	65 ± 10	70
4.6	41 ± 4	c
5.0	37 ± 8	65
5.5	14 ± 4	64
6.0	25 ± 5	71

[a] From reaction $K^-p \to \Lambda\phi(\to K^+K^- + K_1^0K_2^0)$ using world average $\phi \to K^+K^- + K_1^0K_2^0/\phi \to$ totals = 0.817.
[b] From reaction $K^-p \to \Lambda\phi(\to K_1^0K_2^0)$ using world average $\phi \to K_1^0K_2^0/\phi \to$ totals = 0.348.
[c] This experiment.

TABLE LI. Cross sections for $K^-p \to Y_1^{*+}(1385)\pi^-$.

P_K- (GeV/c)	σ (μb)	Reference
1.15–1.30	1130 ± 80	67
1.30–1.45	860 ± 60	67
1.45–1.60	790 ± 50	67
1.60–1.75	510 ± 70	67
1.8	430 ± 35	52
1.95	440 ± 70	52
2.24	207 ± 25	53
3.0	78 ± 8	54
3.5	90 ± 15	56
3.9	79 ± 8	a
4.1	36 ± 21	64
4.6	63 ± 6	a
5.0	55 ± 12	65
5.5	32 ± 4	64
6.0	16 ± 3	60
8.0	37 ± 31	72
10.1	12 ± 4	66

[a] This experiment.

where Y stands for either Λ or Σ^0.

If the production mechanism of reactions (a)–(d) is meson exchange, they can be related to each other by application of SU(3) symmetry at the meson vertex, since the baryon vertex remains the same. Very little needs to be assumed about the nature of the exchanged meson. If K or $K(1420)$ is exchanged in the process, the meson vertex requires the antisymmetric F type of coupling, whereas if the $K(890)$ is responsible for the exchange mechanism, the meson vertex involves the symmetric D-type coupling. In either case, the SU(3) symmetry leads to the following relation for each helicity amplitude[75]:

$$A(K^-p \to Y\rho) = A(K^-p \to Y\omega),$$
$$A(K^-p \to Y\phi) = -A(\pi^-p \to YK(890)), \quad \text{(e)}$$

where we have suppressed the helicity indices. In this derivation we have used the experimentally observed small value of the $\phi \to \rho\pi$ branching ratio as well as the ideal mixing angle between the ω and ϕ (35°, which is essentially equal to the experimental value of 39°). We have in addition assumed that neither the factors in the amplitude which depend on the external masses nor absorptive effects strongly break this equality (e).

This in turn leads to the following relations among the experimentally measured quantities as examined in the peripheral region:

$$\frac{d\bar{\sigma}}{dt}(K^-p \to Y\rho^0) = \frac{d\bar{\sigma}}{dt}(K^-p \to Y\omega), \quad \text{(f)}$$

TABLE LII. Comparison of reactions $K^-p \to \Lambda\rho^0$ and $K^-p \to \Lambda\omega$. σ_T, σ_B, and σ_F denote total, backward, and forward cross section; A is the slope of the differential cross section; and P_Λ is the Λ polarization.

Momentum (GeV/c)	Measured quantity	Reactions $\Lambda\omega$	Reactions $\Lambda\rho^0$	Difference
3.9	σ_T (μb)	98 ± 9	78 ± 10	20 ± 13
3.9	σ_B (μb)	31 ± 4	15 ± 5	16 ± 6
3.9	σ_F (μb)	67 ± 8	53 ± 9	14 ± 12
4.6	σ_T (μb)	65 ± 6	66 ± 6	−1 ± 8
4.6	σ_B (μb)	14 ± 2	21 ± 3	−7 ± 4
4.6	σ_F (μb)	51 ± 6	45 ± 5	6 ± 8
3.9	A (GeV^{-2})	1.8 ± 0.4	2.4 ± 0.6	−0.6 ± 0.7
4.6	A (GeV^{-2})	2.0 ± 0.3	2.2 ± 0.6	−0.2 ± 0.7
3.9 + 4.6	P_Λ	Large and positive in forward direction		

$$P_Y(K^-p \to Y\rho^0) = P_Y(K^-p \to Y\omega), \quad \text{(g)}$$

$$\rho_{mm'}(K^-p \to Y\rho^0) = \rho_{mm'}(K^-p \to Y\omega), \quad \text{(h)}$$

$$\frac{d\bar{\sigma}}{dt}(K^-p \to Y\phi) = \frac{d\bar{\sigma}}{dt}(\pi^-p \to YK(890)), \quad \text{(i)}$$

$$P_Y(K^-p \to Y\phi) = P_Y(\pi^-p \to YK(890)), \quad \text{(j)}$$

$$\rho_{mm'}(K^-p \to Y\phi) = \rho_{mm'}(\pi^-p \to YK(890)), \quad \text{(k)}$$

with

$$\bar{\sigma} \equiv \sum |A|^2 = \frac{P_{\text{in}}}{P_{\text{out}}} s\sigma,$$

s being the square of the center-of-mass energy.[76] P_Y and $\rho_{mm'}$ are the baryon polarization and vector-meson density-matrix elements, respectively.

B. Comparison of $K^-p \to \Lambda\omega$ and $K^-p \to \Lambda\rho$

The experimental data on the reaction

$$K^-p \to \Lambda\omega, \quad (1)$$

$$K^-p \to \Lambda\rho \quad (2)$$

of Sec. III are summarized in Table LII (note since $m_\omega \approx m_\rho$, no corrections for $\bar{\sigma}$ have been made). We observe that the forward ($\cos\theta^* > 0.0$) cross section, as well as the slope of the differential cross section, are in good agreement. In addition, both reactions exhibit large positive Λ polarizations in the forward momentum transfer region.

In Figs. 94(a)–94(e) are shown different combinations of density-matrix elements for the two reactions in both the Jackson and helicity frames. The combination ρ_{00} or $\rho_{11} - \rho_{1\,-1}$ ($\rho_{11} + \rho_{1\,-1}$) is expected to project out the contribution of the unnatural- (natural-) parity exchange.[28] As can be seen in Fig. 94(c), both reactions (1) and (2) have values of $\rho_{11} + \rho_{1\,-1}$ which average between 0.5 and 0.6 (for $|t'| < 1.0$ GeV^2), indicative of approximately equal parts of natural- and unnatural-parity exchange. We observe that the ρ_{ij} combinations for the two reactions are very similar in the peripheral region ($|-t'| < 1.0$ GeV^2) where the SU(3) predictions, cited above, are expected to hold. The only possible exception is a 3-standard-deviation difference in ρ_{00}, in the smallest momentum-transfer region ($|-t'| \leq 0.1$ GeV^2) where reaction (1) exhibits an anomalously large value. It is not clear whether this represents a violation of the SU(3) prediction or of a possible statistical fluctuation.

C. Comparison of Reactions $K^-p \to \Lambda\phi$ and $\pi^-p \to \Lambda K(890)$

We now compare the reaction

$$K^-p \to \Lambda\phi, \quad (1)$$

with

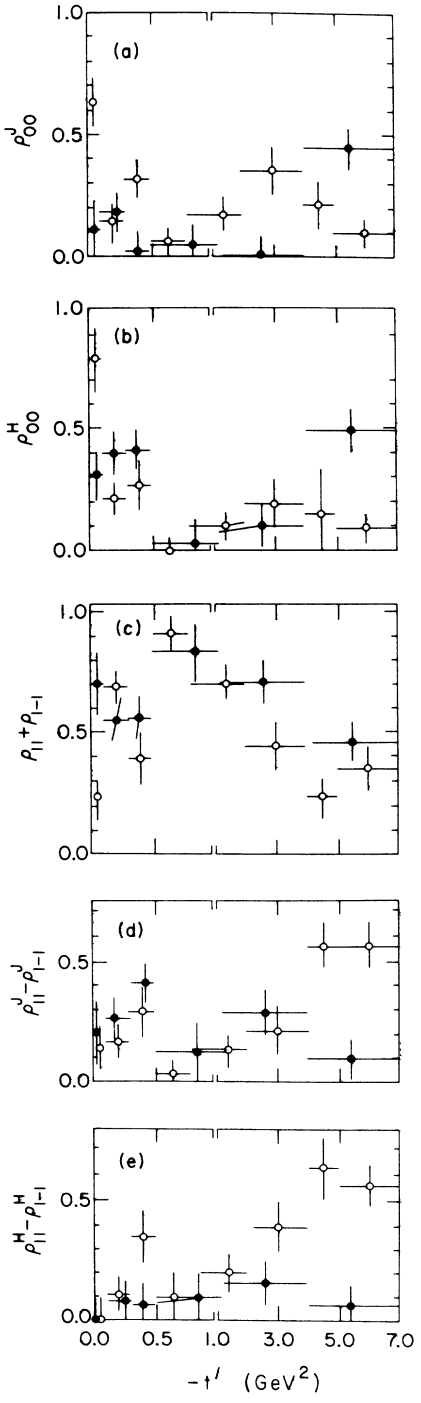

FIG. 94. (a)–(e) Comparison of the density-matrix elements of the vector mesons produced in the reaction $K^-p \to \Lambda\rho$ (closed dots) and $K^-p \to \Lambda\omega$ (open dots).

$$\pi^-p \to \Lambda K(890). \quad (2)$$

The data for reaction (2) come from a recent CERN bubble-chamber experiment at 3.9 GeV/c.[77] The cross section[78] in the momentum transfer region

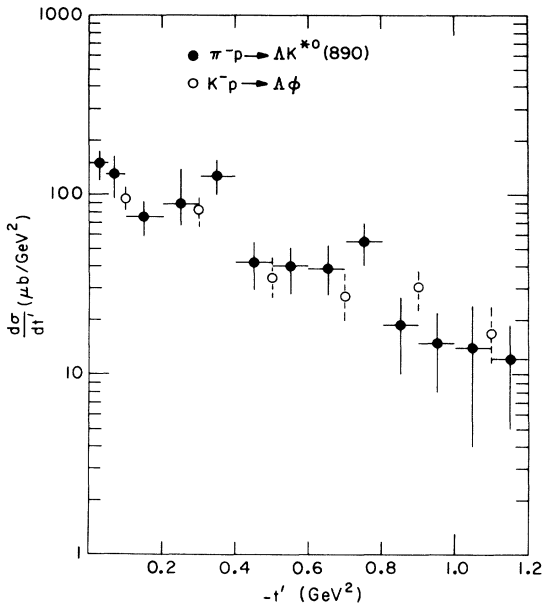

FIG. 95. Comparison of the differential cross section of the reaction $\pi^- p \to \Lambda K(890)$ (closed dots) and $K^- p \to \Lambda\phi$ (open dots) at 3.9 GeV/c.

$-t' < 1.0$ GeV^2 for reaction (1) is 54 ± 6 μb, to be compared to that for reaction (2) which is 64 ± 6 μb. Considering the normalization uncertainties inherent in comparing data from two different experiments, these values are in good agreement with each other. The differential cross sections shown in Fig. 95 are also, bin by bin, in excellent agreement. We have fitted each distribution to the form $d\sigma/dt' \sim e^{At'}$ and obtained

reaction (1a): $A = 1.9 \pm 0.2$ GeV^{-2},

reaction (1b): $A = 2.4 \pm 0.3$ GeV^{-2}.

The ϕ density-matrix elements from reaction 1 are shown in Figs. 96(a)–96(f) as open circles in both the Jackson and helicity frames. The corresponding density-matrix elements from reaction (2) are shown as closed circles in the figure. We observe remarkably good agreement between the values of $\rho_{mm'}$ as a function of momentum transfer. We note that both reactions exhibit a sharp rise in the value of ρ^H_{11} as a function of momentum transfer (corresponding to a dip in ρ^H_{00}, see Fig. 63), while the value of ρ^H_{1-1} remains constant; these observations suggest an increase in both the natural- and unnatural-parity contributions to the vector-meson helicity-one states, accompanied by a corresponding decrease of the unnatural parity contribution to the helicity-zero states.

In Fig. 97(a) the Λ polarization distributions are presented as a function of momentum transfer for the same two reactions. We observe that both reactions exhibit similar polarization in the momentum-transfer region shown. The shape of these distributions is in marked contrast to that in the reactions $K^- p \to \Lambda\rho$ and $K^- p \to \Lambda\omega$, which are shown in Fig. 97(b) for the same momentum-transfer region. It is interesting to note that broken-duality arguments predict a difference between the polarization of $\Lambda\phi$ (which has a planar diagram) and $\Lambda\omega$ or $\Lambda\rho$ (which both have nonplanar diagrams). In addition, we observe that the positive polarizations found in these latter reactions are consistent with that found in the $K^- p \to \Lambda\pi^0$ reaction which also has a nonplanar duality diagram, but which can only proceed through unnatural-parity exchange.

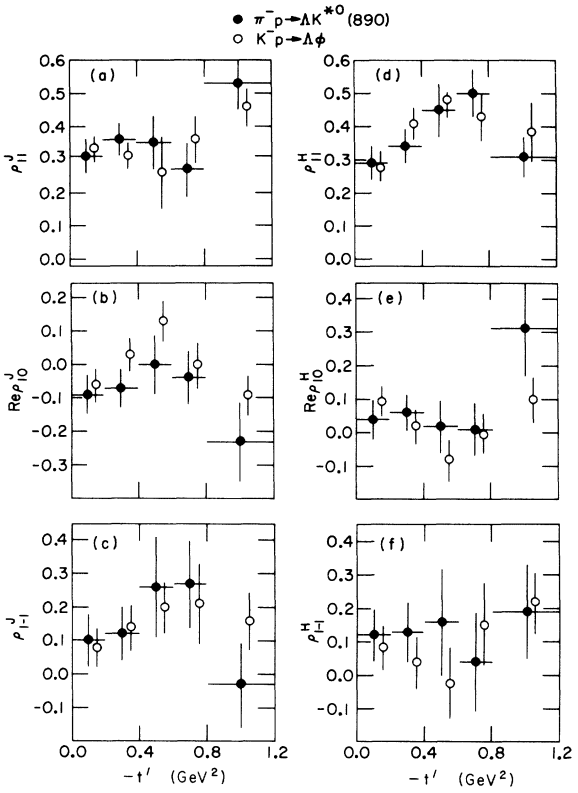

FIG. 96. Comparison of the density-matrix elements for the ϕ (open dots) and $K(890)$ (closed dots) produced off Λ: (a)–(c) Jackson frame; (d)–(f) helicity frame.

D. Comparison of Reactions $K^- p \to \Sigma^0\phi$ and $\pi^- p \to \Sigma^0 K(890)$

We now perform similar comparisons with the Σ^0 reactions:

$$K^- p \to \Sigma^0\phi, \tag{1b}$$

$$\pi^- p \to \Sigma^0 K(890). \tag{2b}$$

The $d\sigma/dt'$ (Ref. 79) and $\rho_{mm'}$ distributions for these reactions are displayed in Figs. 98 and 99, respec-

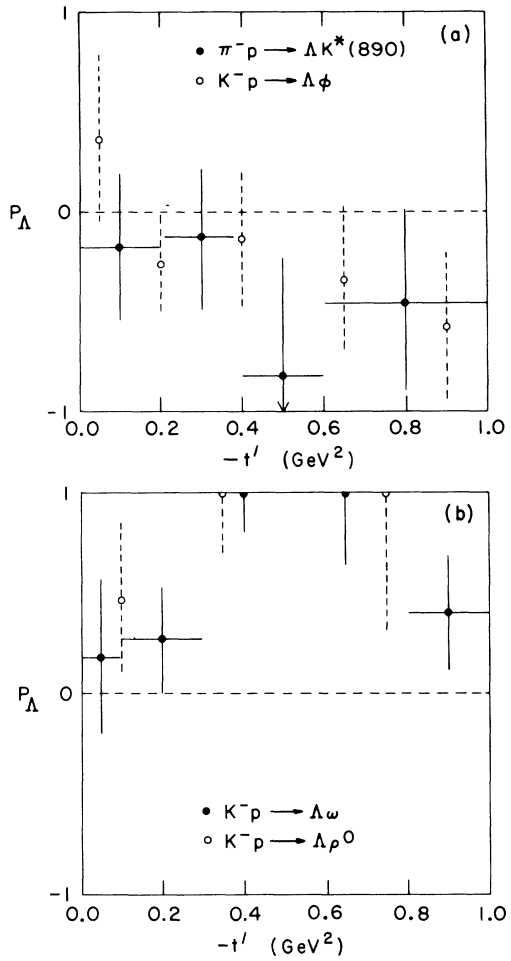

FIG. 97. Comparison of Λ polarization: (a) between the ϕ (open dots) and $K(890)$ (closed dots) reactions; (b) between the ω (closed dots) and ρ (open dots) reactions.

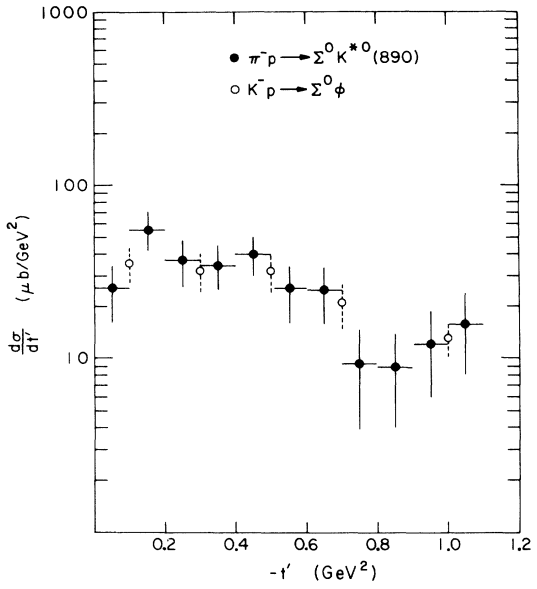

FIG. 98. Comparison of the differential cross section of the reaction $\pi^-p \rightarrow \Sigma^0K(890)$ (closed dots) and $K^-p \rightarrow \Sigma^0\phi$ (open dots) at 3.9 GeV/c.

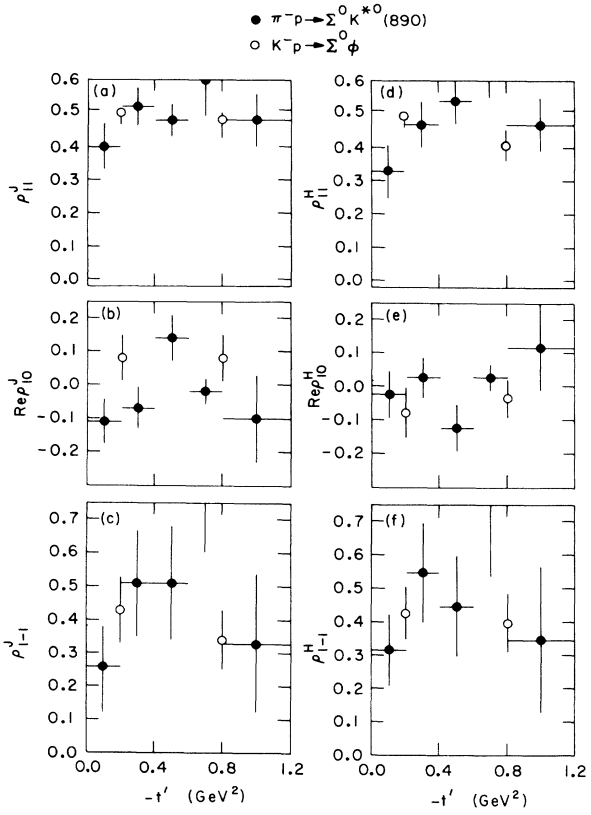

FIG. 99. Comparison of the density-matrix elements for the ϕ (open dots) and $K(890)$ (closed dots) produced off Σ^0: (a)–(c) Jackson frame; (d)–(f) helicity frame.

tively. All distributions are observed to be in good agreement with the equality suggested from this simple SU(3) approach. The cross section for $|-t'| < 1.0$ GeV^2 is found to be 25 ± 5 μb (including the relative correction factor to $\bar{\sigma}$ of 1.05) for reaction (1b) compared to (27 ± 5) μb for reaction (2b), in excellent agreement with each other as are the fitted values of the slope parameters for the two reactions which were found to be

reaction (1b): $A = 1.1 \pm 0.4$ GeV^{-2},

reaction (2b): $A = 1.3 \pm 0.3$ GeV^{-2}.

On the other hand, these slopes are both about 2 standard deviations smaller than in the corresponding Λ reactions whose values are quoted above.

In addition, the values of the $\rho_{mm'}$ density matrix elements are different; the Σ^0 reactions have larger values of both ρ_{11} and ρ_{1-1}, indicative of

dominant natural-parity contributions with little contribution from unnatural-parity exchange. It is then the interference of these natural-parity objects which produces the observed large positive Σ^0 polarization in the $\Sigma^0\phi$ reaction.

In summary, we have found that the simple SU(3) relation (e) is in good agreement with the experimentally observed distributions for both Σ^0 and Λ reactions at an incident momentum of 3.9 and 4.6 GeV/c. This justifies, *a posteriori*, that the mass-dependent kinematic factors (e.g., the threshold and pseudothreshold factors) and absorptive effects do not significantly affect this simple equality. It is indeed remarkable to see that further dynamical considerations, such as these, do not lead to a gross violation of the simple SU(3) picture.

E. Comparison of Line-Reversed Reactions

In this section we compare the line-reversed reactions

$$K^-p \to \Lambda\pi^0 \text{ at } 3.9 \text{ GeV}/c, \tag{1a}$$

$$\pi^-p \to \Lambda K^0 \text{ at } 3.9 \text{ GeV}/c \tag{1b}$$

as well as

$$K^-p \to Y^{*+}(1385)\pi^- \text{ at } 3.9 \text{ GeV}/c, \tag{2a}$$

$$\pi^+p \to Y^{*+}(1385)K^+ \text{ at } 4.0 \text{ GeV}/c. \tag{2b}$$

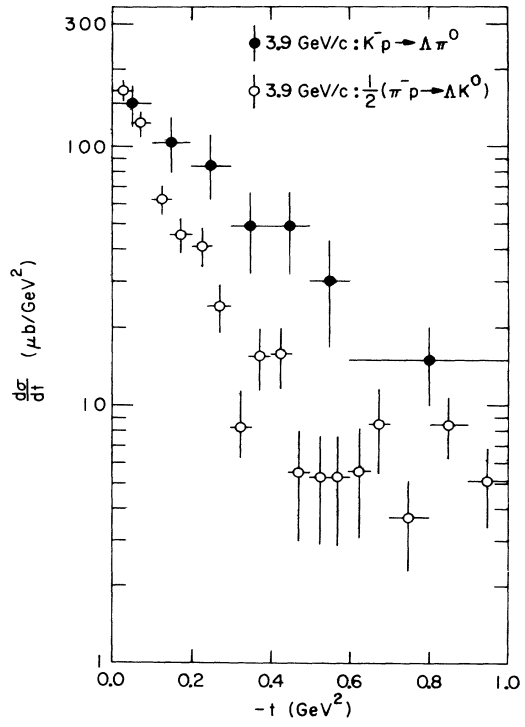

FIG. 100. Comparison of the differential cross section for the reactions $K^-p \to \Lambda\pi^0$ and $\pi^-p \to \Lambda K^0$ at 3.9 GeV/c.

The data for reaction (1b) are from Abramovich *et al.*[80] while those of reaction (2b) are from Ying *et al.*[81]

Each set of reactions has an identical baryon vertex and a meson vertex which we relate, as in the previous section, by coupling of $K^*(890)$ (or any F-type coupling) and $K^*(1420)$ exchange. The SU(3) amplitude for the processes (1) listed above can then be written

$$A = (\tfrac{1}{3})^{1/2}[\tfrac{1}{2}A_F^8 + \tfrac{3}{10}\sqrt{5}\,A_D^8], \tag{1a'}$$

$$A = (\tfrac{2}{3})^{1/2}[-\tfrac{1}{2}A_F^8 + \tfrac{3}{10}\sqrt{5}\,A_D^8] \tag{1b'}$$

and for reactions (2)

$$A = (\tfrac{2}{3})^{1/2}[\tfrac{1}{2}A_F'^8 + \tfrac{3}{10}\sqrt{5}\,A_D'^8], \tag{2a'}$$

$$A = -(\tfrac{2}{3})^{1/2}[-\tfrac{1}{2}A_F'^8 + \tfrac{3}{10}\sqrt{5}\,A_D'^8], \tag{2b'}$$

where A_F^8 (A_D^8) are the antisymmetric (symmetric) SU(3) octet amplitudes. We observe that, without additional dynamical assumptions on the nature of the structure of the amplitudes [e.g., Regge-pole exchange, exchange degeneracy of $K^*(890)$ and $K^*(1420)$, absorption effects, etc.], the sign of the interference term between the F- and D-type exchange diagrams is different between the line-reversed reactions [i.e., (1a) and (1b) as well as (2a)

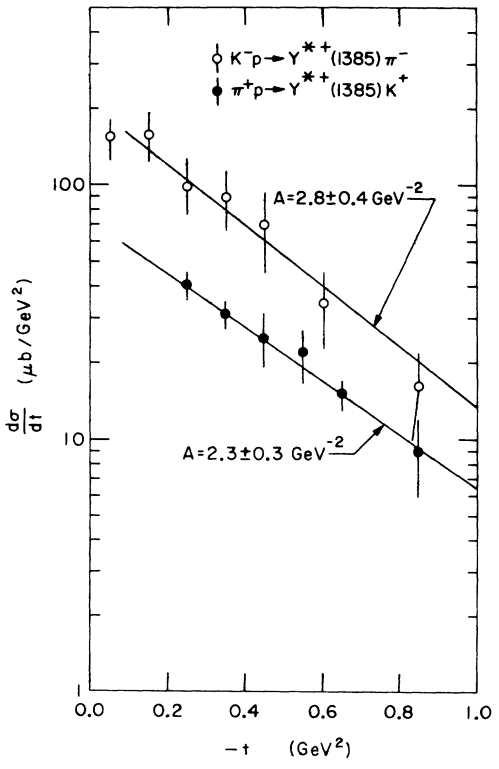

FIG. 101. Comparison of the differential cross section of the reaction $K^-p \to Y^{*+}(1385)\pi^-$ (open dots) and $\pi^+p \to Y^{*+}(1385)K^+$ (closed dots).

and (2b)]. We would then expect the cross sections for the line-reversed reactions to be the same for reaction (2) and in the ratio 1:2 for reaction (1) only if their interference term is equal to zero or if the F- or D-type exchange vanishes.

In Fig. 100 we show $\frac{1}{2}d\sigma/dt$ [reaction (1b)] and $d\sigma/dt$ [reaction (1a)], and in Fig. 101, $d\sigma/dt$ for reactions (2a) and (2b). We observe, in agreement with previous investigations, that the cross sections which involve an incident K^- are larger than the corresponding line-reversed π reactions. These observations suggest that a simple noninterference $K^*(890)$-$K^*(1420)$ model cannot be invoked to describe the experimental data at our energy. Similar conclusions[82] have been deduced from previous investigations via the failure of exchange-degenerate $K^*(890)$-$K^*(1420)$ (even with absorption included) Regge-pole models to account for the difference in cross section [as well as Λ polarization in reaction (1)] of the reactions discussed above. It is interesting to note that (1a) and (1b) have, within the experimental errors, identical cross sections in the forwardmost bin of momentum transfer. We also observe that the slopes of the differential cross sections of reactions (2a) and (2b) are equal, while that of reaction (1b) is almost twice that of (1a).

VIII. COMPARISON OF ρ AND ϕ MESONS PRODUCED WITH Λ, Σ^0, AND $Y^*(1385)$

In this section we summarize the experimental data on vector-meson production (ρ and ϕ) each accompanied by a Λ, Σ^0, or $Y^*(1385)$. We present a detailed comparison of the data with quark [or equivalently SU(6)] model predictions which relate the reactions

$$K^-p \to [\Lambda, \Sigma^0, Y^*(1385)] + V,$$

where V is any vector meson.

We find, in agreement with a previous investigation by Hirsch *et al.*[83] at 3.0 GeV/c, that certain quark-model predictions are in violation with the experimental data. In addition, our data do not agree with a particular broken-SU(6) prediction, proposed by Hirsch *et al.*,[84] which was satisfied at 3.0 GeV/c. We briefly discuss the quark-model prediction with more details to be found in Ref. 43.

A. Quark-Model Predictions

The quark model with the additivity conditions or an exchange model utilizing SU(6) symmetry predicts the following sum rule among the cross sections for vector-meson production in the peripheral region:

$$\bar{\sigma}(\Lambda) = 3[\bar{\sigma}(\Sigma^0) + \bar{\sigma}(Y^{*0})], \tag{13}$$

where $\bar{\sigma}$ is defined as in the previous section.

We now define three combinations of density matrix elements,

$$\rho_{xx} = \rho^J_{11} - \rho^J_{1\,-1},$$

$$\rho_{yy} = \rho^J_{11} + \rho^J_{1\,-1},$$

$$\rho_{zz} = \rho^J_{00},$$

where ρ^J_{ij} are the vector-meson density-matrix elements evaluated in the Jackson frame.

The cross sections for a specific polarization state are then defined as

$$\bar{\sigma}^{(i)} = \rho_{ii}\,\bar{\sigma} \quad (i = x, y, z).$$

The combinations $\bar{\sigma}^{(x)}$ and $\bar{\sigma}^{(y)}$ are predicted to obey the following relationships:

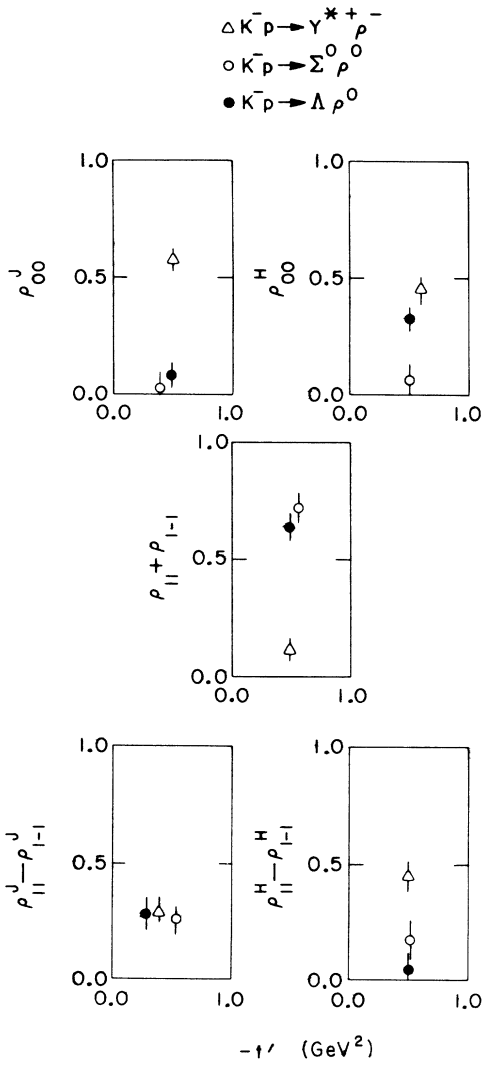

FIG. 102. Comparison of the ρ density-matrix elements for $|t'| < 1.0$ GeV^2 from the reactions $K^-p \to \Lambda\rho^0$ (closed dots), $K^-p \to \Sigma^0\rho^0$ (open dots), and $K^-p \to Y^{*+}\rho^-$ (triangles).

$$\bar{\sigma}^{(x)}(\Lambda):\bar{\sigma}^{(x)}(\Sigma^0):\bar{\sigma}^{(x)}(Y^*)=27:1:8, \quad (14)$$

$$\bar{\sigma}^{(z)}(\Lambda):\bar{\sigma}^{(z)}(\Sigma^0):\bar{\sigma}^{(z)}(Y^*)=27:1:8, \quad (15)$$

while $\bar{\sigma}^{(y)}$ should obey a similar relation to (1), namely,

$$\bar{\sigma}^{(y)}(\Lambda)=3[\bar{\sigma}^{(y)}(\Sigma^0)+\bar{\sigma}^{(y)}(Y^{*0})]. \quad (16)$$

The data[83] at 3.0 GeV/c were observed to violate these predictions for events produced with $\cos\theta^*>0.0$ (θ^* is the center-of-mass angle between the incident and outgoing baryon) for ρ and ω production; however, they were observed to satisfy the following relationship:

$$\frac{\rho_{zz}(\Lambda)}{\rho_{xx}(\Lambda)}=\frac{\rho_{zz}(\Sigma^0)}{\rho_{xx}(\Sigma^0)}=\frac{\rho_{zz}(Y^*)}{\rho_{xx}(Y^*)}, \quad (17)$$

$$\rho_{yy}(\Sigma)\geq\rho_{yy}(\Lambda)\geq\rho_{yy}(Y^{*0}), \quad (18)$$

which led the authors of Ref. 84 [based on a broken-SU(6) analysis] to suggest that (17) and (18) should be generally valid even if (13) to (16) are violated.

B. Reactions Involving the ρ Meson

We now compare the production properties of the ρ meson produced off Λ, Σ^0, and $Y^*(1385)$. Instead of using the lesser statistical sample of $K^-p\to Y^{*0}(1385)\rho^0$ events we have used the data on the reaction $K^-p\to Y^{*+}(1385)\rho^-$ whose cross sections are related by

$$\sigma(Y^{*+}\rho^-)=4\sigma(Y^{*0}\rho^0)$$

if, as we have previously shown, the $I=\frac{3}{2}$ exotic t-channel exchange contribution can be neglected. We have tested the quark-model prediction on the Λ^0, Σ^0, and $Y^*(1385)$ reactions in the forward region of momentum transfer, $|t'|<1.0$ GeV^2, with cross sections determined from the averaged 3.9- and 4.6-GeV/c data sample (for the $\bar{\sigma}$ corrections we used an average incident K^- momentum of 4.25 GeV/c). In Fig. 102 are shown the density-matrix element combinations referred to in the last section. We observe, in the Jackson frame, that the Σ^0 and Λ^0 have similar values of ρ_{ii}, which are very different from those of the $Y^*\rho$ reaction, which, as previously mentioned, has a small natural-parity contribution (small $\rho^J_{11}+\rho^J_{1-1}$ and large ρ^J_{00}). All relevant experimental data on the reactions are given in Table LIII. We have tested quark relations (13)–(16) with the results given in the table where

$f_1=1$ for Λ,
$=3$ for Σ^0 or Y^*,
$f=\frac{1}{27}$ for Λ,
$=1$ for Σ^0,
$=\frac{1}{8}$ for Y^*.

We observe a strong violation of relation (13) with the Y^* plus Σ^0 cross sections almost 6 standard deviations larger than predicted by the quark model. In addition, the Λ^0/Σ^0 ratio of 1.93 ± 0.38 vio-

TABLE LIII. Test of quark-model predictions for reactions $K^-p\to\{\Lambda,\Sigma^0,Y^{*0}\}\rho^0$.

Measured quantity	Reaction: $K^-p\to$ $\Lambda\rho^0$	$\Sigma^0\rho^0$	$Y^{*+}\rho^-$
$\langle\sigma\rangle$ (μb)	39.4 ± 4.8	19.8 ± 3.0	13.5 ± 1.3[a]
$\bar{\sigma}$ (μb GeV^2)	403 ± 49	209 ± 32	156 ± 15
Slope (GeV^{-2})	2.3 ± 0.4	1.9 ± 0.5	2.7 ± 0.5
$\rho_{zz}=\rho^J_{00}$	0.08± 0.05	$0.02^{+0.08}_{-0.02}$	0.58± 0.05
$\rho_{yy}=\rho^J_{11}+\rho^J_{1-1}$	0.64± 0.06	0.72± 0.06	0.12± 0.03
$\rho_{xx}=\rho^J_{11}-\rho^J_{1-1}$	0.28± 0.06	0.26± 0.06	0.30± 0.03
Relation[b]			
(13) $f_1\bar{\sigma}$	403 ± 49	1095± 106	
(14) $f\bar{\sigma}^{(x)}$	4.2 ± 1.0	54.3 ± 15.0	5.9 ± 0.8
(15) $f\bar{\sigma}^{(z)}$	1.2 ± 0.8	$4.2^{+16.8}_{-4.2}$	11.3 ± 1.5
(16) $f_1\bar{\sigma}^{(y)}$	258 ± 40	506± 79	
(17) $\left(\frac{\rho_{zz}}{\rho_{xx}}\right)$	0.29± 0.19	$0.08^{+0.32}_{-0.08}$	1.93± 0.25

[a] As discussed in the text, we use the relation $\sigma(K^-p\to Y^{*0}\rho^0)=\frac{1}{4}\sigma(K^-p\to Y^{*+}\rho^-)$.

[b] The values of f_1 and f are given in the text.

lates by 3 standard deviations a previous prediction of Lipkin[85] [based on the SU(6) model] of

$$\bar{\sigma}(\Lambda^0) \geq 3\bar{\sigma}(\Sigma^0).$$

Also as observed in Table LIII predictions (14)–(16) are grossly violated.

In addition, while relation (18) is consistent with the data, relation (17) fails between Λ and Y^* by 5 standard deviations.

We comment that the ρ^J_{00} density-matrix elements for the ρ^0 in both the Σ^0 and Λ reaction are significantly smaller than those obtained in the 3.0-GeV/c analysis in which relations (17) and (18) were found to be satisfied. This discrepancy may be caused by the different production dynamics between 3.0 and 4.0 GeV/c or by the different t region investigated, or else by the difference in the method of extraction of the density-matrix elements in the two experiments. As commented previously, we have explicitly handled the resonance and background term on an equal footing through a mass-dependent analysis. It is also clear that failure to include the S-wave background will produce a distortion of the resonance angular distribution in such a direction as to flatten the true $\cos\theta$ resonance terms and produce a larger (or smaller) value of ρ_{00} if its true value is less (or greater) than 0.33.[25]

C. Reactions Involving the ϕ Meson

In Fig. 103 we present a comparison of the density-matrix elements of the ϕ meson produced with Λ, Σ^0, and $Y^*(1385)$ for the combined data at 3.9 and 4.6 GeV/c. We restrict the remainder of this discussion to the data in the very peripheral region of $|-t'|<0.5$ GeV^2. Here we observe a difference between the density-matrix elements of the ϕ in the Λ^0 and Σ^0 reactions. The former reaction is observed to be dominated by natural-parity ex-

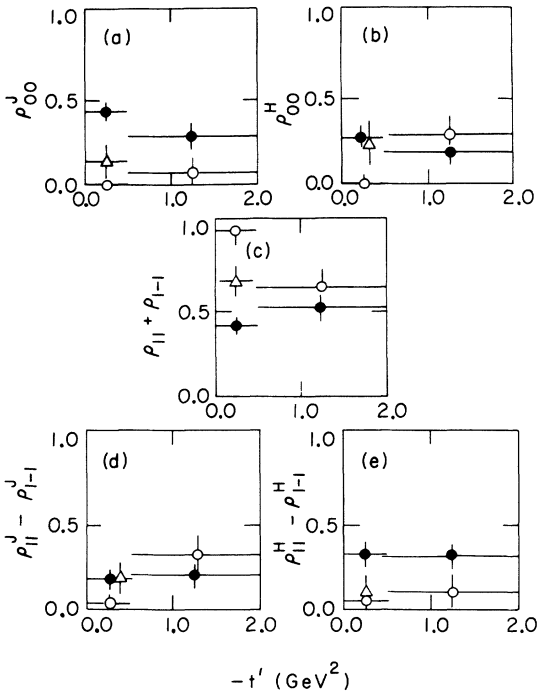

FIG. 103. Comparison of the ϕ density-matrix elements from the reactions $K^-p \to \Lambda\phi$ (closed dots), $K^-p \to \Sigma^0\phi$ (open dots) and $K^-p \to Y^{*0}(1385)\phi$ (triangles).

TABLE LIV. Test of quark-model predictions for reactions $K^-p \to \{\Lambda, \Sigma^0, Y^{*0}\}\phi$.

Measured quantity	Reaction: $K^-p \to$ $\Lambda\phi$	$\Sigma^0\phi$	$Y^{*0}\phi$
$\langle\sigma\rangle$ (μb)	24.5 ± 2.0	8.1 ± 1.4	11 ± 1.7
$\bar{\sigma}$ (μb GeV^2)	276 ± 23	95 ± 16	146 ± 23
Slope (GeV^{-2})	2.0 ± 0.2	1.1 ± 0.4	2.8 ± 0.8
$\rho_{zz}=\rho^J_{00}$	0.43± 0.05	$0.00^{+0.02}_{-0.00}$	0.15± 0.09
$\rho_{yy}=\rho^J_{11}+\rho^J_{1-1}$	0.41± 0.05	$0.98^{+0.02}_{-0.08}$	0.68± 0.09
$\rho_{xx}=\rho^J_{11}-\rho^J_{1-1}$	0.16± 0.05	$0.02^{+0.08}_{-0.02}$	0.18± 0.09
Relation[a]			
(13) $f_1\bar{\sigma}$	276 ± 23	723± 84	
(14) $f\bar{\sigma}^{(x)}$	1.6 ± 0.5	$1.9^{+7.6}_{-1.9}$	3.3 ± 1.7
(15) $f\bar{\sigma}^{(z)}$	4.4 ± 0.6	$0.0^{+1.9}_{-0.0}$	2.7 ± 1.7
(16) $f_1\bar{\sigma}^{(y)}$	113 ± 17	576± 79	
(17) $\left(\frac{\rho_{zz}}{\rho_{xx}}\right)$	2.7 ± 0.9	···	0.83± 0.65

[a] The values of f_1 and f are given in the text.

change mechanism ($\rho^J_{00} = 0.0$; $\rho_{11} + \rho_{1\,-1} = 1.0$) while the latter reaction has contributions from both natural- and unnatural-parity exchange.

In Table LIV are presented the results of the test of the quark-model predictions (13)–(16). We observe as in the ρ case that relations (13) and (16) are in gross violation with the experimental data, however, here relations (14) and (15) are consistent with the experimental observation. In addition, the inequality relation (17) is also violated by the experimental data [i.e., $\rho_{yy}(Y^{*0}) \geq \rho_{yy}(\Lambda)$] by ~3 standard deviations.

D. Summary of Quark-Model Predictions

As discussed above we have found the additivity quark-model or SU(6) predictions to be in gross violation with the experimental data in both ϕ and ρ production. We have found the relations (17) and (18) suggested by Hirsch *et al.*[84] to be similarly violated.

IX. TEST OF A QUARK-MODEL PREDICTION IN WHICH THE BARYON VERTEX REMAINS INVARIANT

We have seen that the predictions of the quark model are in violation with the experimental data for reactions in which the baryon vertex changes with the meson vertex remaining the same. We now test the following quark-model relation[86] in which the baryon vertex is invariant, and in which the meson vertex changes:

$$\bar{\sigma}(K^- p \to \Lambda\eta) + \bar{\sigma}(K^- p \to \Lambda\eta') = \bar{\sigma}(K^- p \to \Lambda\pi^0) + \bar{\sigma}(\pi^- p \to \Lambda K^0). \quad \text{(a)}$$

The relevant experimental cross sections are (at 3.9 GeV/c):

$K^- p \to \Lambda\eta$: $\sigma = 26 \pm 6$ μb; $\bar{\sigma} = 236 \pm 55$ μb GeV^2,

$K^- p \to \Lambda\eta'$: $\sigma = 45 \pm 7$ μb; $\bar{\sigma} = 469 \pm 73$ μb GeV^2,

$K^- p \to \Lambda\pi^0$: $\sigma = 67 \pm 6$ μb; $\bar{\sigma} = 576 \pm 52$ μb GeV^2,

$\pi^- p \to \Lambda K^0$ (Ref. 80): $\sigma = 58 \pm 3$ μb; $\bar{\sigma} = 545 \pm 28$ μb GeV^2,

so that the left-hand side ($\bar{\sigma} = 705 \pm 91$) differs from the right-hand side ($\bar{\sigma} = 1121 \pm 59$) of (a) by almost 4 standard deviations. As can be seen, this violation of the quark-model relation (a) is caused by the relatively small cross section for η production in our energy region. In addition, we note that the shape of the differential cross sections in the peripheral region for the four reactions are different (see Figs. 23, 26, 35, and 100). We thus conclude that the quark-model prediction (a) is in disagreement with the experimental data in our intermediate energy region.

ACKNOWLEDGMENTS

We acknowledge the help in many stages of this experiment of Dr. V. E. Barnes, Dr. D. Bassano, Dr. E. Flaminio, Dr. M. Goldberg, Dr. J. B. Kinson, and Dr. D. Pandoulas. We particularly thank Dr. K. Jaeger, whose thesis was on the final states discussed in the present analysis and from which most of the numbers in the compilation of cross sections (Tables XLV–LI) have been taken. We acknowledge many helpful and stimulating discussions with Dr. R. Field. We also thank the AGS and 80-in. bubble-chamber staffs and crews for their help in obtaining the pictures, and our data-handling personnel for their efforts.

---

*Work supported by the U. S. Atomic Energy Commission.

[1]M. Aguilar-Benitez, R. L. Eisner, and J. B. Kinson, Phys. Rev. D 4, 2583 (1971).

[2]As in the remainder of the paper, $t' = t - t_{max}$ where t is the momentum transfer between target proton and outgoing baryon and t_{max} is the minimum momentum transfer for a given event.

[3]As in the remainder of the paper the Λ polarization was extracted using a maximum-likelihood technique with the form

$$W(\cos\theta) = \tfrac{1}{2}(1 + \alpha_\Lambda P_\Lambda \cos\theta),$$

where P_Λ is the Λ polarization and $\alpha_\Lambda = 0.645$. The angle θ is the angle between the outgoing proton in the Λ rest frame and the normal to the production plane defined as $\hat{p}_{in} \times \hat{\Lambda}_{out}$ where $\hat{p}_{in}$ ($\hat{\Lambda}_{out}$)is the direction of the target proton (Λ) in the over-all center-of-mass system.

[4]D. J. Crennell *et al.*, Phys. Rev. Letters 23, 1347 (1969).

[5]W. L. Yen *et al.*, Phys. Rev. Letters 22, 963 (1969).

[6]All cross sections in this paper have been corrected for Λ visibility and losses as well as for probability cuts where needed. Total cross sections have been corrected for unseen resonance decay modes using Particle Data Group, Rev. Mod. Phys. 43, S1 (1971).

[7]Particle Data Group, Ref. 6.

[8]A. Rittenberg, Ph. D. thesis, LBL Report No. UCRL 18863, 1969 (unpublished).

[9]V. I. Oglievetsky, W. Tybor, and A. N. Zaslavsky, Phys. Letters 35B, 69 (1971).

[10]The resonance region is defined as 0.930–0.980 GeV. The control regions are 0.905–0.930 GeV and 0.980–1.005 GeV.

[11]The $\pi^+\pi^-$ background distribution has been normalized to the central value of the η' mass using the method employed in Ref. 8.

[12]The matrix element used is $\sim K^2 q^2 m^2 \sin^2\theta$ where $K(q)$

is the $\gamma(\pi^+)$ momentum, θ is the angle between the γ and π^+, and m is the dipion effective mass (all evaluated in the dipion rest frame).

[13]$\cos(\pi^+,\eta)$ is the angle between the π^+ and η in the $\pi^+\pi^-$ rest frame.

[14]J. P. Dufey *et al.*, Phys. Letters 29B, 605 (1969).

[15]G. W. London, Phys. Rev. 143, 1034 (1966).

[16]See ρ^0 analysis in Sec. III B 1 b for further discussion.

[17]M. Aguilar-Benitez *et al.*, Phys. Rev. Letters 25, 1635 (1970).

[18]Note that since no probability selections were imposed on the $K^-p\pi^+\pi^-\pi^0$ hypothesis, events of the type $K^-p \to K^-pK^+K^-$ are also included in this mass spectrum so that we are mainly observing the $\phi \to K^+K^-$ decay mode.

[19]All events that fitted the 4c reactions $K^-\pi^-\pi^+p$ and $K^-K^+K^-p$ were removed. Reaction (b) was selected if its χ^2 probability was greater than any of the other 1c hypotheses. See Ref. 17 for more details.

[20]Events in the $Y^{*+}(1385)$ band have been removed and the region then repopulated with conjugate events according to the method of P. Eberhard and M. Pripstein, Phys. Rev. Letters 10, 351 (1963). This method has been employed for the entire sample in order to obtain an estimate of the background under the conjugate resonance sample. This approach assumes no interference between $\pi\pi$ resonance and $Y^*(1385)$; however, after removal of the narrow Y^{*+} [$1.34 \le M(\Lambda\pi^+) \le 1.42$ GeV], there is no significant difference in the number of ρ^0 events obtained between the repopulated and nonrepopulated sample so that strong interference effects can be ruled out between Y^* and ρ.

[21]This assumes that the helicity angular distribution of the signal and the background are symmetric; however, because of the narrow $Y^{*+}(1385)$ selection, even if this were not the case in our data, it would present only a small systematic error in the resonance density-matrix elements so obtained.

[22]See, for example, E. Malamud and P. E. Schlein, Phys. Rev. Letters 19, 1057 (1967).

[23]Of course, the ϵ^0 and correspondingly any S-wave $\pi\pi$ background in the ρ^0 region may be produced by K exchange and be incoherent with the ρ^0 production. This would lead to no observed interference effects in the ρ^0 angular distribution.

[24]See, for example, R. L. Eisner *et al.*, Phys. Rev. 164, 1699 (1967).

[25]If one uses this traditional approach of neglecting the S-wave background, it is easy to show that one obtains a value ρ'_{00} which is related to the true value ρ^T_{00} by

$$\rho'_{00} = \tfrac{1}{3} + \epsilon_P{}^2\{\rho^T_{00} - \tfrac{1}{2}\} = \tfrac{1}{3}\epsilon_S{}^2 + \epsilon_P{}^2\rho^T_{00},$$

where $\epsilon_P{}^2$ ($\epsilon_S{}^2$) is the fraction of P wave (S wave) in the given region and $\epsilon_S{}^2 + \epsilon_P{}^2 = 1$.

[26]M. Aguilar-Benitez *et al.*, preceding paper, Phys. Rev. D 6, 11 (1972).

[27]S. M. Berman and M. Jacob, Phys. Rev. 139, B1023 (1965).

[28]As shown in J. Ader *et al.*, Nuovo Cimento 56A, 952 (1968), the quantity of $\rho_{11} + \rho_{1-1}$ projects out the contribution of the natural-parity exchange, and ρ_{00} ($\rho_{11} - \rho_{1-1}$) projects out the unnatural-parity contribution to the helicity-zero (-one) states.

[29]The average experimental resolution in the ϕ region for this channel is $\sigma = 1.18$ MeV.

[30]The branching ratio obtained at 3.9 GeV/c was 0.90 ± 0.14, and at 4.6 GeV/c was 0.89 ± 0.14.

[31]The width was fixed at the value obtained from the K^+K^- decay mode of the ϕ. The experimentally determined resolution was folded into the resonance shape.

[32]To correct for the $MM^2 > 0.01$ GeV^2 selection, the number of $\pi^+\pi^-\pi^0$ events has been multiplied by the ratio of ω's found in total to that observed with $MM^2 > 0.01$ GeV^2.

[33]See references in Sec. VI for production of the reaction $K^-p \to \Lambda\phi$.

[34]We have not performed a mass-dependent analysis because of the narrow width of the ϕ as well as the observed small backgrounds relative to signals [see Figs. 60(a)–60(d)].

[35]There is no significant $Y^{*+}(1385)$ reflection into the backward-produced f^0 sample.

[36]The cross sections quoted have been corrected for unobserved resonance decay modes as well as for the tails of the A_2 and ρ.

[37]V. E. Barnes *et al.*, Phys. Rev. Letters 15, 322 (1965).

[38]We use the ϕ decay rates as given in the $K^-p \to \Lambda\phi$ section.

[39]There is no significant reflection from ρ^0 or f^0 in the $Y^*(1385)$ sample.

[40]This condition is derived in M. Doncel, L. Michel, and P. Minneart, Laboratoire de Physique Théorique Report No. PTB-37 (unpublished). Note that, by nature of the Schwarz inequality, $|\rho_{3+1}|^2 \le \rho_{33}\rho_{11}$ so that $|\mathrm{Re}\rho_{31}|$ and $|\mathrm{Re}\rho_{3-1}|$ are required to be less than 0.25.

[41]L. Stodolsky and J. J. Sakurai, Phys. Rev. Letters 11, 90 (1963).

[42]A fit was also performed which allowed the resonance fraction and background term to vary with the values of the $\rho_{mm'}$ fixed at the Stodolsky-Sakurai predictions. The resultant log of the likelihood differed by five units from that of the fit quoted in the text.

[43]A. Białas and K. Zalewski, Nucl. Phys. B6, 449 (1968); B6, 465 (1968); B6, 478 (1968); B6, 483 (1968).

[44]The quoted errors encompass 1-standard-deviation errors from the two methods of determining the number of quasi-two-body events.

[45]The method consisted of dividing the $\Lambda\pi^+\pi^-\pi^0$ triangular plot into rectangular areas A, B, C, D, E and X_i ($i = 1,4$) which are defined by

A: $0.64 \le M(\pi^-\pi^0) \le 0.92$ GeV; $1.34 \le M(\Lambda\pi^+) \le 1.42$ GeV,
B: $0.96 \le M(\pi^-\pi^0) \le 1.12$ GeV; $1.34 \le M(\Lambda\pi^+) \le 1.42$ GeV,
C: $0.48 \le M(\pi^-\pi^0) \le 0.60$ GeV; $1.34 \le M(\Lambda\pi^+) \le 1.42$ GeV,
D: $0.64 \le M(\pi^-\pi^0) \le 0.92$ GeV; $1.26 \le M(\Lambda\pi^+) \le 1.30$ GeV,
E: $0.64 \le M(\pi^-\pi^0) \le 0.92$ GeV; $1.46 \le M(\Lambda\pi^+) \le 1.50$ GeV,
X_1: $0.48 \le M(\pi^-\pi^0) \le 0.60$ GeV; $1.46 \le M(\Lambda\pi^+) \le 1.50$ GeV,
X_2: $0.48 \le M(\pi^-\pi^0) \le 0.60$ GeV; $1.26 \le M(\Lambda\pi^+) \le 1.30$ GeV,
X_3: $0.96 \le M(\pi^-\pi^0) \le 1.12$ GeV; $1.26 \le M(\Lambda\pi^+) \le 1.30$ GeV,
X_4: $0.96 \le M(\pi^-\pi^0) \le 1.12$ GeV; $1.46 \le M(\Lambda\pi^+) \le 1.50$ GeV,

so that to a good approximation the number of $Y^*\rho$ events in A, N, can be written

$$N = A - (B + C + D + E) + \sum_i X_i$$

where A, B, C, D, E, and X_i now represent the number of events in the corresponding grid location. This method fails to find the total number of $Y^*\rho$ events by missing the events in the Y^* and ρ tails.

[46]The same factor found in the $Y^{*+}\rho^-$ analysis was used.

[47]The background estimate of non-$Y^*\rho$ events in this

band was found to be ~ 25% from the method of fitting the $\Lambda\pi^+$ (or $\pi^-\pi^0$) mass spectrum as a function of $\pi^+\pi^-$ (or $\Lambda\pi^+$) effective mass. The errors quoted on the values of the $T^{LL'}_{mm'}$ should be large enough to encompass any systematic error from the background. As a check we have found that the values of the $\rho_{mm'}$ (i.e., for ρ^0 or Y^{*+}) obtained from our mass-dependent fits and those obtained without a background subtraction are not significantly different.

[48]The transversity [Jackson transversity] frame has the x axis along the direction of the decaying particle in the over-all center of mass system [(target proton) direction in $\rho(Y^*)$ rest frame].

[49]A. Białas, A. Gula, and M. Muryn, Phys. Letters 24B, 428 (1967); A. Białas and K. Zalewski, *ibid.* 26B, 170 (1968). See also M. Aderholz *et al.*, Nucl. Phys. B8, 485 (1968), for a similar analysis of the reaction $\pi^+p \to \Delta^{++}\rho^0$ and $\pi^+p \to \Delta^{++}\omega$.

[50]See compilation of coupling constants, G. Ebel *et al.*, Nucl. Phys. B33, 317 (1971).

[51]C. G. Wohl *et al.*, Phys. Rev. Letters 17, 107 (1966).

[52]L. T. Smith *et al.*, in *Proceedings of the Athens Second Topical Conference on Resonant Particles, Athens, Ohio, 10-12 June 1965,* edited by B. A. Munir (Ohio University Press, Athens, Ohio, 1965).

[53]G. London *et al.*, Phys. Rev. 143, 1034 (1966).

[54]J. Badier *et al.*, CEA Report No. CEA 68-7 (unpublished).

[55]R. Barloutaud *et al.*, Nucl. Phys. B9, 493 (1969).

[56]M. Hague *et al.*, Phys. Rev. 152, 1148 (1966).

[57]W. L. Yen *et al.*, Phys. Rev. 188, 2011 (1969).

[58]Case-Western Reserve data as reported by B. Musgrave, in *Phenomenology in Particle Physics, 1971,* proceedings of the Conference held at Caltech, 1971, edited by C. B. Chiu *et al.* (Caltech, Pasadena, 1971).

[59]University of Kansas data, as reported by B. Musgrave (Ref. 58).

[60]D. C. Colley *et al.*, Nuovo Cimento 53A, 522 (1968).

[61]Johns Hopkins data as reported by B. Musgrave (Ref. 58).

[62]S. M. Flatté and C. G. Wohl, Phys. Rev. 163, 1441 (1967).

[63]W. Hoogland, Thesis, Universiteit van Amsterdam, 1968 (unpublished).

[64]J. Mott *et al.*, Phys. Rev. 177, 1966 (1968).

[65]K. Jaeger, Ph. D. thesis, Syracuse University, 1970 (unpublished).

[66]M. Aderholz *et al.*, Nucl. Phys. B5, 606 (1968).

[67]D. O. Huwe, Phys. Rev. 181, 1824 (1969).

[68]S. M. Flatté, Phys. Rev. 155, 1517 (1967).

[69]J. S. Lindsey and G. A. Smith, Phys. Rev. 147, 913 (1966).

[70]G. S. Abrams *et al.*, Phys. Rev. Letters 18, 620 (1967).

[71]D. G. Scotter *et al.*, Nuovo Cimento 62A, 1057 (1969).

[72]D. Birnbaum *et al.*, report presented at the Fourteenth International Conference on High Energy Physics, Vienna, 1968.

[73]See, for instance, the review by G. Fox, in *Phenomenology in Particle Physics,* Ref. 58.

[74]We have previously reported on the SU(3) comparison of reactions (c) and (d): M. Aguilar-Benitez *et al.*, Phys. Rev. Letters 28, 574 (1972).

[75]In particular, the following relations are obtained in the peripheral region:

$$F \text{ coupling: } -A(K^-p \to Y\phi) = A(\pi^-p \to YK(890)) = -\sqrt{2}\,A(K^-p \to Y\rho) = -\sqrt{2}\,A(K^-p \to Y\omega) = -(1/\sqrt{6})A_F^8,$$

$$D \text{ coupling: } -A(K^-p \to Y\phi) = A(\pi^-p \to YK(890)) = \sqrt{2}\,A(K^-p \to Y\rho) = \sqrt{2}\,A(K^-p \to Y\omega) = (\tfrac{3}{10})^{1/2}A_D^8,$$

where A_F^8 (A_D^8) are the antisymmetric (symmetric) SU(3) octet amplitudes. For more details see H. J. Lipkin, Nucl. Phys. B7, 321 (1968); G. Alexander *et al.*, Phys. Rev. Letters 17, 412 (1966).

[76]This uses the definition of S. Meshkov, G. A. Snow, and G. B. Yodh, Phys. Rev. Letters 12, 87 (1964).

[77]M. Abramovich *et al.*, Nucl. Phys. (to be published).

[78]The $\Lambda\phi$ cross section has been multiplied by 1.04 to take into account its relative correction to σ with respect to the $\Lambda K(890)$ cross section. This same factor also multiplied the $d\sigma/dt'$ distribution shown in Fig. 95.

[79]Because of the limited statistics in the $\Sigma^0\phi$ channel, the data at 3.9 and 4.6 GeV/c have been combined and then normalized to the total cross section at 3.9 GeV/c. The resultant $d\sigma/dt'$ distribution has been multiplied by the relative correction factor between $\Sigma^0\phi$ and $\Sigma^0K(890)$ of 1.05.

[80]M. Abramovich *et al.*, Nucl. Phys. B27, 477 (1971).

[81]S. P. Ying *et al.*, Phys. Letters 30B, 289 (1969).

[82]See, for instance, the summary by K. W. Lai and J. Louie, Nucl. Phys. B19, 205 (1970).

[83]E. Hirsch *et al.*, Phys. Letters 36B, 139 (1971).

[84]E. Hirsch *et al.*, Phys. Letters 36B, 385 (1971).

[85]H. J. Lipkin and F. Scheck, Phys. Rev. Letters 18, 347 (1967).

[86]The theoretical equality was exhibited in Ref. 43 and by G. Alexander, H. J. Lipkin, and F. Scheck, Phys. Rev. Letters 17, 412 (1966). We test this relation without any t' selection because of the relatively small backward cross sections in these processes.